

**UNCLASSIFIED**

**AD 409422**

**DEFENSE DOCUMENTATION CENTER**

**FOR**

**SCIENTIFIC AND TECHNICAL INFORMATION**

**CAMERON STATION, ALEXANDRIA, VIRGINIA**



**UNCLASSIFIED**

**NOTICE:** When government or other drawings, specifications or other data are used for any purpose other than in connection with a definitely related government procurement operation, the U. S. Government thereby incurs no responsibility, nor any obligation whatsoever; and the fact that the Government may have formulated, furnished, or in any way supplied the said drawings, specifications, or other data is not to be regarded by implication or otherwise as in any manner licensing the holder or any other person or corporation, or conveying any rights or permission to manufacture, use or sell any patented invention that may in any way be related thereto.

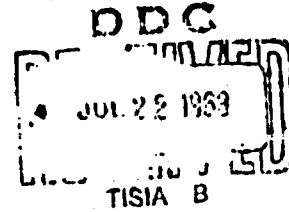
TR 63-205.3

# THIN FILMS FORMED BY ELECTROCHEMICAL REACTIONS

Contract DA No. 36-039 SC-90744  
(Continuation of Contract No. DA 36-039 SC-87305)  
DA Project No. 3A99-15-003 & 3G93-34-001

FINAL REPORT

June 1, 1961 - January 31, 1963



ELECTRONIC COMPONENTS DEPARTMENT  
U.S. ARMY ELECTRONICS RESEARCH AND DEVELOPMENT LABORATORY  
FORT MONMOUTH, NEW JERSEY

GENERAL TELEPHONE & ELECTRONICS LABORATORIES  
INCORPORATED

DAYSIDE LABORATORIES, BAYSIDE, NEW YORK



NO. 079

409422

CATALOGED BY DDC 40942  
AS AD No. \_\_\_\_\_

**Qualified Requestors May Obtain Copies Of  
This Report From ASTIA. ASTIA Release  
To OTS Not Authorized.**

**THIN FILMS FORMED BY ELECTROCHEMICAL REACTIONS**

**Contract No. DA 36-039 SC-90744**  
**(Continuation of Contract No. DA 36-039 SC-87305)**  
**DA Project No. 3A99-15-003 & 3G93-34-001**

**FINAL REPORT**

**June 1, 1961 - January 31, 1963**

**Prepared by E. R. Bowerman**  
**J. Warren Culp**  
**P. F. Hudock**

**Approved by A. L. Solomon**  
**Scientist-in-Charge**  
**Chemical Electronics**



TABLE OF CONTENTS (Cont'd.)

	<u>Page</u>
1.1.6.4 Electron Micrographs	39
1.1.6.5 Tantalum Oxide Film Density	39
1.1.7 Electrical Measurements	43
1.1.7.1 Apparatus and Procedures	44
1.1.7.2 Results	45
1.2 Thin-Film Resistors	73
1.2.1 Selection and Treatment of Substrates	75
1.2.2 Film Deposition Techniques	75
1.2.2.1 Sputtering	75
1.2.2.2 Evaporation	78
1.2.3 Measuring Techniques	79
1.2.3.1 Interferometry	79
1.2.3.2 DC Resistance	79
1.2.4 Resistor Patterns	79
1.2.5 Anodization	81
1.2.5.1 Apparatus	81
1.2.5.2 Electrolytes	85
1.2.5.3 Current Density	86
1.2.5.4 Automatic Method of Anodization	88
1.2.6 Heat Treatment of Anodized Films	89
1.2.7 Resistor Properties	92
1.2.7.1 Temperature Coefficient of Resistance	92
1.2.7.2 Stability of Resistance	102
2. CONCLUSIONS	111
2.1 Thin-Film Capacitors	111
2.2 Thin-Film Resistors	113

TABLE OF CONTENTS (Cont'd.)

	<u>Page</u>
3. REFERENCES	114
4. RECOMMENDATIONS FOR FUTURE WORK	115
4.1 Thin-Film Capacitors	115
4.2 Thin-Film Resistors	115
APPENDIX I   Electrical Testing Unit for Thin-Film Capacitors	117
APPENDIX II   Measurement of Capacitance and Dissipation Factor Over a Frequency Range	119
APPENDIX III  Multiple-Beam Interferometry for Thin-Film Measurement Below 300 A	121
Man Hours Expended by Key Personnel	123

## PURPOSE

The aim of this study is the development of techniques for preparing thin-film resistors and capacitors by complete or partial anodic oxidation of selected metal deposits in predetermined patterns. The metals of interest are aluminum, tantalum, titanium, tungsten and zirconium. The methods of patterning deposits of these metals should be both capable of obtaining high resolution and economically adaptable to the mass production of microelectronic circuits. Reliability and tolerance limits should be comparable to levels currently attainable with vacuum deposition methods.

## ABSTRACT

The technique of forming thin-film capacitors by the anodic oxidation of the surfaces of vacuum-deposited films of aluminum, tantalum, tungsten, titanium and zirconium has been investigated. Of these metals, tantalum was found to approach closest the objectives specified in the contract. Methods of selecting and cleaning glass substrate surfaces have accounted in large part for increasing the voltage at which capacitor breakdown occurred. Breakdown voltages equal to or greater than the anodization forming voltage have been obtained, resulting in a usable capacitance-voltage product of  $13.5 \mu\text{f} \cdot \text{v}/\text{cm}^2$ . The uniformity of capacitance measured for a large number of test samples fell within a standard deviation of 3 percent. Electrical properties over a range of frequency and temperature have been evaluated.

The preparation of thin-film resistors by forming vacuum-deposited metal in a predetermined pattern and then partially anodizing the deposited metal to a precise resistance has been studied for tantalum and tungsten. The properties of vacuum-deposited films of titanium and zirconium that are related to their use as resistors has also been investigated. Anodized, evaporated tungsten films best fulfilled the objectives specified in the contract. Film patterns were prepared with a resistor density of 6 megohms/in.<sup>2</sup> and with a temperature coefficient of resistance (TCR) nominally zero. The corresponding sheet resistivity at zero TCR was 300 ohms/sq; the sheet resistivity at a TCR of  $-200 \text{ ppm}/^\circ\text{C}$  was 2000 ohms/sq. The resistance of anodized tungsten films has been stabilized within 10 ppm/hr by heat treatment in vacuum without appreciably changing the resistance from that obtained after anodization. The precision of resistance to which a preselected value could be obtained was better than 1.5 percent. Stability of resistance under load over a temperature range is described.

## PUBLICATIONS, LECTURES, REPORTS AND CONFERENCES

### PUBLICATIONS

<u>Quarterly Reports</u>	<u>Date Issued</u>
Contract DA 36-039-sc-87305	
First	Oct. 1961
Second	Jan. 1962
Third	Mar. 1962
Fourth	Aug. 1962
Contract DA 36-039-sc-90744	
First	Nov. 1962
Second	Mar. 1963

A paper, "Anodized Tungsten Thin-Film Capacitors and Resistors," by E.R. Bowerman, J.W. Culp, P.F. Hudock, F. Leder and H.J. Degenhart was presented at the 1963 Electronics Components Conference held May 7-9, 1963 in Washington, D.C. and accepted for publication in the IEEE Transactions, Component Parts.

### CONFERENCES TO REVIEW THE PROGRESS OF THE PROJECT

June 30, 1961	Dr. E. Both of USAELRDL visited
Sept. 5, 1961	GT&E Labs.
Oct. 6, 1961	Dr. H.J. Degenhart and Mr. I.H. Pratt of
Dec. 14, 1961	USAELRDL visited GT&E Labs.
Oct. 13, 1961	Mr. W. Weintraub and Lt. J. Bennett of
	USAELRDL visited GT&E Labs.
Mar. 14, 1962	Dr. A. L. Solomon, Mr. E.R. Bowerman
	and Dr. A.S. Esbitt of GT&E Labs
	visited USAELRDL.
June 8, 1962	Dr. H.J. Degenhart, Mr. I.H. Pratt
	and Mr. A.J. Raffalovich of USAELRDL
	visited GT&E Labs.
Nov. 29, 1962	Dr. A. L. Solomon and Mr. E.R. Bowerman
	of GT&E Labs visited USAELRDL.

## 1. FACTUAL DATA

### 1.1 THIN-FILM CAPACITORS

Thin-film capacitors were formed by anodic oxidation of the surfaces of metal films deposited on glass substrates, followed by the deposition of a metallic top or counter electrodes. The metals investigated were aluminum, tantalum, tungsten, titanium and zirconium. Electrical characteristics of the capacitors were evaluated and compared with those specified as objectives in the contract. Significant physical characteristics of the oxide layers were determined.

#### 1.1.1 General Procedure

The structure of a glass panel containing five test capacitors is represented schematically in Fig. 1. A film of the metal to be anodized was deposited on the substrate by sputtering or evaporation with part of the area masked off. The film was anodically oxidized except for the circular portion which was masked for the electrical base connection. Top electrodes were deposited by evaporation through a mask in a pattern to form the five capacitors with contact tabs extending over the unmetallized area of the substrate. A sixth top electrode made contact with the unanodized area of the base film and therefore with the metal film lying underneath the oxide, which served as a common bottom electrode.

Substrates were generally cut from glass microscope slides with a diamond scribe and measured 1.6 cm x 5.1 cm (5/8 in. x 2 in.) as indicated in Fig. 1. The anodized area measured 4.3 cm<sup>2</sup> (0.67 in.<sup>2</sup>). Each capacitor had an area of 0.20 cm<sup>2</sup> (1/8 in. x 1/4 in. or 0.031 in.<sup>2</sup>).

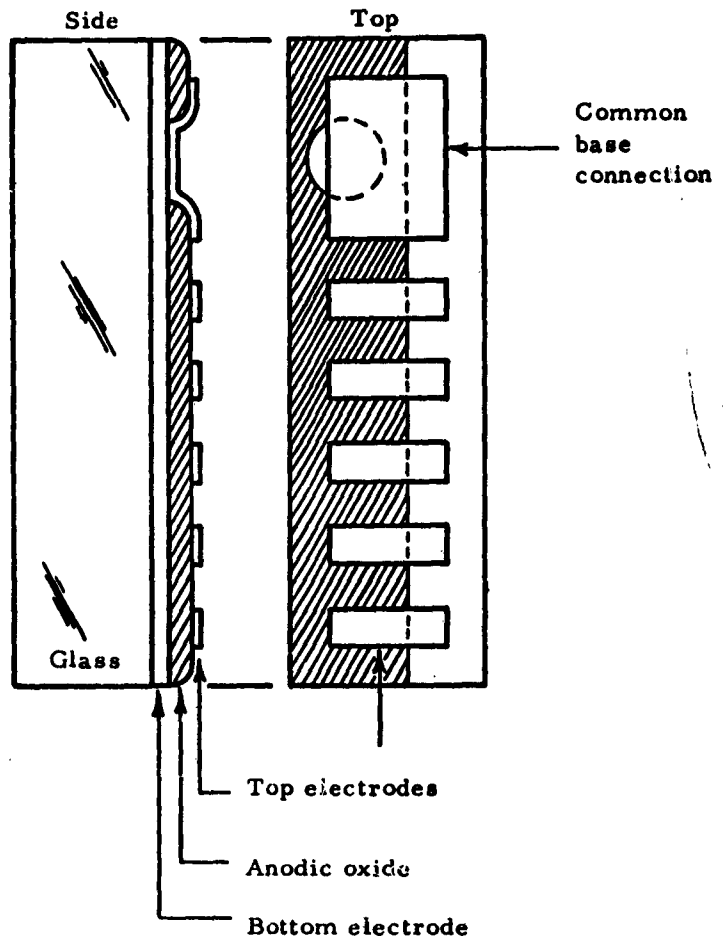


Fig. 1. Panel containing five test capacitors with common base connection

The following sections will describe procedures for and results of selecting and cleaning of substrates, deposition of metallic base films, anodic oxidation, deposition of top electrodes, examination of physical characteristics of the oxide, and measurement of electrical characteristics of the test capacitors.

Electron microscopes were made at several stages in the procedure. Surface replicas were prepared by preshadowing with platinum, depositing a carbon film, and stripping the replica from the specimen with dilute hydrofluoric acid.

#### 1.1.2 Substrates

It is desirable to form thin-film passive components on a substrate having low electrical and high thermal conductivity, and a smooth, chemically inert surface. Although the micro slide glass surface chosen for this study does not meet the last three requirements as well as was hoped, careful selection and cleaning did meet the critical requirement of smoothness.

##### 1.1.2.1 Materials

The suitability of ceramic substrates was investigated in the initial phases of this work. It appeared that a ceramic should meet all the desired properties from a consideration of mechanical strength, thermal and electrical characteristics, and the convenience of molding small, precise shapes. Tests showed, however, that metallized Alsimag 614 alumina micromodule wafers had a surface roughness of 5000 Å, which was excessive for the formation of oxide films of 1000 Å thickness. Glazing the wafers by heating with a zinc borosilicate frit for a short time at 700°C made them sufficiently smooth for use as substrates. For the present experimental investigation, however, it was decided to use

glass micro slides because of their ease of handling, the availability of a wide variety of glasses, and their superior surface smoothness.

As the program proceeded, it became evident that the use of smoother glass surfaces resulted in films with higher electrical breakdown strengths. Although an early investigation of increasing the capacitance per unit area by roughening the glass surface showed that up to a 20 percent increase could be obtained by sandblasting, an attending loss in breakdown strength far overshadowed the gain.

#### 1.1.2.2 Defects in Glass Surfaces

Eleven types of micro slides and cover glasses were examined by optical microscopy for surface defects. Attempts were also made to relate these defects to sites of electrical breakdown in capacitors prepared on these surfaces.

Preliminary studies narrowed the choice to four types of micro slides:

- A1 - ground edges; individually selected by the manufacturer as free of bubbles, pits and scratches.
- A2 - ground edges; selected as above, but by plate and not individually.
- A3 - unground, fire-polished edges; otherwise selected like A2.
- B1 - unground edges as cut; packed with paper separators.

Figure 2 shows that the unground-edge samples, B1 and A3, had fewer defects. Since the A3 glass yielded, for undetermined reasons, capacitors of higher breakdown strength, it was adopted as the preferred substrate material. Selection of individual slides from a given lot was required, and one side of the slide was found to be preferable.

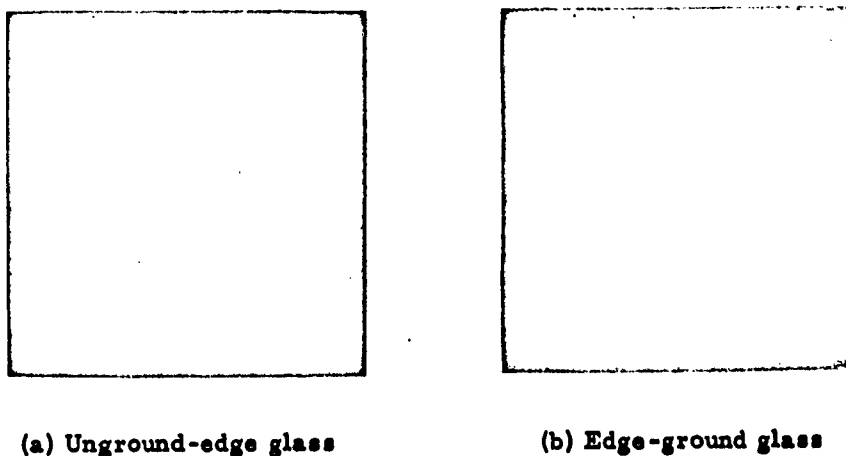


Fig. 2. Negatives of photographs at 10X under oblique top illumination, showing unground-edge and edge-ground micro slide substrates (metallized with sputtered tantalum films).

Much of the optical examination of glass surfaces was done with standard equipment. Areas up to 2 mm in diameter were photographed at 10X magnification with a 35-mm reflex camera mounted above a Zeiss 2006 interference microscope with the eyepiece removed. This instrument was also used in examining surface contours by means of interference fringes under green (5400 A) or white vertical illumination. Additional illumination by transmitted and oblique light was provided. Extraneous reflections of transmitted light were reduced by stopping the 10X objective down to 2 mm. Visual observation at 75 to 600X and photography up to 800X were possible with a Unitron U-11 metallographic microscope.

To identify breakdown sites with glass defects in the same area, photographs of a capacitor before and after breakdown were compared with a photograph of the original substrate surface. A triple comparator was

constructed for the purpose. This instrument superimposes two photographs in the field of one eye of the observer and locates a third photograph in the field of the other eye. Superimposition is obtained with a beam-splitting mirror and an erecting mirror. Low-magnification prismatic oculars cause the two eye fields to merge. Three separate illuminators of different colors with independent brightness controls and blackout provision allow easy location of differences among the three images.

The larger defects observed on glass micro slides were classified as indentations, chips and ridges. Indentations, which were detected with the interference microscope before metallizing, appeared to have resulted from the glass lying on a rough surface while still soft during its fabrication. Three types of slide from one manufacturer (A1, A2 and A3) had indentations as deep as 5000 A and only on one side, while another type (B1) from another source had none. Although no direct association could be drawn between indentations and capacitor properties, where possible, the opposite side was selected for film deposition.

Chips are small fractures with radiating cracks and flakes still attached. Similar fractures have been produced by pressing fine abrasive powder between two slides. Chips are visible under strong oblique light especially after metallization (Fig. 2a). Glass slides were selected to eliminate large defects of this type.

Ridges are fine, widely separated, parallel elevations of heights up to 500 A. They were visible to the unaided eye after glass was metallized and could be found with the interference microscope before metallizing. This defect appeared extensively on both surfaces of one manufacturer's micro slides (A1, A3). Ridges prominently interfered with the anodization of titanium. The current tended to concentrate

initially at ridge elevations and oxygen evolution, typical of titanium anodization in aqueous electrolytes resulted in lines of bubbles covering the ridges. Areas with ridges became insulated from the electrolyte by the bubbles and ceased to form oxide. The result is shown in Fig. 3.

In addition to these large defects, which could be identified and eliminated by glass selection, there remained a large number of small defects that could not be sufficiently resolved optically for classification. To study the relation between these small defects and sites of electrical breakdown, 1-mm square capacitors were photographed and the negatives enlarged for more detailed observation of the breakdown.

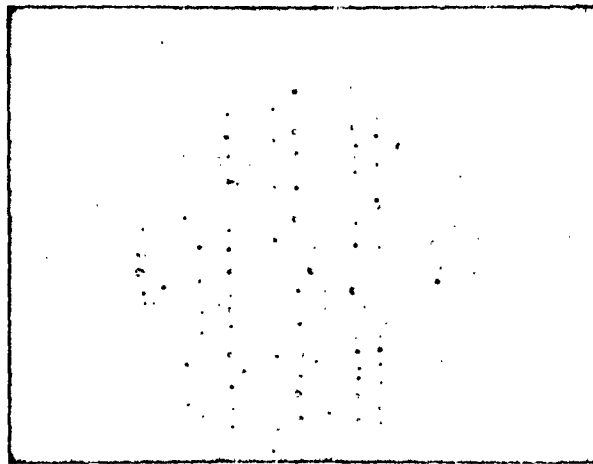


Fig. 3. Anodized titanium deposit on a glass substrate having ridge-type defects. (Photograph by transmitted light. Diameter of field — 10 mm.)

The triple comparator was used for this purpose. An example of these photographs and an enlargement of a breakdown site, which appears in this case as a series of four craters, are illustrated in Fig. 4. Typically, a pit was centered in each crater, and it is believed to be the origin of the electrical discharge that caused breakdown. Although a surface defect in the glass was found at the site in the photograph before breakdown, the location of the defect did not coincide with that of the central pit. We were not able in this investigation to establish fully the relation between small defects and capacitor breakdown.

#### 1. 1. 2. 3 Cleaning

Glass micro slide substrates were individually cleaned ultrasonically in Alconox detergent, rinsed with running distilled water, immersed in hot chromic-sulfuric acid, rinsed, quickly flooded with 1 percent hydrofluoric acid, rinsed again, and rapidly dried with a jet of clean compressed air. The air drying took place within a pressurized dust-free work space, which also enclosed the sputtering chamber. Substrates were transferred directly to the sputtering jig or to a covered Petri dish when the metal was to be deposited by vacuum evaporation. Sample slides were periodically diverted for test. If black breath figures were obtained, the cleaning was considered adequate.

The hydrofluoric acid treatment was instituted when electron micrographs (Fig. 5) showed that chemical residues and grease remained after the chromic-sulfuric acid cleaning. It is postulated that the hydrofluoric acid removes a thin layer of silica gel on the glass surface and any foreign material attached to it. The foreign material was removed as shown in Fig. 6, and capacitors prepared on these surfaces showed fewer initial shorts and higher breakdown voltages with no change in capacitance or dissipation factor.

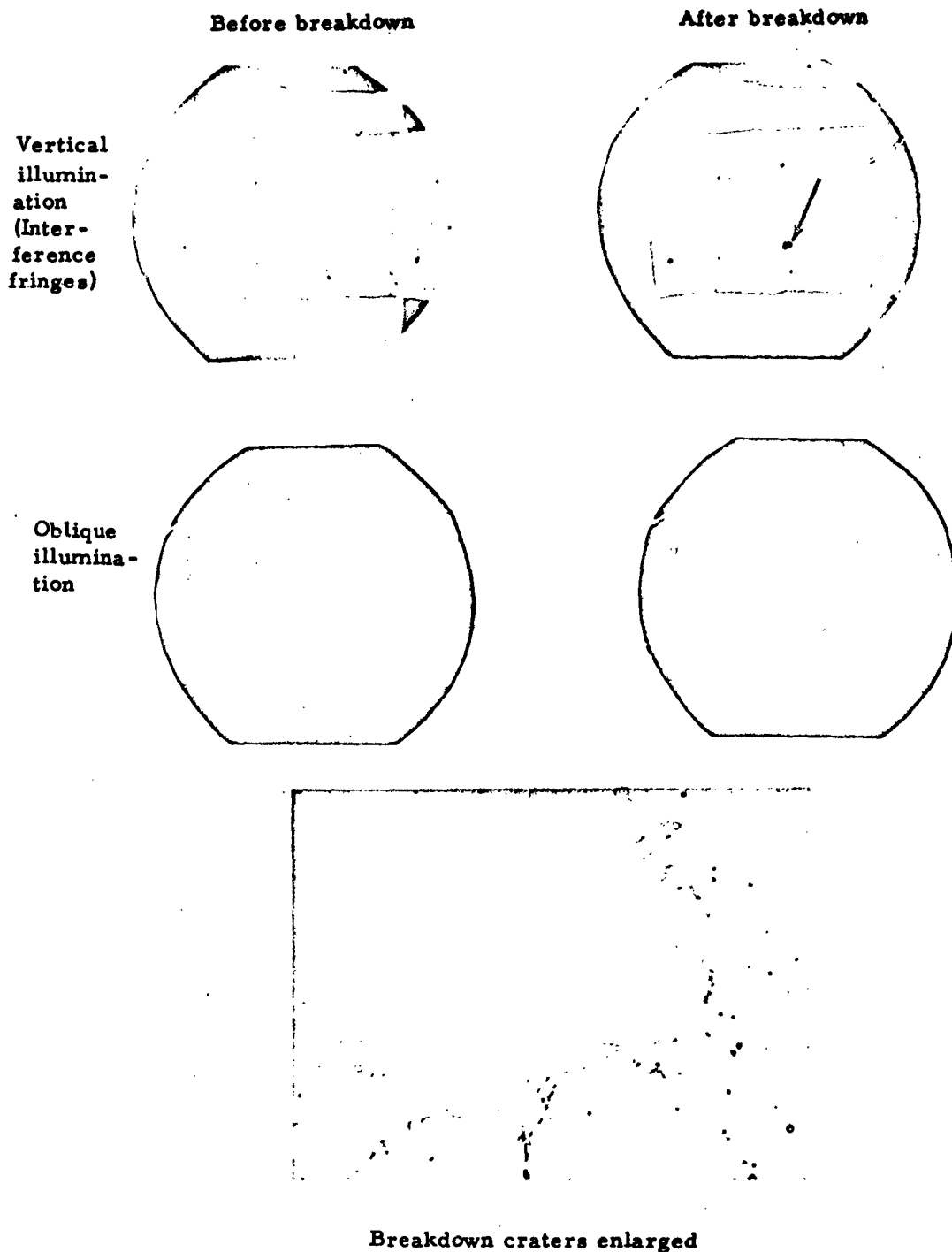


Fig. 4. Top: Photographs of a tantalum capacitor of 32X magnification before and after breakdown (by vertical illumination using interference fringes and by oblique illumination).  
Below: Breakdown crater shown above, at 800X magnification.

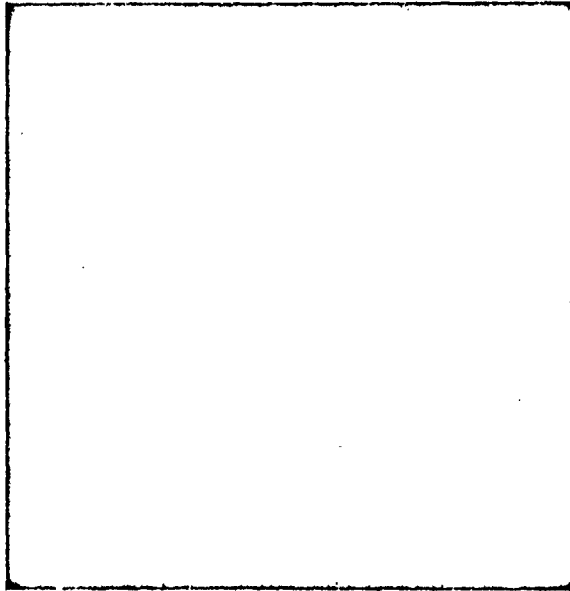


Fig. 5. Electron micrograph of glass slide, after chromic-sulfuric acid cleaning. (13,000X)

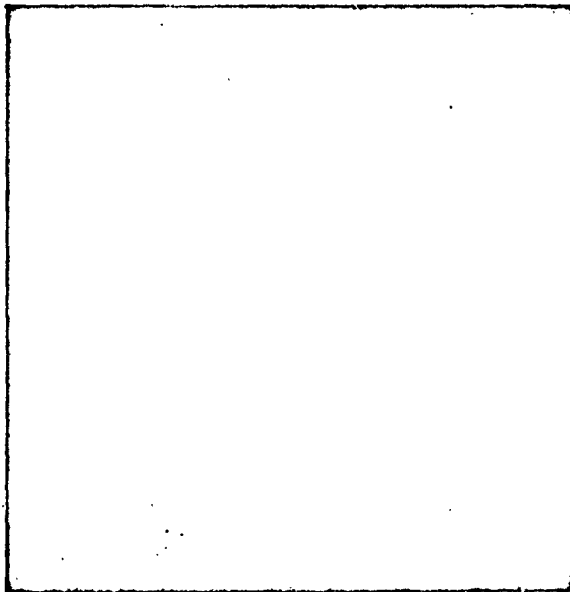


Fig. 6. Electron micrograph of glass slide, after chromic-sulfuric acid cleaning and hydrofluoric acid treatment. (13,000X)

#### 1.1.2.4 Summary

Micro slide glass was chosen for substrate material in this work because of its superior surface smoothness, availability, and ease of handling. The bulk of the work was done with the unground, fire-polished edge type of micro slide designated in this report as A3. Selection from a given lot was required, and selection of the smoother side was preferred. A direct association of glass surface defects with sites of electrical breakdown could not be established. It was observed that ridge defects had a deleterious effect on the anodization of metal films. A glass substrate cleaning treatment was developed which included flooding with dilute hydrofluoric acid to remove traces of foreign materials.

#### 1.1.3 Deposition of the Metal Base Film

Base films of the metals to be anodized were deposited on substrates as soon as possible after cleaning. The materials deposited during the course of this research included aluminum, tantalum, titanium, tungsten, and zirconium. The methods of deposition employed were vacuum evaporation from a resistively heated filament, sputtering in argon, and vacuum evaporation by electron bombardment. Aluminum and titanium were evaporated from filaments; tantalum and tungsten were both sputtered and evaporated by electron bombardment, and zirconium was sputtered. Detailed descriptions of these three methods follow.

##### 1.1.3.1 Evaporation from a Filament

Evaporation of aluminum and titanium was carried out in a Consolidated Vacuum Corp. LC1-18B vacuum system with a 45-cm bell jar. The evaporant, in wire form, was placed inside or wrapped on the filament. The filament had five turns of triple-strand 30-mil tungsten

wire and was operated at currents up to 110 amp. An inner cylindrical shell shielded the bell jar from the filament for ease in cleaning. Substrates to be coated with aluminum were mounted 15 cm below the filament in a work holder (Fig. 7) provided with water cooling. Masks were of glass. Substrates to be coated with titanium were mounted 15 cm above the filament to reduce exposure to settling dust, with either glass masks or steel masks held by magnets. A thermocouple indicated the work-holder temperature.

Before evaporation, substrates were further cleaned by ion bombardment in a glow discharge. The glow was maintained for 20 to 30 minutes, until the work-holder temperature reached 250°C for aluminum and 90°C for titanium. Glow currents of 200 to 400 ma were passed at approximately 3 kv with the pressure preferably adjusted to locate the substrate within the negative glow, thereby reducing the amount of organic contaminants. A liquid-nitrogen trap below and a water-cooled baffle above the main valve were employed to minimize the backstreaming of oil. In the case of titanium, air was leaked into the system and pumped out continuously during the glow to oxidize and flush out impurities such as water and pump oil. It was important to use a pure titanium glow cathode for cleaning. When an aluminum glow cathode was used, the subsequent titanium deposit had a poor appearance probably because of the effect of aluminum sputtered during the cleaning. Evaporation was carried out after the substrates had cooled to 80°C for titanium and 100°C for aluminum where water cooling of the work holder aided the process. Pressure at the start of evaporation was  $5 \times 10^{-6}$  Torr or better. The charge was melted down with a shield protecting the substrates from flying particles, and then evaporation was completed as rapidly as possible. Films evaporated in this manner had a relatively small number of pinholes, metallic brightness on both sides

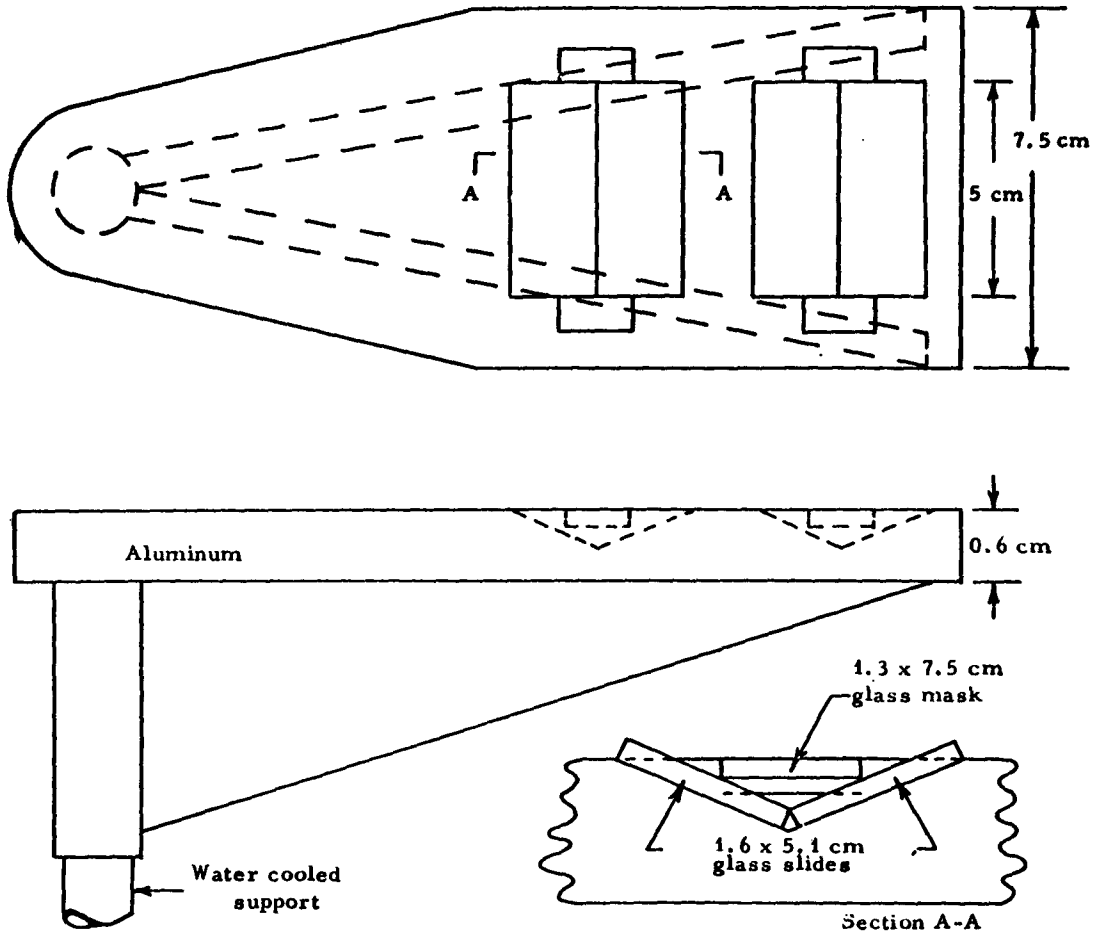


Fig. 7. Work holder for evaporation of aluminum.

of the film, and good adherence to the substrate both in a Scotch tape test and during anodization.

#### 1.1.3.2 Sputtering

Tantalum, tungsten, and zirconium were sputtered in a modified Kinney SC-3 vacuum system with a 30-cm bell jar. An electrically insulated, water-cooled cathode support and a grounded cathode shield were built into the jar (Fig. 8). A sheet cathode of the desired metal was mounted by means of a threaded stud. A water-cooled copper table 4 cm below the cathode served as the anode and supported the jigs containing the substrates and their masks. Clean glass was preferred as the masking material. A copper mask, employed for a time to give higher precision, contaminated the edge of the film with submicroscopic particles that were deposited electrostatically.

Argon of 99.995% purity was leaked into the system, which was continuously pumped. Pressure was measured with a CVC type GP-110 Pirani gauge corrected for argon. Substrates were shielded during a preliminary period of intermittent sputtering while the cathode was cleaned and the chamber was degassed. Next the shield was removed and sputtering was carried out in 5-sec bursts alternated with 30-sec cooling periods until 60 sec of on-time was completed. Some deviations from this cycle were tried, notably with tantalum where extension of the cooling periods to 54 seconds lowered the average cathode temperature and improved the physical characteristics of the films. Sputtering voltages, current densities, argon pressures and rates of deposition are listed in Table I for the different metals. The dark space was maintained short enough (2.5 cm) so that the substrates were outside this region of high electrostatic fields.

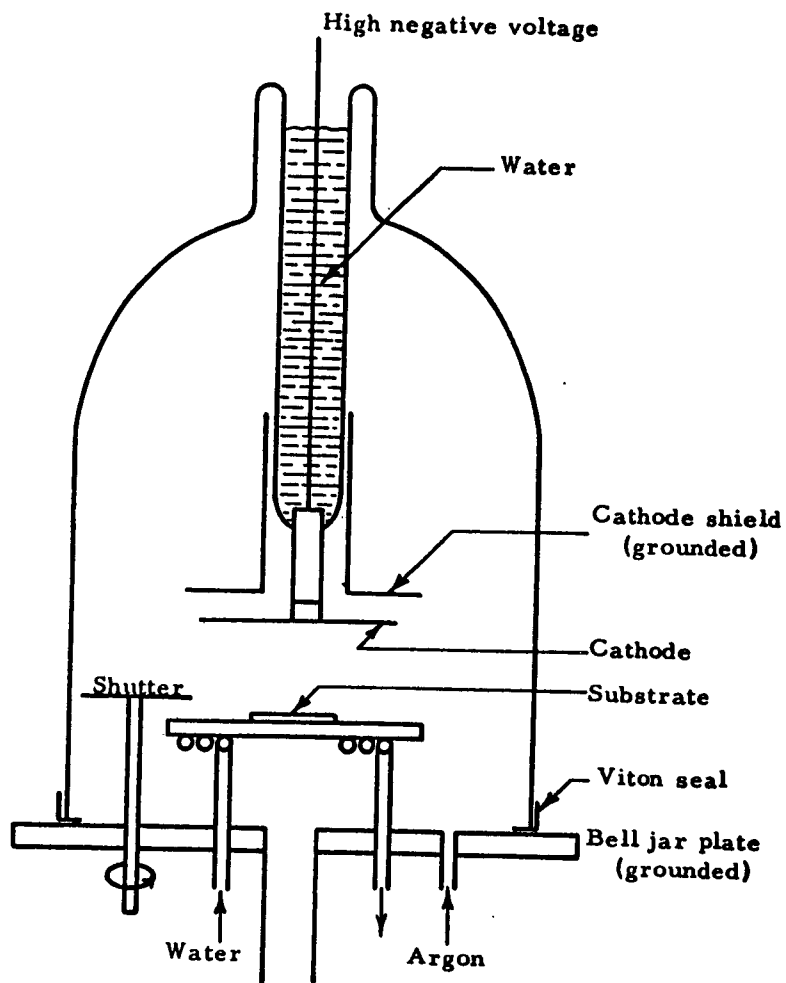


Fig. 8. Sputtering system.

TABLE I

Sputtering Parameters for Different Capacitor Metals

Metal	Argon pressure (Torr)	Current density (ma/cm <sup>2</sup> )	Voltage (kv)	Rate (A/sec)
Tantalum	$7.5 \times 10^{-2}$	2.5	6.0	13
Tungsten	$5.5 \times 10^{-2}$	1.9	4.5	16
Zirconium	$7.5 \times 10^{-2}$	1.7	5.0	18

A good vacuum prior to the introduction of argon was found to be essential. Tantalum-base films sputtered at an initial pressure of  $5 \times 10^{-4}$  Torr, instead of the usual maximum of  $3 \times 10^{-6}$  Torr, yielded capacitors with reduced capacitance and high dissipation factors. This deterioration was ascribed to oxygen and other contaminants in the sputtered film.

Impurities in the argon during the sputtering cycle were monitored by spectrographic analysis, using the glow discharge as a source. Films taken with a Gaertner 165 spectrograph were subsequently plotted on a microdensitometer. The results indicated that the precleaning operation, with substrates shielded, reduced the intensity of nitrogen bands to a low value. Hydrogen lines increased in intensity during sputtering, while a CO bandhead remained constant. Figure 9 shows a typical series of spectra during the cycle.

1.1.3.3 Evaporation by Electron Bombardment

Tantalum and tungsten were also evaporated by heating a rod of the pure metal by bombardment with electrons emitted from an incandescent filament and accelerated with a potential of 8 to 10 kv.

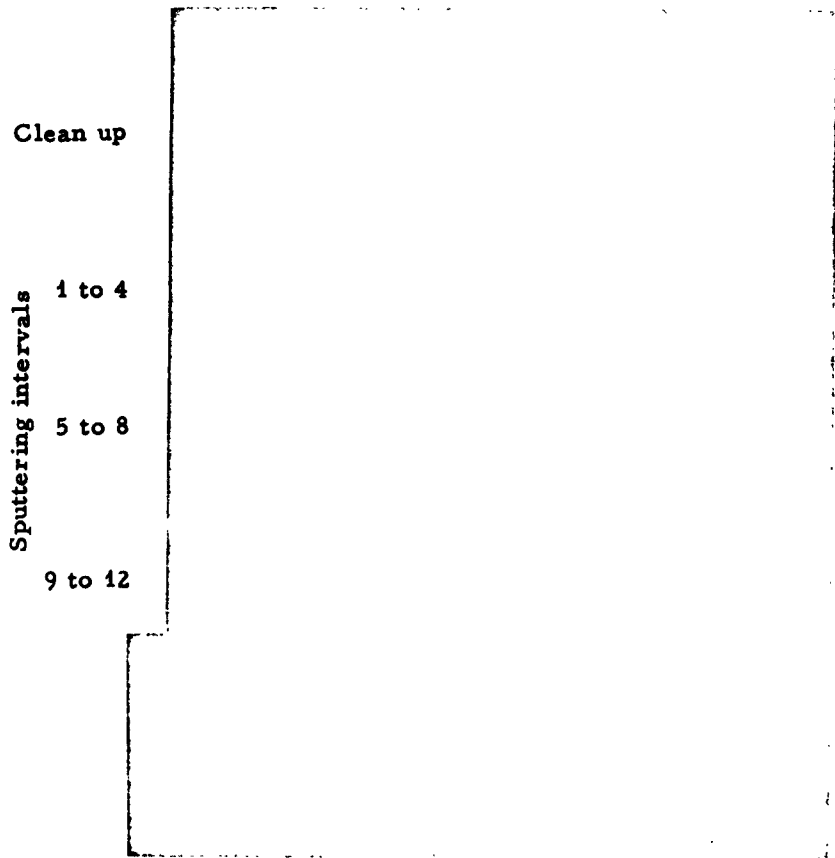


Fig. 9. Spectrum of glow discharge for tantalum sputtering in argon at 5 sec intervals.

A vacuum system constructed for this purpose, Figs. 10(a) and 10(b), included an oil diffusion pump with a mechanical back pump and a liquid nitrogen trap, and an Evapor-Ion titanium gettering pump with a mechanical roughing pump. Chamber pressure was measured with a Bayard-Alpert ionization gauge.

The anode rod of tantalum (3.2 mm diameter) or tungsten (1.6 mm for easier melting) was manually adjusted to the center of the grid cavity (Fig. 11) and was electrically grounded. The grid was ordinarily self-biased and served to focus the electron current on the anode. Only the tip of the rod was melted to form a hanging drop from which evaporation took place. Monitoring of evaporation was aided by an optically projected image of the drop. A shutter protected the substrates during preliminary outgassing. Evaporation was carried out for 20 minutes at electron currents from 25 to 30 ma. The power supply schematic is shown in Fig. 12.

The evaporation cycle involved the following steps:

<u>Operation</u>	<u>Pressure (Torr)</u>
1. Start roughing pump	Atmospheric
2. Start diffusion pump	$4 \times 10^{-2}$
3. Start titanium pump	$1 \times 10^{-5}$
4. Bake vacuum system and cool	$1 \times 10^{-6}$
5. Evaporate	$3 \times 10^{-7}$

Masks for evaporation were made of 2-mil and 5-mil spring steel.

#### 1.1.3.4 Film Quality

With regard to the absence of pinholes and blisters in the films, sputtered films ranked first, filament-evaporated films second and

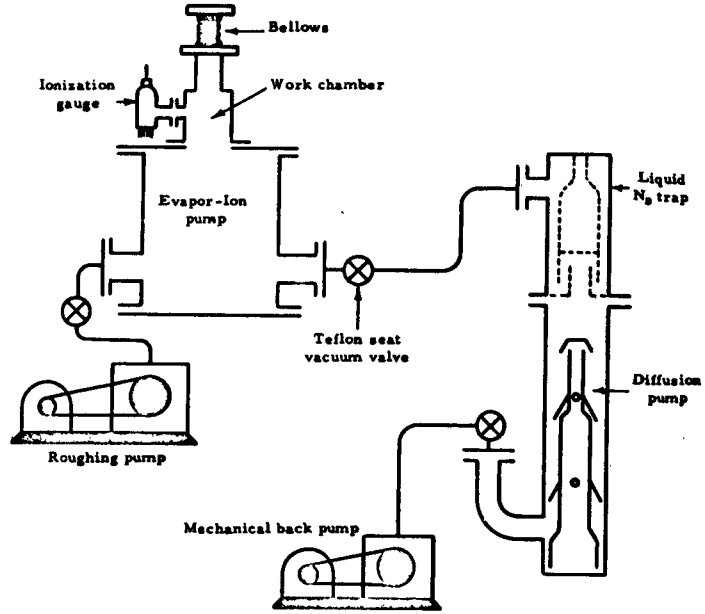


Fig. 10(a). Electron bombardment evaporation vacuum system.

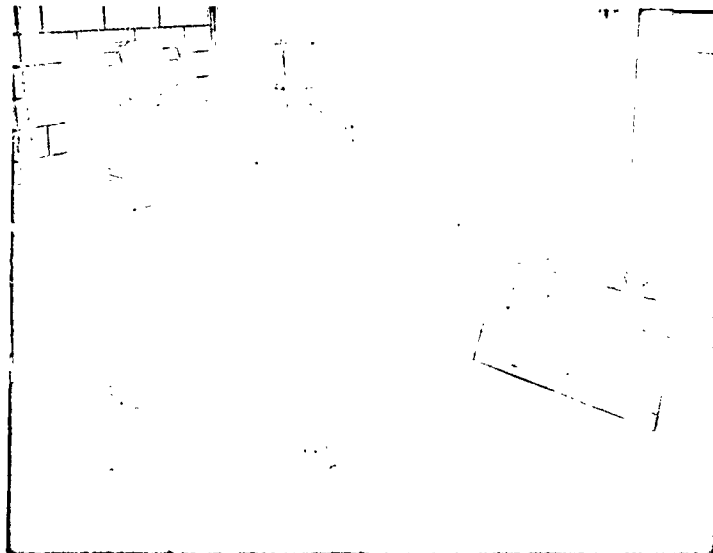


Fig. 10(b). Photograph of electron bombardment evaporator.

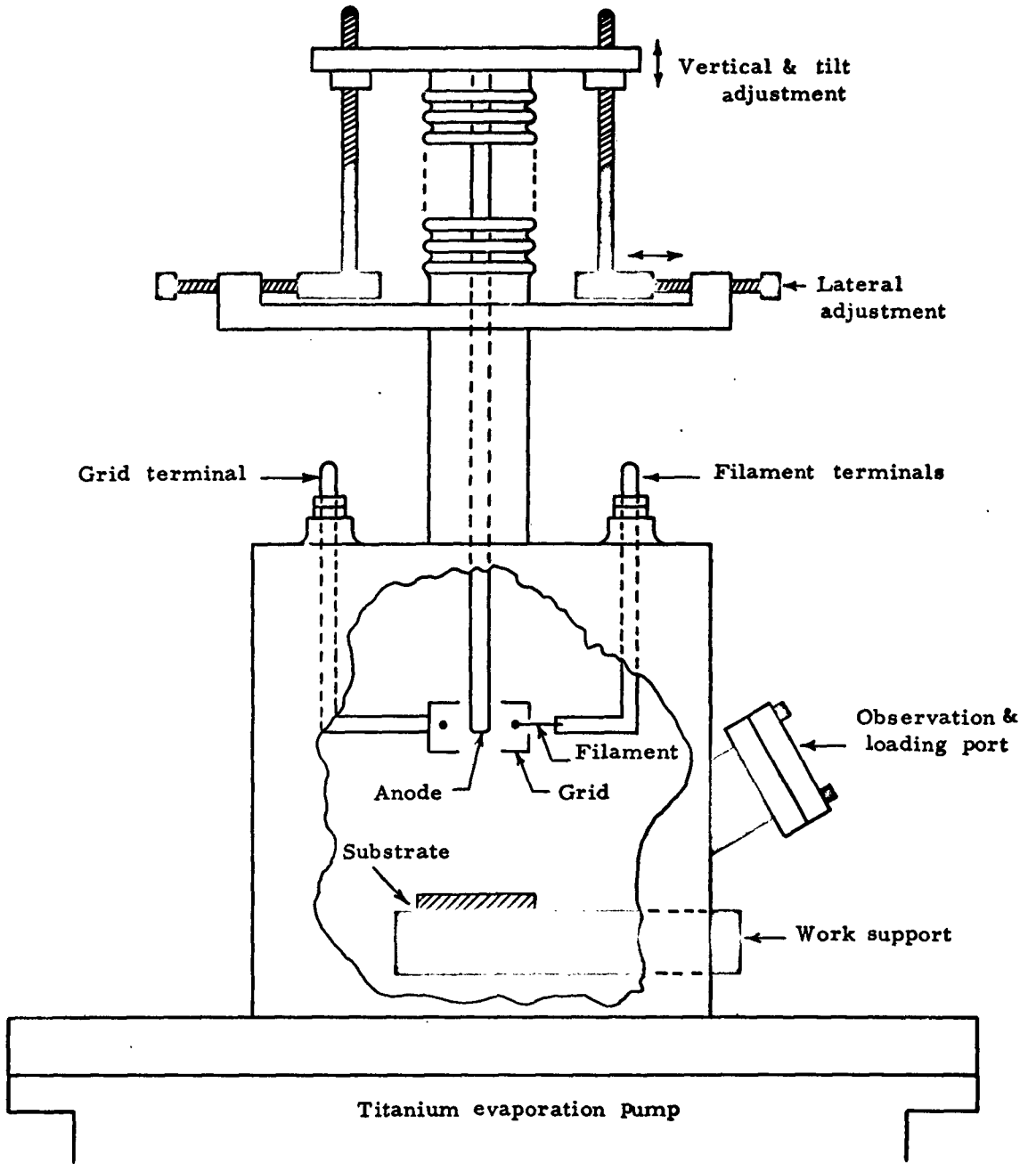


Fig. 11. Electron bombardment evaporator.

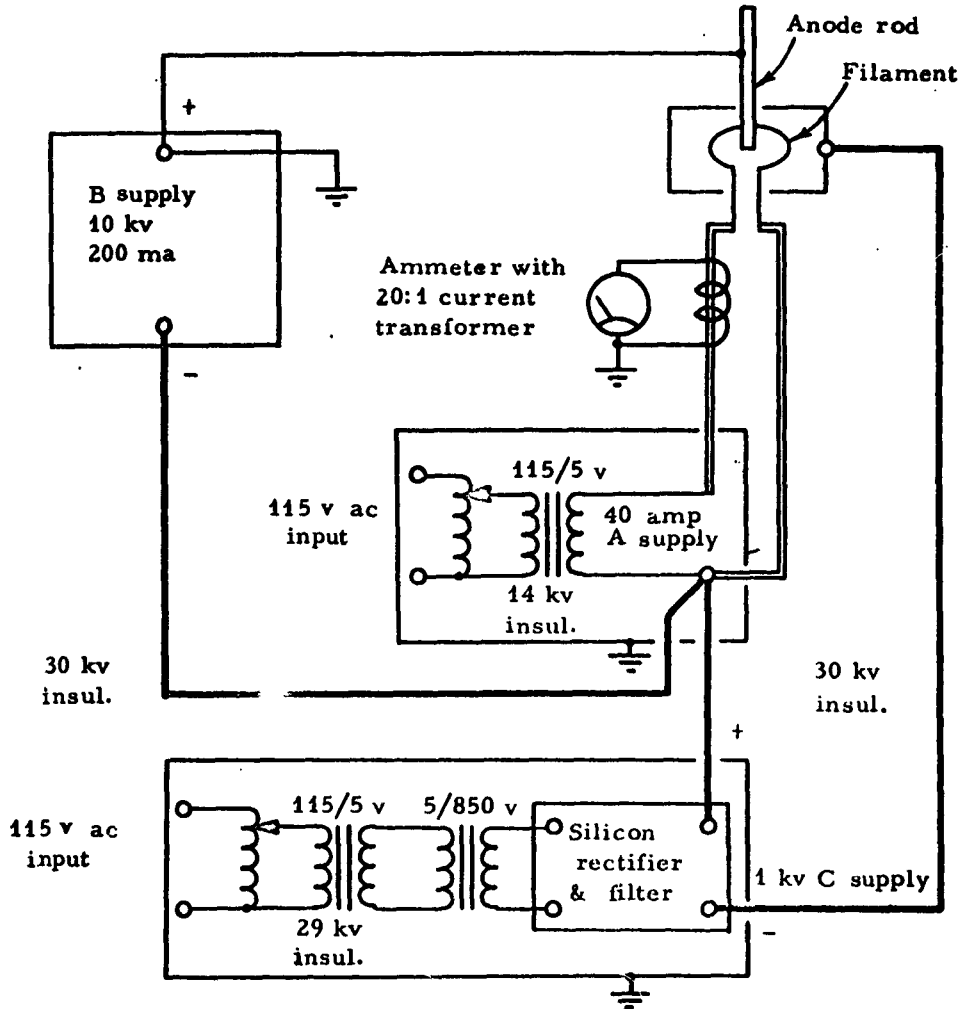


Fig. 12. Power supplies for electron bombardment evaporator.

electron beam evaporated films third. With regard to uniformity of thickness, the order was approximately the same. Ranking according to uniformity of thickness was determined roughly by visually comparing optical densities with transmitted light.

The smoothness of sputtered tantalum and tungsten deposits was examined by electron microscopy. A freshly sputtered tantalum deposit is shown in Fig. 13, a sputtered tantalum deposit after standing for two days at room temperature in Fig. 14. The fresh deposit shows no significant localized irregularities, although it is slightly rougher than the substrate. Heights of surface features vary from 50 to 125 Å. The aged deposit shows a clustered laminar pattern. A sputtered tungsten deposit, shown in Fig. 15, is seen to be similar in surface characteristics to freshly sputtered tantalum.

#### 1.1.4 Anodic Oxidation (see also Section 1.2.5)

##### 1.1.4.1 Equipment and General Procedure

Equipment for anodic oxidation included an electrolytic cell, a power supply, and measuring apparatus. The cells were mounted inside a dust-free, pressurized enclosure which also contained the sputtering chamber and a small sink with running distilled water.

The electrolytic cell was a covered resin reaction kettle fitted with a glass stirrer, electrode holders, and a thermometer. The cathode was a helix made from 25 cm of 40-mil platinum wire. The metallized substrate was clamped at one end in a Teflon support. Electrical connection was made with a pad of conductive silicone rubber. The contact area was insulated from the electrolyte by a Viton O-ring compressed between the substrate and the support.

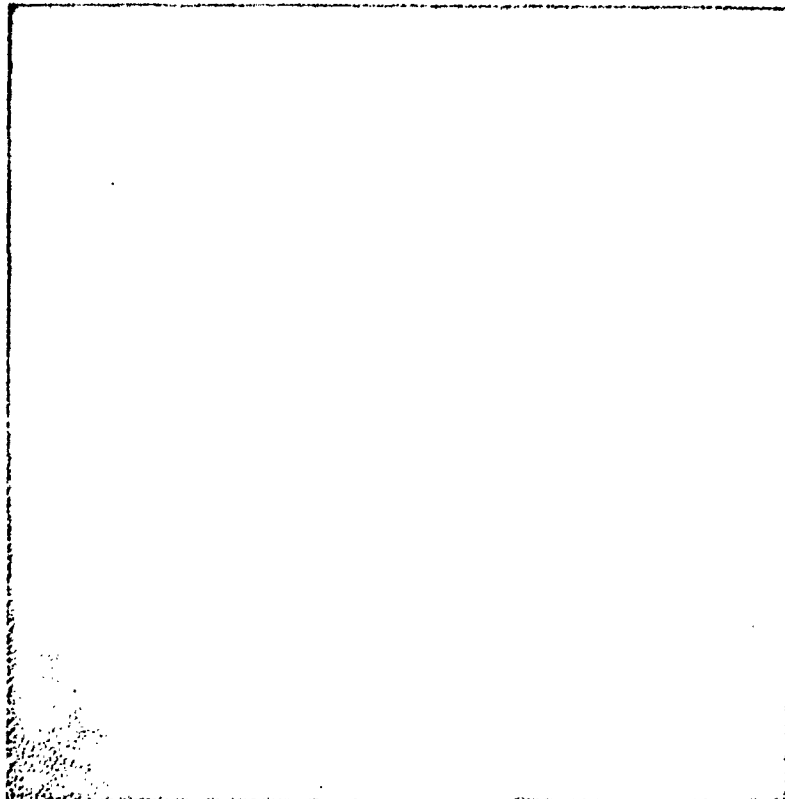
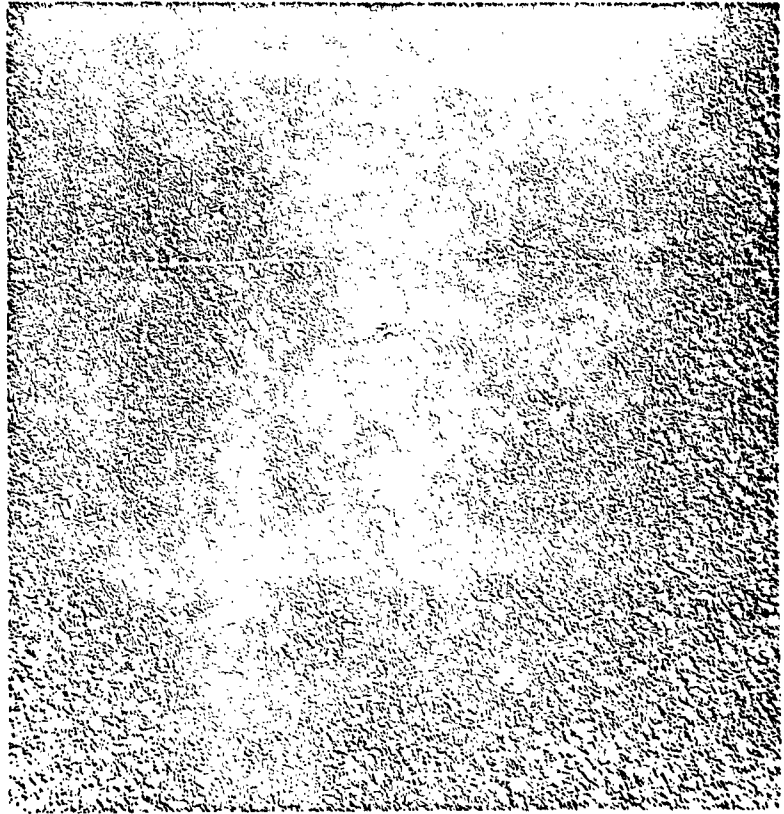
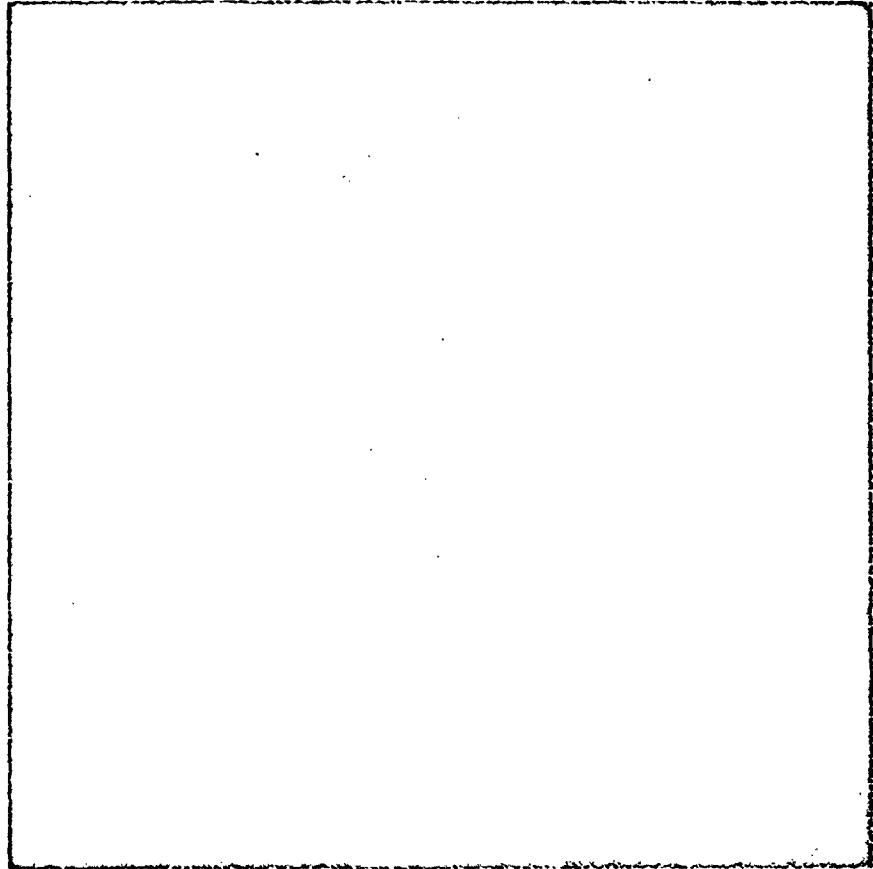


Fig. 13. Electron micrograph of freshly sputtered tantalum film on hydrofluoric acid treated slide (17,500X).



→ || ← 1000 A

Fig. 14. Electron micrograph of sputtered tantalum layer on hydrofluoric acid treated slide; stored two days before replication (17,500X).



10,000 A

Fig. 15. Electron micrograph of sputtered tungsten film  
(20, 300X).

The normal procedure was to apply a constant current until the voltage across the cell rose to a chosen level, then to apply a constant voltage until the current dropped to a suitable level. The initial constant current was selected to give a linear increase in voltage. Constant current and constant voltage were furnished by a Kepco HB-2M supply modified to reduce the minimum available current to 1.2 ma. Cell voltage at the terminals was measured with a high-impedance Keithley 610A electrometer, whose output was plotted on a Brown strip chart recorder. Cell current was measured with a Simpson 269 multi-range meter.

Electrolytic solutions were prepared from reagent-grade chemicals and distilled water. The solutions were filtered through fritted glass to remove suspended particles that might be attracted to the anode. The absence of such particles was verified by searching for the Tyndall effect with a bright lamp and a black backdrop. Stirring was used to maintain a uniform composition of electrolyte near the anode. The pH was measured with a Beckman 72 pH meter.

#### 1.1.4.2 Electrolytes and Specific Procedures

Anodizing electrolytes were selected, where possible, on the basis of van Rysselberghe's unitary formation rate<sup>1</sup> and the final current density. Unitary formation rate is defined as the rate of voltage increase per unit current density,  $(dV/dt)/i$ , observed during the constant-current phase. A high unitary rate and a low final-current density indicate favorable barrier-type oxide growing conditions.

The choice of electrolytes used in anodizing films of aluminum, tantalum, titanium, tungsten and zirconium will be discussed individually for each metal.

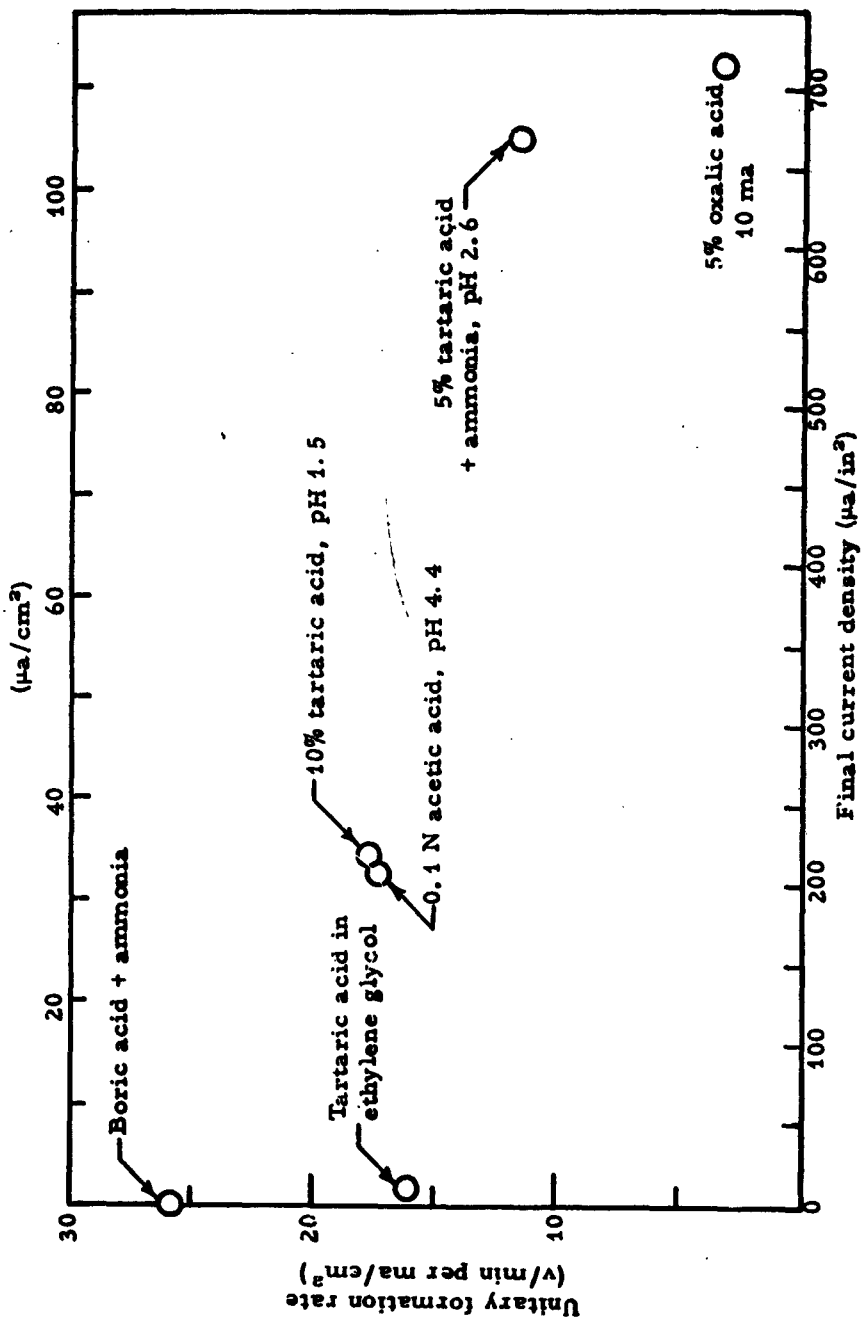


Fig. 16. Effect of electrolyte on the unitary formation rate for aluminum.

1. Aluminum. Electrolytes showed a tendency to attack the oxide film on aluminum and to form a soft, porous layer. An electrolyte was sought which would favor the growth of a barrier oxide layer with a minimum of attack. Results of tests on various solutions are presented in Fig. 16, where the unitary formation rate is plotted against the final current density. The formation rate was measured at a current of  $0.46 \text{ ma/cm}^2$  between 20 and 50 volts. As mentioned, a high formation rate and a low final current are desirable characteristics. The best of these solutions is seen to be boric acid solution neutralized with ammonia.

The effect of the pH on the formation rate of 2 percent boric acid electrolytes with additions of ammonia is plotted in Fig. 17. Aluminum capacitors were prepared using an electrolyte having a pH of 6.5 to 7.0, which gave the highest formation rate as well as a minimum of attack on the film. Current density was  $0.46 \text{ ma/cm}^2$ .

The effect of solution temperature was also studied. Although the formation rate increased with temperature, chemical attack of the anodized film also increased. A compromise temperature of  $20^\circ\text{C}$  was adopted.

2. Tantalum. Three different anodizing solutions were tested for the preparation of tantalum capacitors:

- a. A 3 percent boric acid solution adjusted to pH 6.9 with  $\text{NH}_4\text{OH}$ ,
- b. A 3 percent tartaric acid solution adjusted to pH 6.5 with  $\text{NH}_4\text{OH}$ ,
- c. A solution of 17 percent oxalic acid, 33 percent water, and 50 percent ethylene glycol, measuring pH 1.5 as prepared.

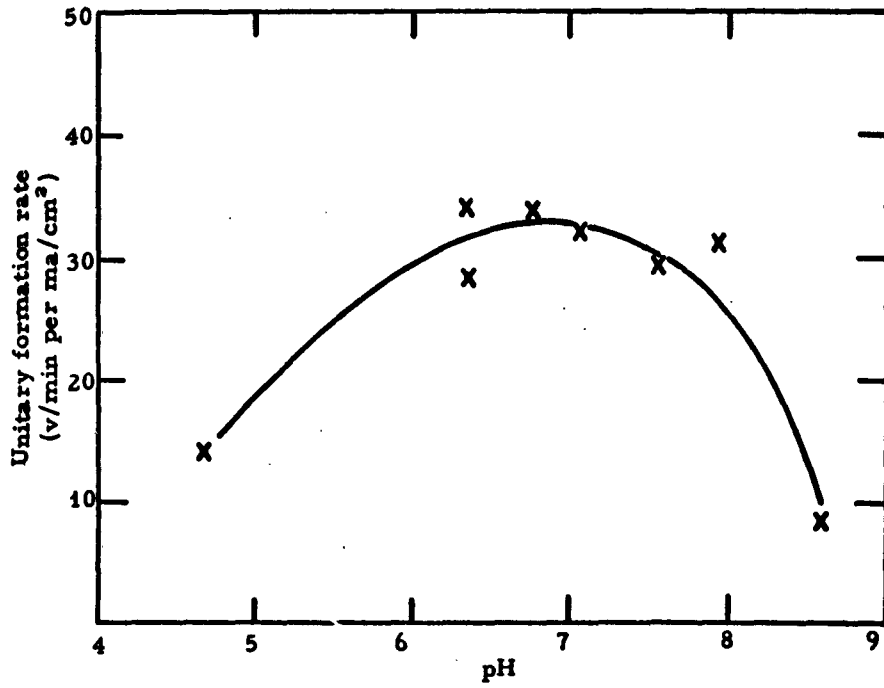


Fig. 17. Effect of pH on the unitary formation rate for aluminum in boric acid-ammonia solutions.

Films were anodized at room temperature at  $0.72 \text{ ma/cm}^2$ . After the selected forming voltage of 60 was reached, the anodization was continued at constant voltage for three hours or until the current had dropped below  $0.7 \mu\text{a/cm}^2$ .

The unitary formation rates at the operating current for the three electrolytes were as follows:

- |                  |                                 |
|------------------|---------------------------------|
| a. Boric         | 26.8 v/min per $\text{ma/cm}^2$ |
| b. Tartaric      | 26.8                            |
| c. Oxalic-glycol | 28.2                            |

The three were therefore considered to be equivalent in this respect. Equivalent values of final current were also observed. The oxalic-glycol solution resulted in capacitors with the highest breakdown voltages and was adopted as the standard solution for tantalum capacitor anodizing.

3. Titanium. A search was made for an electrolytic solution that would result in unblemished anodized titanium films. Solutions based on oxalic, tartaric, and acetic acids yielded poor capacitors or dissolved the films. The following solutions gave better results:

- a. 0.1 M citric acid adjusted to a pH of 4 to 8 with ammonia.
- b. 67 percent 0.1 M citric acid and 33 percent ethylene glycol.

Reproducible results were obtained with the first citric acid solution by anodizing at  $1.04 \text{ ma/cm}^2$  at room temperature. The unitary formation rate was  $15.5 \text{ v/min per ma/cm}^2$ . The lowest final current obtained was  $1.5 \mu\text{a/cm}^2$ .

The effect of pH on the final current density after one hour is shown in Fig. 18. The final current was found to be not critically dependent on pH in the range of 4 to 7.5.

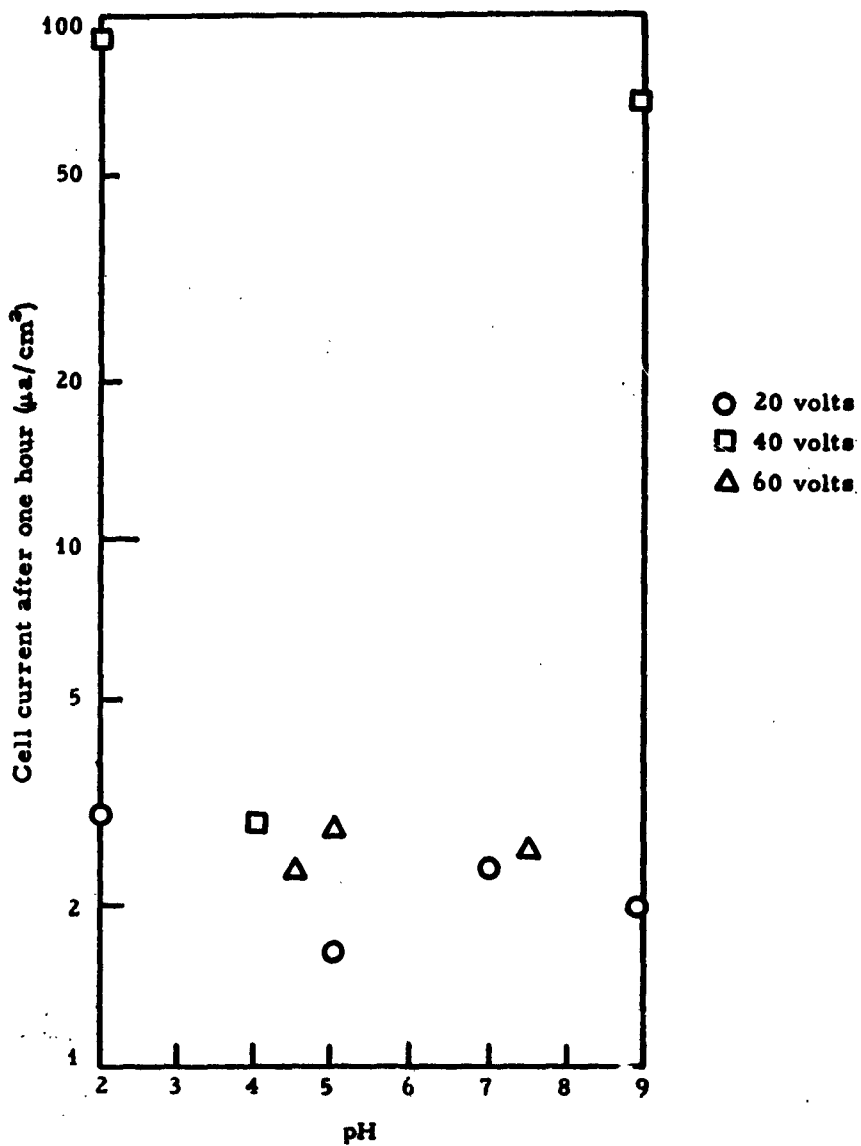


Fig. 18. Cell current density after one hour measured for evaporated titanium in 0.1M citric acid + ammonia solutions of different acidity.

Good results in terms of fairly low final currents and dissipation factors generally below 2 percent were obtained with each of the citric acid solutions by applying 40 volts initially (without a prior constant-current phase). The current initially rose to the limit of the supply, 60 ma/cm<sup>2</sup>, and gas evolved at the anode, as might be expected at a high current.

4. Tungsten. A number of electrolytes were employed in anodizing tungsten films. Included were solutions based on sulphuric acid, lead acetate, phosphoric acid, acetic acid, formic acid and several other acids. Neutral or high pH solutions yielded poor capacitors or dissolved the films, probably the result of increased solubility of tungsten oxide in increasingly alkaline solutions. None of the solutions could be described as satisfactory for obtaining low dissipation factors and reproducible capacitance values.

The effect of pH on the final current density was studied with 1 M solutions of potassium phosphate having the pH adjusted with ammonia. Over the range of pH from 2 to 9, the only reproducible results were obtained with a pH of 4 or less. In all other cases the films broke down or dissolved. Final currents, after periods greater than one hour, ranged from 16 to 32  $\mu$ a/cm<sup>2</sup> for the good films.

The largest group of tungsten capacitors was formed in solutions of from 0.08 to 11 ml of concentrated sulphuric acid in 1000 ml of water. Oxide films formed at 50 volts had a wide range of capacitances and thicknesses, independent of the solution concentration. Interference colors ranged through yellow, magenta and blue. The oxide often had a frosty appearance. Six samples formed in sulfuric acid solutions at temperatures from 4 to 13°C were indistinguishable from samples prepared at room temperature.

5. Zirconium. Two different anodizing solutions were tested for the preparation of zirconium capacitors:

- a. 10 percent ethyl acid phosphate (pH 1.0) or with ammonia added to increase the pH to 2.0, 3.0, 5.2, and 7.0.
- b. 3 percent boric acid (pH 3.0) or with ammonia added to increase the pH to 6.0.

Films were anodized at room temperature at current densities up to  $1.4 \text{ ma/cm}^2$ , or in some cases with the constant voltage of 50 applied initially. Anodization was continued for two to three hours. Final currents as low as  $0.9 \mu\text{a/cm}^2$  were observed for ethyl acid phosphate electrolytes and increased rapidly as the pH was raised. Although somewhat higher final currents were obtained with boric acid, dissipation factors of the resulting capacitors had a lower average value.

Low pH appeared to result in capacitors with high dissipation factors for boric acid solutions. No conclusion could be drawn in this respect for the small number of samples formed in phosphate solutions.

#### 1.1.5 Deposition of Top Electrodes

Top electrodes were applied as soon as possible after anodization of the metallic base film to avoid settling of airborne contaminants. Metal was deposited through a photoengraved spring steel mask by evaporation or, in some earlier work, by sputtering in argon.

##### 1.1.5.1 Materials and Procedure

The final preferred method of forming top electrodes was evaporation of gold from a tungsten filament. The filament, mounted 20 cm above the masked substrates, contained 400 mg of gold wire. Evaporation took place in a vacuum of  $10^{-4}$  Torr or better. The preferred film thickness was 800 Å.

Materials investigated for use as top electrodes were gold, aluminum, tantalum and indium. For aluminum capacitors, top electrodes were of evaporated aluminum. For tantalum capacitors, top electrodes of evaporated gold were found to be preferable to evaporated aluminum and sputtered gold, aluminum and tantalum. Evaporated indium was tested with a few titanium capacitors. For all other capacitors, the top electrode material was evaporated gold.

Sputtering of gold took place at 2 kv with a cathode current density of  $0.3 \text{ ma/cm}^2$  in argon at  $6 \times 10^{-2}$  Torr. Current was carried in 10-second bursts alternating with 30-second cooling periods for a total of 2 minutes on-time, giving a film thickness of 700 A. Sputtering of tantalum took place at 2 kv with current density of  $0.8 \text{ ma/cm}^2$  in argon at  $7.5 \times 10^{-2}$  Torr. Current bursts 40 sec long were alternated with 30-second cooling periods for a total of 8 minutes on-time, giving a film thickness of 2000 A.

Two panels with anodized titanium films were coated by evaporation partly with indium and partly with gold as top electrodes. No significant difference in the capacitors was found.

#### 1.1.5.2 Results and Discussion

Electrical characteristics are presented in Table II for tantalum capacitors prepared with various top electrode materials. All were formed at 60 volts in an oxalic acid - ethylene glycol solution. Evaporated gold demonstrated a superiority in breakdown characteristics which was maintained in subsequent tests. Capacitors with sputtered-gold top electrodes developed substantial leakage above 40 to 45 volts, and consequent heating soon caused them to spark. Capacitors with evaporated-gold top electrodes could be taken up to forming voltage before breaking down suddenly after giving evidence of only small leakage.

TABLE II  
Electrical Characteristics of Tantalum Capacitors  
Having Various Top Electrodes

Top electrode	Number formed	Dissipation factor	Average breakdown voltage (volts)	Breakdown voltage (% of forming voltage)	Shorts before test (%)
Sputtered gold	105	0.0092	49	82	0
Evaporated gold	15	0.0100	60	100	0
Sputtered tantalum	25	0.04 - 0.15	6.4	11	50
Evaporated aluminum	10	0.0100	35	58	0

Capacitors with sputtered tantalum and evaporated aluminum top electrodes were inferior to the gold electrodes.

The thickness of the gold electrodes had little influence on dissipation factor. Tantalum capacitors with gold electrodes sputtered to thicknesses of 200, 800 and 1600 A had identical dissipation. As will be discussed, dissipation occurred principally in the base metal conductor and in the oxide film. A thickness of 800 A was adequate to prevent easy removal by wiping.

1.1.6 Physical Characteristics of Oxide Film

One important value needed to characterize thin-film capacitors is the thickness of the dielectric layer. The thickness of a transparent oxide film over a metal film cannot be measured by ordinary interferometric methods without a knowledge of the index of refraction, and the absorption and phase shift constants of both films. Methods of measuring

oxide-film thickness were developed for special cases, all depending to some degree on interferometric measurements. Tantalum oxide films were measured by two methods and tungsten oxide films by a third.

Surfaces of tantalum and tungsten oxide films were examined by electron microscopy of replicas.

An estimate of the density of the tantalum oxide film was obtained.

#### 1.1.6.1 Determination of Thickness by Total Oxidation

The thickness of a tantalum oxide film formed by anodization at 60 volts was calculated from a measurement of the total thickness of the base metal and the anodized layer and subtracting the estimated thickness of the remaining base metal. This estimate was obtained by completely anodizing a tantalum film of the same thickness (as that above previous to anodization) and computing from the forming voltage required the equivalent metal thickness that was converted to oxide at the lower 60 volts forming voltage.

A number of test panels were prepared with 800-A-thick tantalum films. All but one were anodized at 60 volts in an oxalic acid - ethylene glycol solution. The average total tantalum-tantalum oxide thickness was 1450 A with variations from panel-to-panel of 200 A. Thicknesses were measured by a Zeiss 2006 interference microscope. The remaining sample was then anodized at constant current and the voltage allowed to rise until the tantalum was completely oxidized. At 300 volts the current fell steeply and the interference colors of the oxide film were visible through the glass substrate. Since 300 volts was five times the value of 60 volts used in the partial anodization, it was estimated

that 160 A of the 800 A tantalum film was converted to oxide at 60 volts. Subtracting the thickness of the remaining tantalum from the total thickness of 1450 A, the estimated thickness of an anodized layer formed at 60 volts is 810 A.

#### 1. 1. 6. 2 Determination of Thickness by Wedge Measurement

Another method, suggested by Hass,<sup>2</sup> of measuring thickness of partially oxidized films was applied to tantalum capacitors. The tantalum was deposited with a tapered edge. Anodic oxidation resulted in a uniform layer of oxide blanketing a residual layer of metal whose tapered edge ended abruptly along a line where all of the base metal deposit was oxidized (Fig. 19). A groove was scribed through the gold across this line and the elevation of the oxide film above the substrate was measured interferometrically. Measurements could be made on many of the tantalum capacitors without modification because the sputtering mask produced the necessary taper at the edge of the deposit. This method could also be used to measure the thickness of some of the anodized tungsten films.

The thickness of anodized tantalum formed at 60 volts and measured by this technique was 810 A, which is in close agreement with the calculation derived from total oxidation.

#### 1. 1. 6. 3 Determination of Thickness by Dissolving Oxide

For some materials interferometric measurements of oxide thickness could be made at a step created by stripping the oxide just next to a top gold electrode. Measurement of the step height gave the combined thickness of oxide and gold, from which was subtracted the gold thickness measured at a point where the gold was deposited on glass alone.

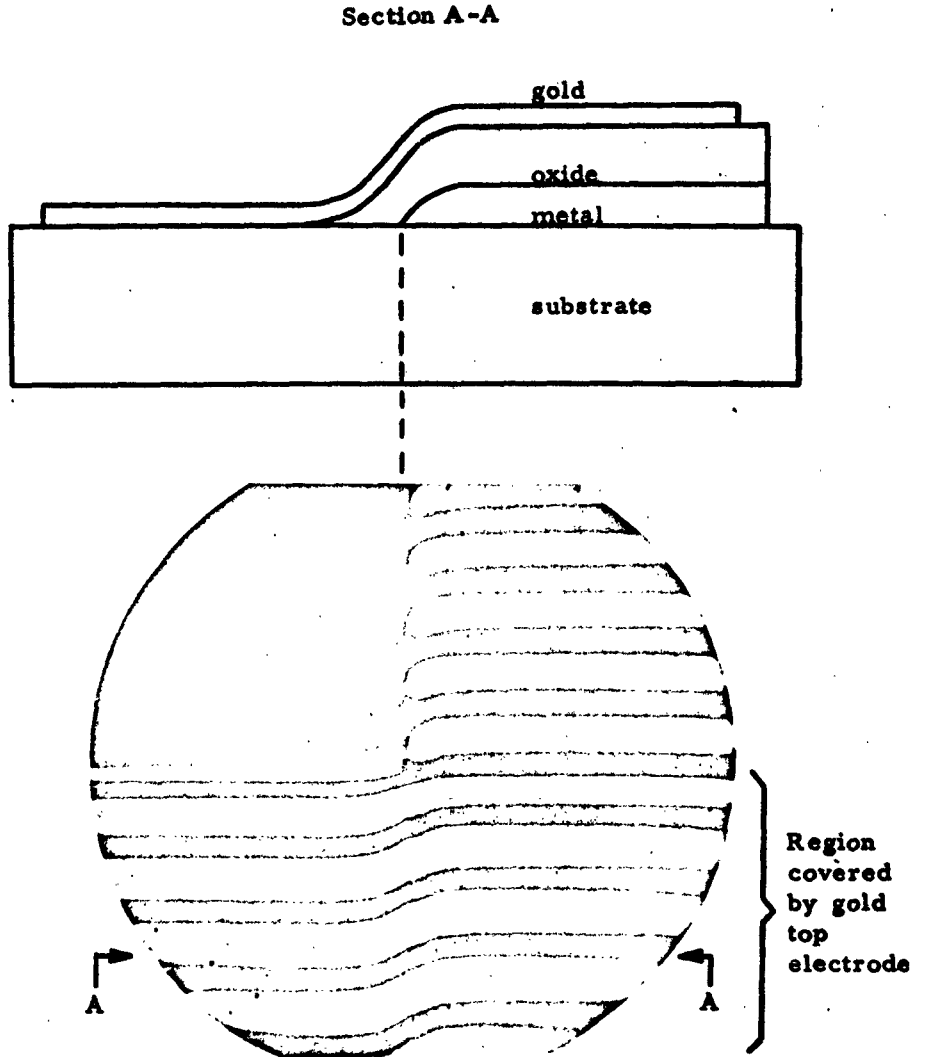


**Fig. 19. Profile of film configuration and interference micrograph used for determination of dielectric layer thickness by the Hass method.**

A number of tungsten capacitors were measured by this method. Tungsten oxide films formed in dilute sulfuric acid could be dissolved readily in 10 percent ammonium hydroxide without affecting the underlying metal. Interference colors followed an order in agreement with the step measurements of thickness and measurements by the Hass wedge method were in general agreement.

#### 1.1.6.4 Electron Micrographs

The surface of an anodically formed tantalum oxide is shown at two magnifications in the electron micrographs of Figs. 20 and 21. Some smoothing of the surface has occurred in comparison with the original metallic surface (Fig. 13). A small number of localized defects are present, although their depth of penetration cannot be determined from the replica micrographs.

The surface of anodically formed tungsten oxide is shown in the micrograph of Fig. 22. In comparison with the original metallic surface (Fig. 15), the oxide has a coarser finish and has developed a number of scattered protrusions. Examination of similar micrographs after the oxide film was stripped indicated that the underlying metal contains craters distributed similarly to the oxide protrusions. This suggests that the protrusions are regions of faster oxide growth.

#### 1.1.6.5 Tantalum Oxide Film Density

An estimate of the density of anodized tantalum films can be made from the thickness data derived from total oxidation (Section 1.1.6.1) and a few additional assumptions. The first assumptions are that the tantalum is anodized to the pentoxide  $Ta_2O_5$  and that the tantalum oxide is not dissolved in the electrolytic solution. We may then write



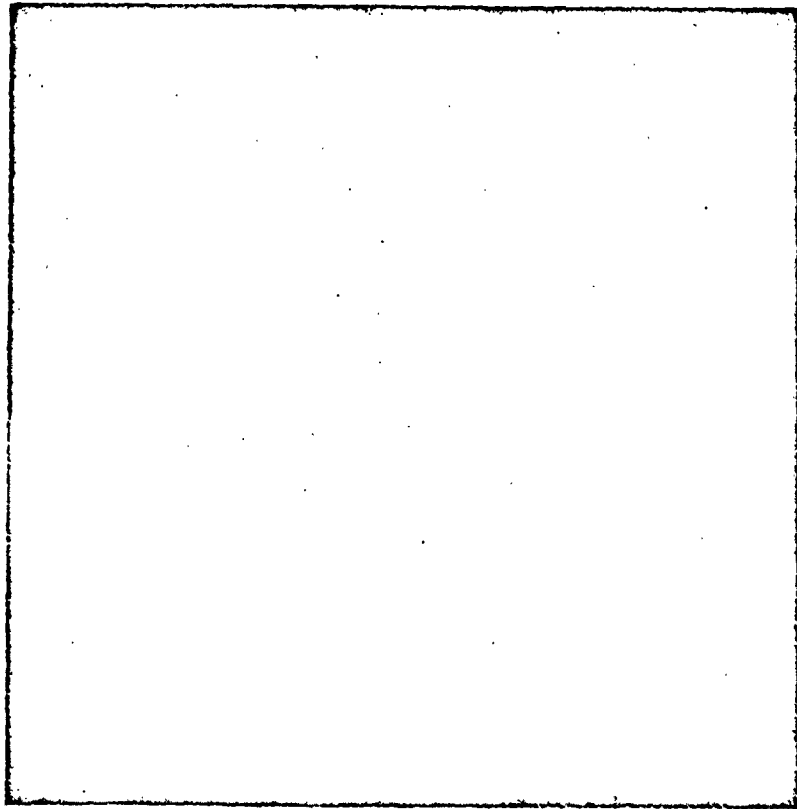
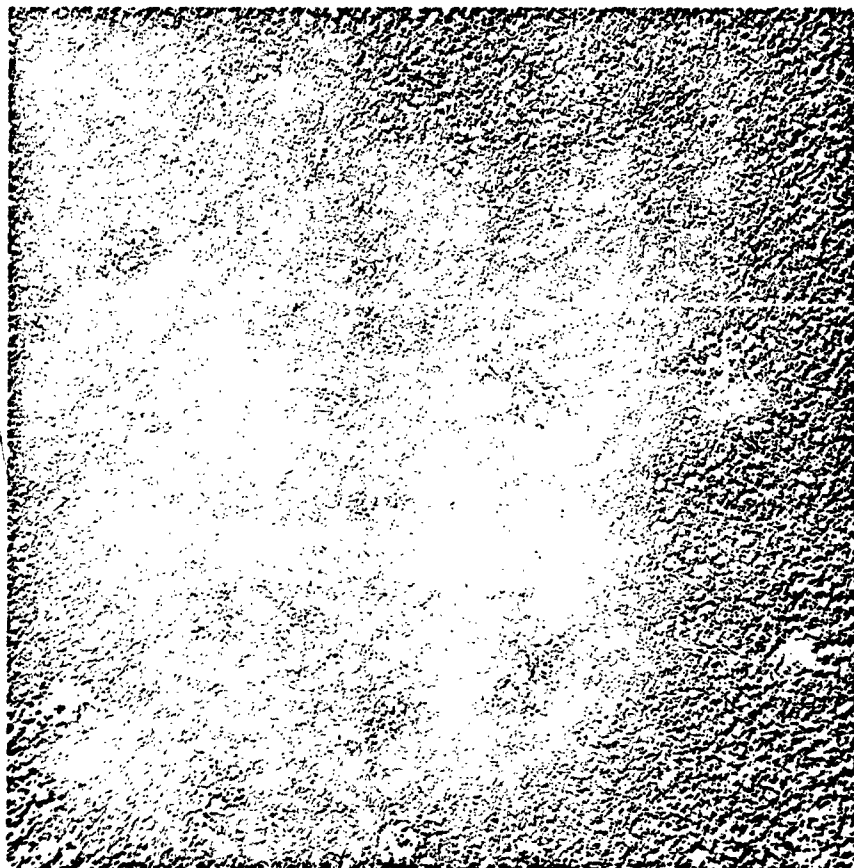


Fig. 21. Electron micrograph of anodized tantalum film (96,000X).



10,000 A

Fig. 22. Electron micrograph of surface of anodized tungsten film (20, 300X).

$$\frac{g_m}{g_o} = \frac{2W_m}{W_o}$$

where  $g_m$  is the mass of tantalum metal converted to the equivalent mass of oxide  $g_o$ ,  $W_m$  is the atomic weight of tantalum, and  $W_o$  is the molecular weight of  $Ta_2O_5$ . Since the areas of the metal and oxide films may be assumed to be the same, the  $g_m/g_o$  ratio is also equal to  $D_m t_m / D_o t_o$  where  $D_m$  and  $t_m$  are the respective density and film thickness. Using the thickness values obtained in Section 1.1.6.1, i.e.,  $t_m = 160 \text{ \AA}$ , and  $t_o = 810 \text{ \AA}$ , and assuming that the tantalum film density is the bulk density of 16.6 g/cc, we obtain

$$D_o = \frac{t_m W_o D_m}{2 t_o W_m} = 4.0 \text{ g/cc.}$$

Since this value is 46% of the density of bulk  $Ta_2O_5$ , 8.7 g/cc, it is inferred that the anodized film is either porous or hydrated.

#### 1.1.7 Electrical Measurements

Electrical measurements were designed to characterize the films as fully as possible and to provide a basis for comparison with the objectives specified in the contract:

1. Minimum capacitance for 50 volt formation:  $0.31 \mu\text{f}/\text{cm}^2$  ( $2\mu\text{f}/\text{in.}^2$ ).
2. Maximum dissipation factor at 1 kc: 0.05.
3. Minimum insulation resistance at 75% of forming voltage: 1000 ohm-farads.
4. Operating range: -55 to 125°C.
5. Maximum temperature coefficient of capacitance over the operating range:  $\pm 250 \text{ ppm}/^\circ\text{C}$ .

#### 1.1.7.1 Apparatus and Procedures

Tests made on capacitors included examination for initial short circuits and measurement of capacitance, dissipation factor, breakdown voltage and leakage current as a function of applied voltage. A brief description of the apparatus and procedures used in these tests is given in this section. The apparatus for short-circuit and breakdown testing is described in Appendix I.

Examination for initial short circuits was made by gradually applying an ac voltage at a frequency of 1 kc from a high-impedance source until peak-to-peak supply voltage reached 4 volts. If the capacitor voltage failed to approach 4, as indicated on an oscilloscope, constructive clearing was attempted by repeatedly discharging a 1- $\mu$ f capacitor into the film capacitor after charging to successively higher voltages. This process often cleared short circuits by melting back the top electrode in the vicinity of the short.

Capacitance and dissipation factor were measured with a General Radio 1650-A impedance bridge. The standard frequency was 1 kc. Additional tests were made with the bridge at other frequencies through use of external oscillators, a null detector, and a decade resistor box as described in Appendix II.

Breakdown voltage was measured by applying a gradually increasing dc voltage to the capacitor through a high resistance and comparing the supply and capacitor voltages as indicated by dual oscilloscope traces. Sparking without permanent breakdown sometimes occurred. A procedure for constructive clearing could often be followed, in which the voltage was slowly increased while repeated sparking took place and weak spots in the film were gradually eliminated. Some capacitors

developed substantial leakage before breaking down. For this type, the voltage was recorded at which leakage current exceeded a specified amount, for example,  $2 \mu\text{a}$ , as indicated by the oscilloscope.

Leakage current was measured with a Keithley 610A electrometer. A calibrated voltage was applied to the capacitor through the electrometer. Current was allowed to stabilize for two minutes at each voltage setting.

Testing at temperatures other than room temperature was carried out with the capacitors in a Wyle C106-640 temperature test chamber.

#### 1.1.7.2 Results

Results of electrical measurements on capacitors formed with films of aluminum, tantalum, titanium, tungsten and zirconium are presented individually for each metal.

1. Aluminum. The inverse of capacitance per unit area is plotted against forming voltage in Fig. 23. Capacitance per unit area at 50 volts, derived from the straight line plot, was  $0.088 \mu\text{f}/\text{cm}^2$  ( $0.57 \mu\text{f}/\text{in.}^2$ ). Considerable spread appeared in the data for different samples, most of which were constructed before procedures were standardized. These samples were anodized in solutions of boric acid and ammonia at pH 5.5 to 7.9 and had final anodizing currents no greater than  $3.1 \mu\text{a}/\text{cm}^2$ . The capacitance-formation voltage product, derived from the curve, was  $4.4 \mu\text{f}\cdot\text{v}/\text{cm}^2$  ( $28.5 \mu\text{f}\cdot\text{v}/\text{in.}^2$ ).

The effect of ambient temperature on capacitance of an aluminum capacitor at 1 kc is shown in Fig. 24. Capacitance increased almost linearly with temperature, giving a temperature coefficient of 539 parts per million per  $^{\circ}\text{C}$ .

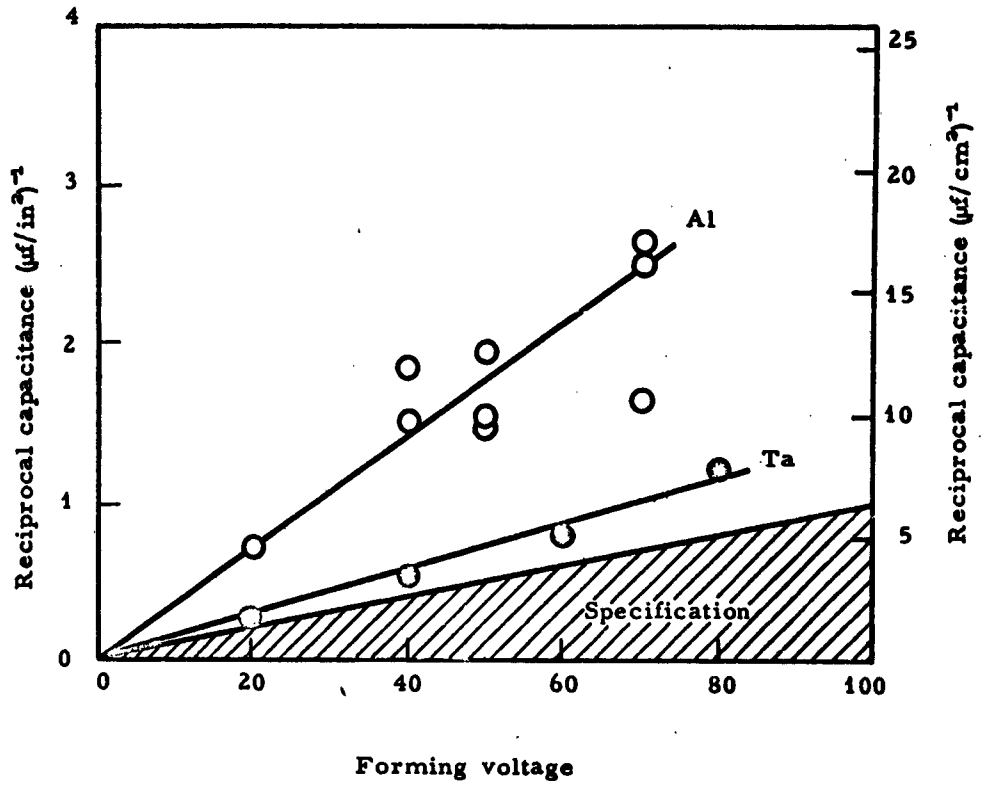


Fig. 23. Reciprocal of capacitance per unit area as a function of forming voltage for aluminum and tantalum capacitors, compared with the contract specification.

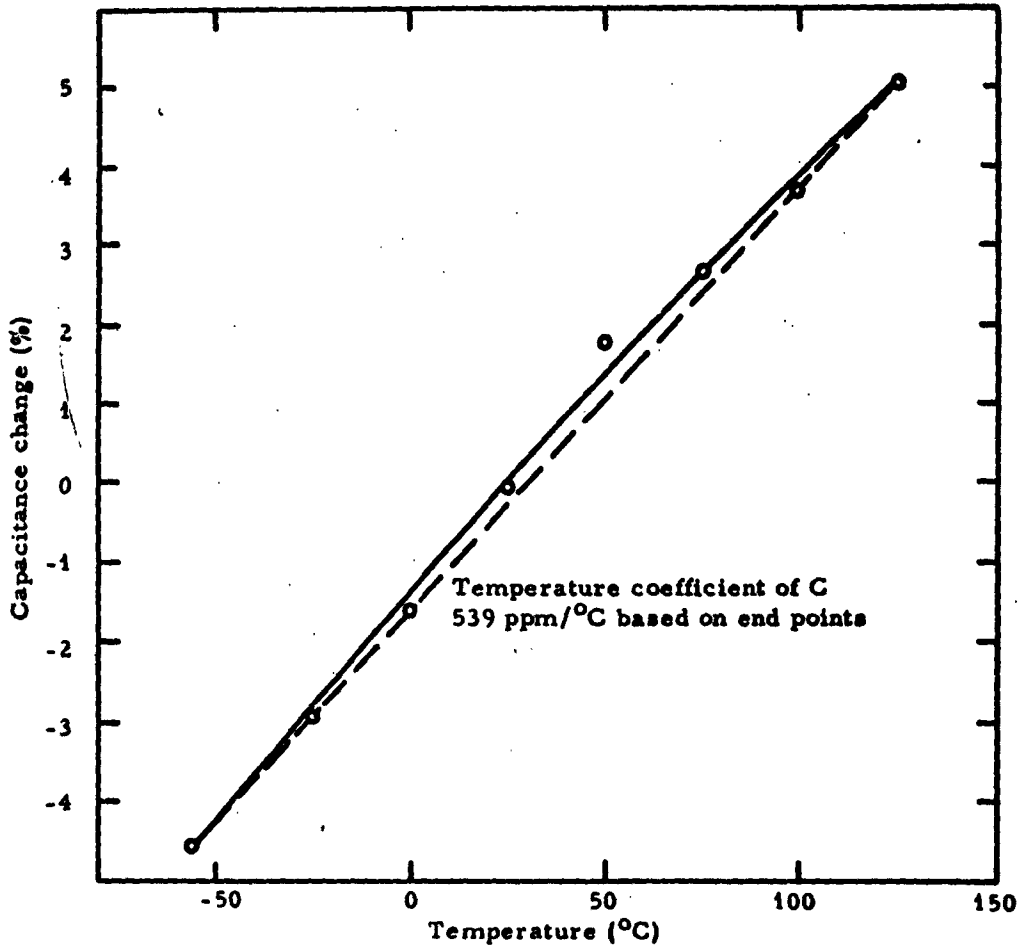


Fig. 24. Percentage capacitance change at 1 kc relative to room temperature value as a function of temperature for an aluminum capacitor.

Dissipation factors ranged from 0.005 to 0.01 for aluminum capacitors at 1 kc.

Breakdown voltage generally ranged between 80 and 96 percent of the forming voltage.

The leakage current of an aluminum capacitor that withstood at least 80 percent of the forming voltage is plotted as a function of applied voltage in Fig. 25. The reverse current was considerably larger than the current in the forward (anodization) direction. The apparent resistance as a function of voltage application time was derived from measurements of leakage current at a fixed voltage; an example is shown in Fig. 26.

The insulation resistance determined from leakage current at 75% of forming voltage was 1450 ohm-farads.

2. Tantalum. The inverse of capacitance per unit area is plotted against forming voltage in Fig. 23. Capacitance per unit area at 50 volts was  $0.22 \mu\text{f}/\text{cm}^2$  ( $1.43 \mu\text{f}/\text{in.}^2$ ). (Different electrolytes modify this capacitance value by approximately 20 percent.) These samples were anodized in solutions of boric acid and ammonia at pH 7.6 and had final anodizing currents no greater than  $3.1 \mu\text{a}/\text{cm}^2$ . The capacitance-formation voltage product, averaged over a large number of capacitors formed at 60 volts, was  $13.6 \mu\text{f}\cdot\text{v}/\text{cm}^2$  ( $88 \mu\text{f}\cdot\text{v}/\text{in.}^2$ ). This value compares favorably with values of 6.7 to  $12.4 \mu\text{f}\cdot\text{v}/\text{cm}^2$  (43 to  $80 \mu\text{f}\cdot\text{v}/\text{in.}^2$ ) reported in the literature.<sup>3</sup>

Uniformity of capacitance was compared among 92 panels constructed with only minor processing differences. Six panels were rejected for masking flaws. A probability plot for the center capacitors

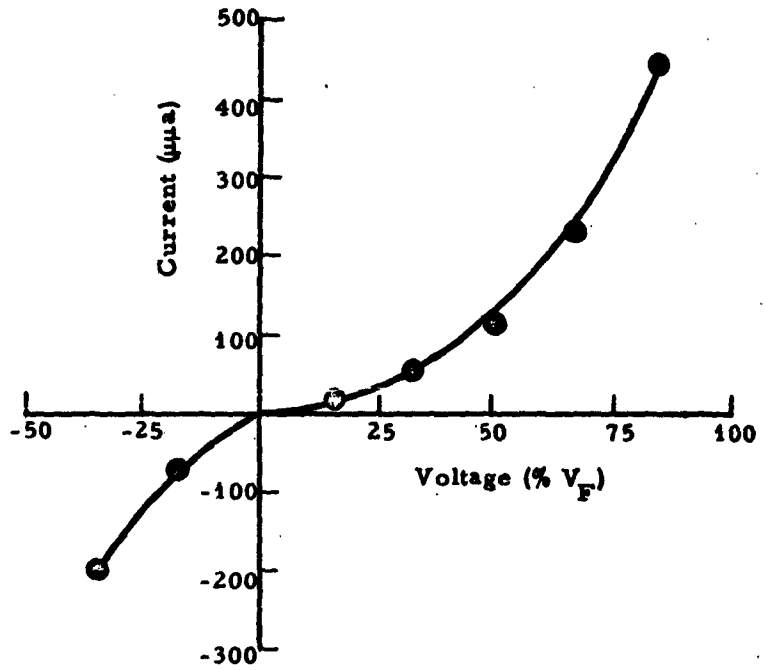


Fig. 25. Leakage current as a function of applied voltage expressed in % of forming voltage for an aluminum capacitor formed at 60 volts.

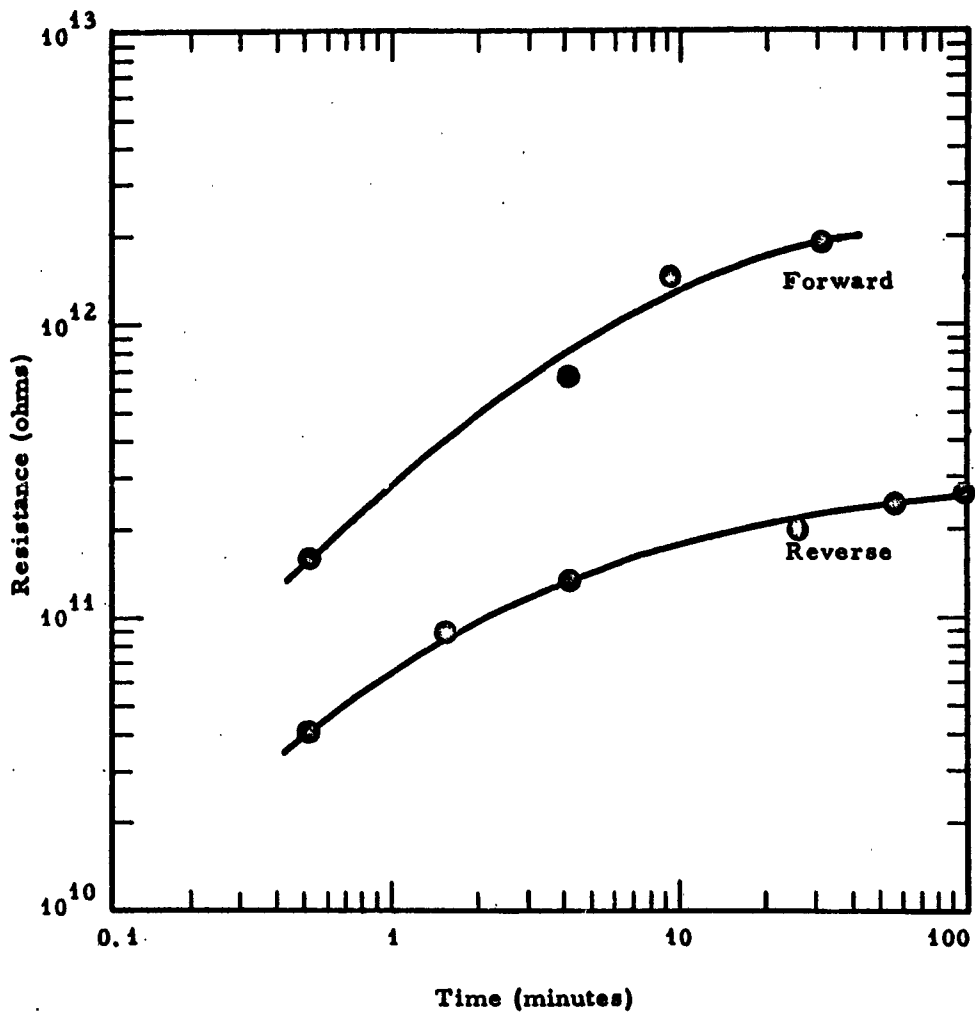


Fig. 26. Apparent resistance as a function of time of voltage application at forward (anodization) and reverse polarities for an aluminum capacitor at 8 volts; forming voltage was 60 v.

of the remaining 86 panels, Fig. 27, shows a mean capacitance of 0.0423  $\mu\text{f}$  with a standard deviation of 0.0012 or 2.8 percent.

The effect of ambient temperature on the capacitance of a tantalum capacitor at 1 kc is shown in Fig. 28. Capacitance rose in a slightly sublinear fashion with temperature over the range of  $-60$  to  $125^{\circ}\text{C}$ . The temperature coefficient computed from the end points was 222 parts per million per  $^{\circ}\text{C}$ .

The effect of frequency on capacitance is shown in Fig. 29. The percentage change in capacitance relative to room temperature value at 1 kc is plotted at  $-55$ ,  $25$ , and  $125^{\circ}\text{C}$  over a frequency range of 0.1 to 100 kc. Between 0.1 and 10 kc the capacitance change was 2 percent of the 1-kc value. Between 10 and 100 kc the capacitance decreased by not more than 6 percent of the 1-kc value.

The dissipation factor for tantalum capacitors (formed at 60 volts) at 1 kc was approximately 0.01. The capacitor nearest the base electrode contact on a test panel typically had only half the dissipation of the capacitor farthest away on the panel; consequently the contribution of the base electrode resistance to dissipation had to be considered. An equivalent circuit for a capacitor being tested at a fixed frequency is shown in Fig. 30. Dissipation factor for this circuit is given by

$$D = \frac{R_s}{X} + \frac{X}{R_p}, \text{ where } X = 1/2\pi fC.$$

In this equation the series resistance  $R_s$  of the base and top electrodes is seen to account for one part of the dissipation and the parallel resistance,  $R_p$ , of the oxide accounts for the other part.

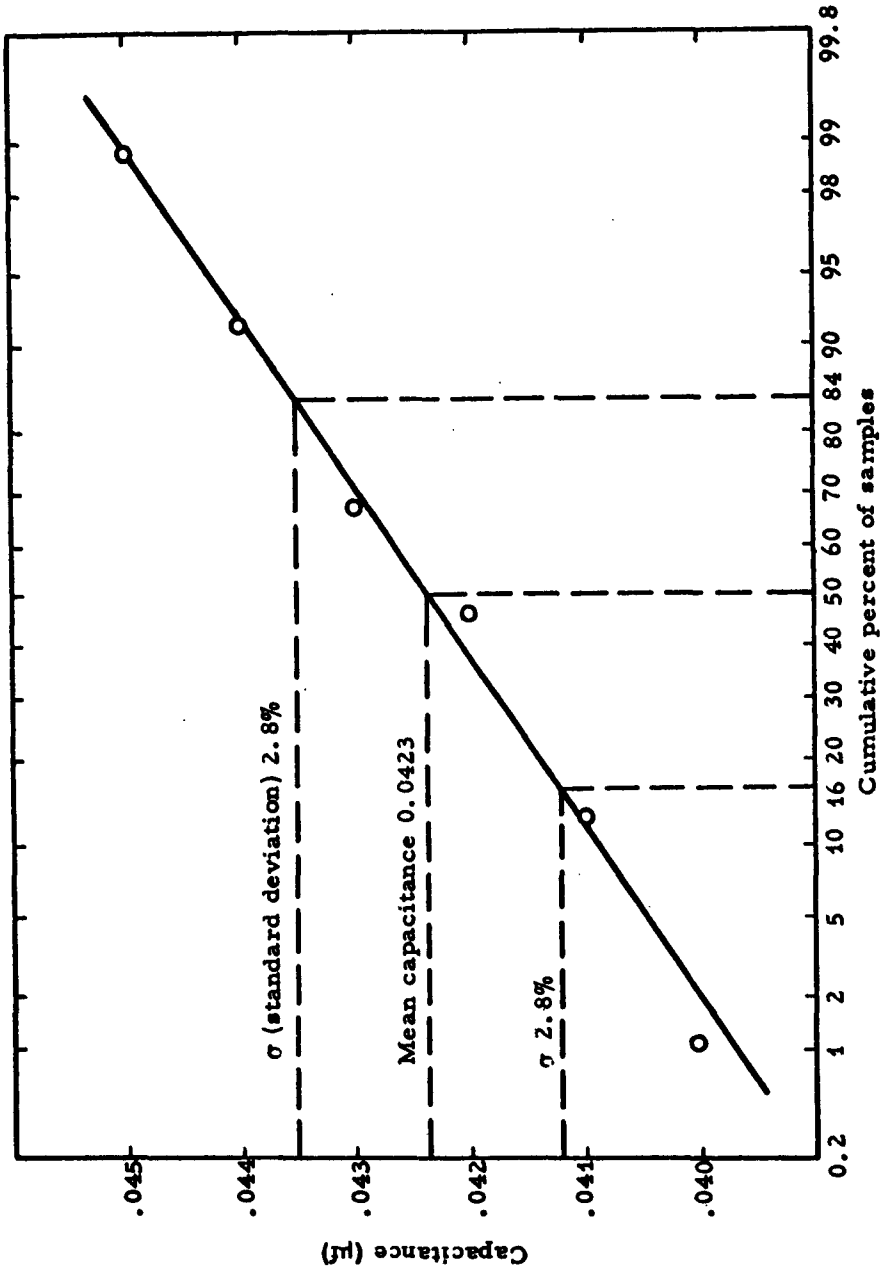


Fig. 27. Uniformity of capacitance for 86 tantalum panels; capacitors 1/4 inch x 1/8 inch, formed at 60 volts.

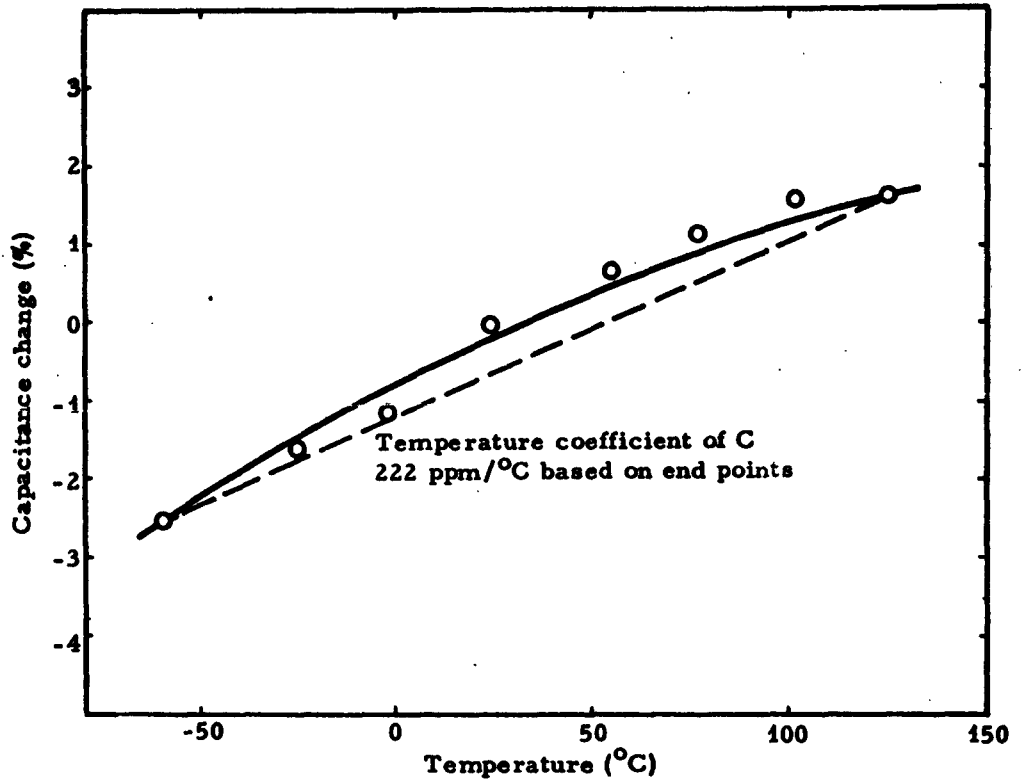


Fig. 28. Percentage capacitance change at 1 kc relative to room temperature value as a function of temperature for a tantalum capacitor.

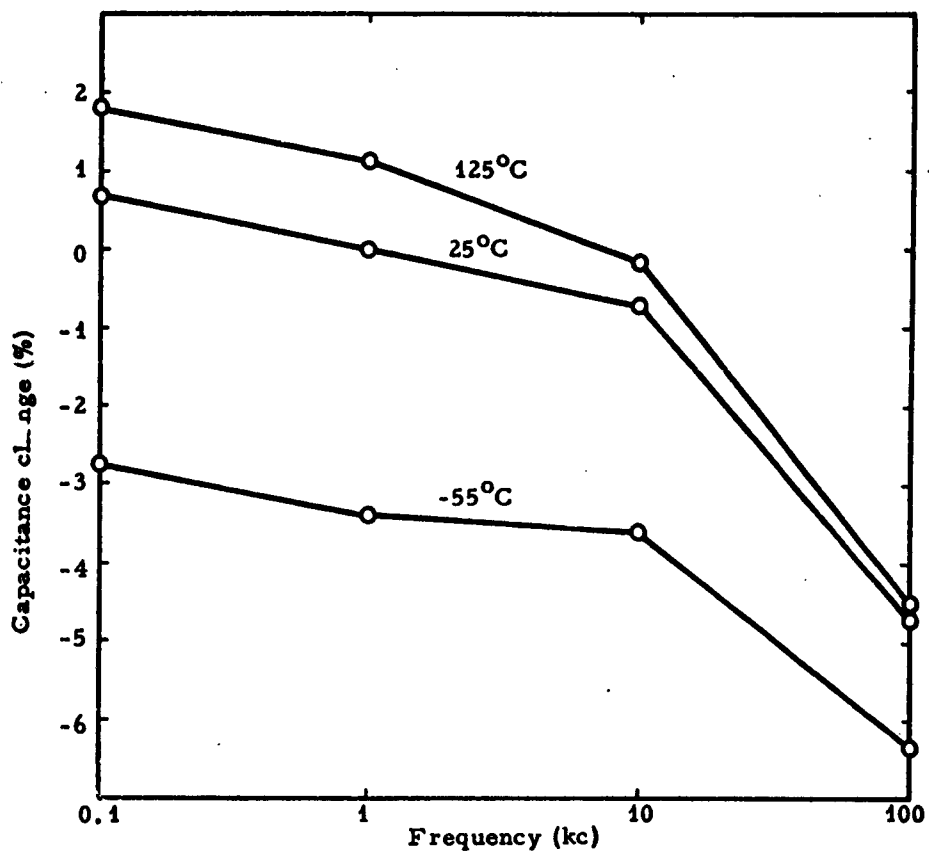


Fig. 29. Percentage change in capacitance of a tantalum capacitor relative to room-temperature value at 1 kc, as a function of frequency, with temperature as the parameter.

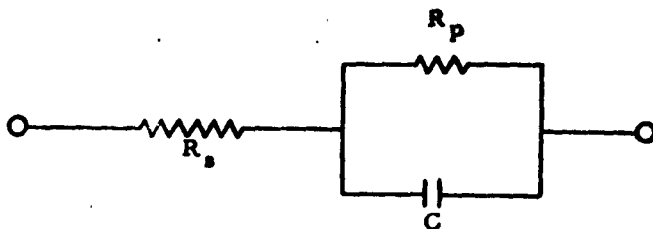


Fig. 30. Equivalent circuit of a single capacitor.

The series resistance of the electrodes was measured for each of the five capacitors on a panel by breaking down the capacitors in turn and shorting them completely with silver paint. As indicated in Section 1.1.6.2, the gold electrodes contributed little to the resistance. The separate contributions of the electrodes and the oxide were calculated by substituting values of  $D$ ,  $R_s$ , and  $C$ , all measured at 1 kc.

Dissipation values are listed in Table III for a typical tantalum capacitor and for capacitors having thinner and thicker base electrode layers (previous to anodization at 60 volts). The values of  $R_s/X$  are clearly a function of base film thickness and of distance to the contact area. Two conclusions were drawn from these data and were borne out by further experiments. First, the resistance of the underlying metal layer in this range of thickness accounted for a major portion of the dissipation of tantalum capacitors. Second, dissipation of the oxide layer increased with base metal thickness. A probable explanation for this lies in the influence of greater stresses to be found in a thicker film on the formation of the anodized layer. In any event, a compromise must be reached in base metal thickness to obtain the lowest dissipation factor.

TABLE III

Contributions of Base and Oxide Film Resistances  
to the Dissipation Factor of Tantalum Capacitors  
Measured at 1 kc.

Base Film Thickness	Capacitor	C (μf)	D	$R_s/X$ (Base)	$X/R_p$ (Oxide)
800 A (Normal)	1	.0488	.0074	.0043	.0031
	2	.0485	.0088	.0049	.0039
	3	.0487	.0098	.0067	.0031
	4	.0483	.0117	.0094	.0023
	5	.0483	.0132	.0109	.0023
	Mean	.0485	.0102	.0072	.0029
270 A (Thin)	1	.0421	.0082	.0048	.0034
	2	.0413	.0103	.0067	.0036
	3	.0412	.0124	.0104	.0020
	4	.0405	.0150	.0129	.0021
	5	.0414	.0200	.0166	.0034
	Mean	.0413	.0132	.0103	.0029
1500 A (Thick)	1	.0448	.0062	.0023	.0039
	2	.0446	.0076	.0031	.0045
	3	.0443	.0080	.0033	.0047
	4	.0432	.0092	.0049	.0043
	5	.0432	.0097	.0051	.0046
	Mean	.0440	.0081	.0037	.0045

The effect of ambient temperature on the dissipation factor of a tantalum capacitor at 1 kc is shown in Fig. 31. Dissipation increased linearly with temperature and had a temperature coefficient of 2970 ppm per °C.

The effect of frequency on dissipation factor is shown in Fig. 32. Values are plotted for temperatures of -55, 25 and 125°C over a frequency range of 0.1 to 100 kc. At high frequencies, the capacitive reactance becomes so small that the term  $X/R_p$  is an insignificant part of the dissipation factor. There remains the contribution of the series resistance of the base electrode  $R_s/X$ , which is proportional to frequency. Therefore each curve approaches a line of 45° slope on this plot at high frequency. At low frequencies, the decrease of one term tends to balance the increase of the other.

At low frequencies, the dissipation curves of Fig. 32 show that lowering the temperature substantially decreased dissipation. It was also observed that immersing the capacitor in liquid nitrogen permitted operation at higher voltage before sparking set in. Since temperature had little effect at high frequencies, where the resistance  $R_s$  of the base electrode dominated the dissipation, it may be deduced that the effect of low temperature was to increase the resistance  $R_p$  of the oxide.

The breakdown voltage of tantalum capacitors was improved to the point where it was equal to or greater than the forming voltage. Capacitors were generally subjected to voltages no greater than the forming voltage to avoid destruction.

The leakage current of a tantalum capacitor as a function of applied voltage is plotted in Fig. 33 in both forward (anodization) and reverse directions. The two curves rise with voltage in the same manner, but the voltage is 20 to 50 percent higher in the forward direction for a given current. Current is linear with voltage below approximately 8 volts.

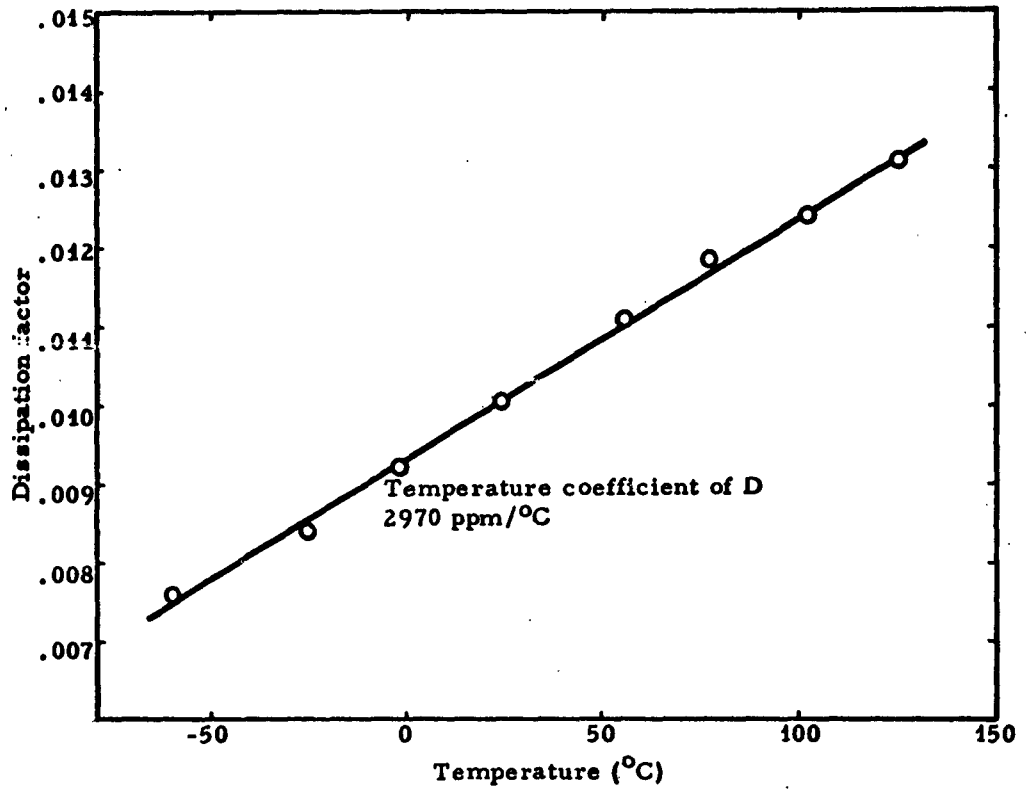


Fig. 31. Dissipation factor of a tantalum capacitor at 1 kc as a function of temperature.

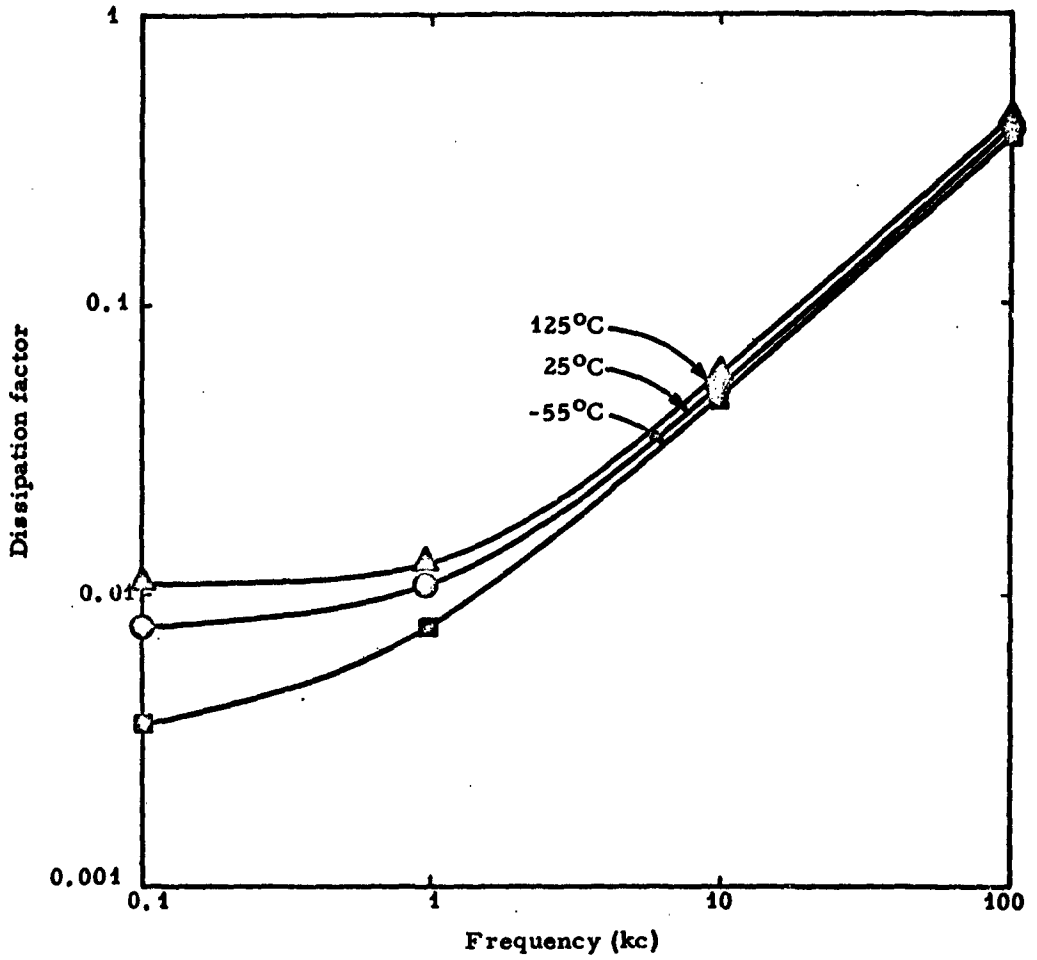


Fig. 32. Dissipation factor of a tantalum capacitor as a function of frequency, with temperature a parameter.

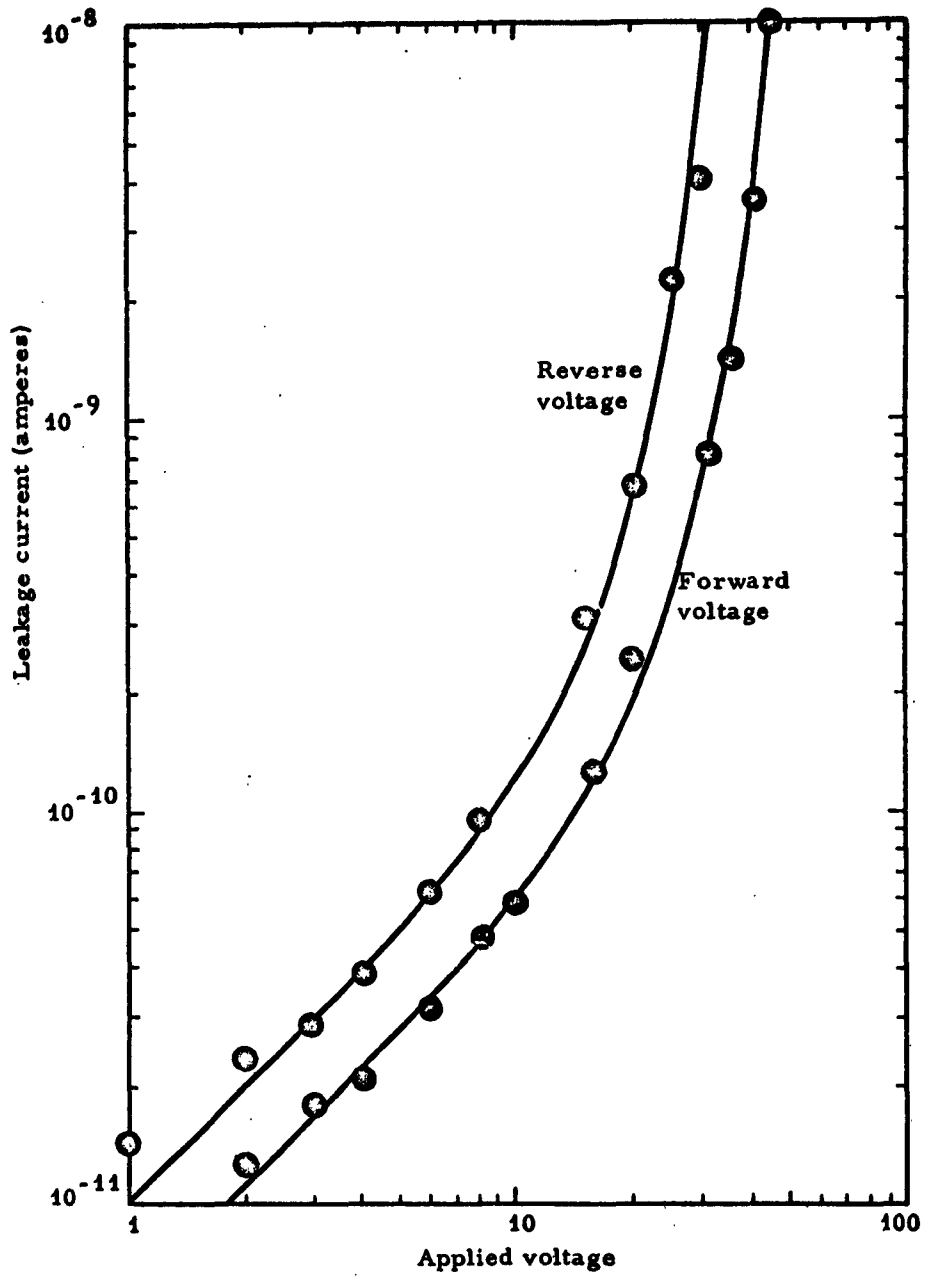


Fig. 33. Leakage current at 25°C as a function of applied voltage in forward (anodization) and reverse directions, for a tantalum capacitor anodized at 60 volts.

The leakage current as a function of applied voltage at different temperatures is plotted in Fig. 34. In this example the low-voltage values of current increased by a factor of 10 when the temperature was raised to 125°C. After returning to room temperature the current was found to be lower than its original value by a factor of 13. Reduction of temperature to -55°C produced a further reduction of current measured at low voltage. The current at voltages above 40 was little influenced by temperature, except at high temperatures.

The insulation resistance of tantalum capacitors at room temperature, determined from leakage current measured at 75 percent of forming voltage, was as high as 400 ohm-farads. Below 17 percent of forming voltage, it exceeded 1000 ohm-farads.

The dielectric constant, estimated from the capacitance and the oxide thickness value of 810 Å, was 21. This figure compares favorably with the values given in Refs. 4 and 6.

3. Titanium. The inverse of capacitance per unit area is plotted against forming voltage in Fig. 35 for titanium anodized in citric acid and ammonia. Capacitance per unit area at 50 volts, as derived from the straight line, was 0.15  $\mu\text{f}/\text{cm}^2$  (0.94  $\mu\text{f}/\text{in.}^2$ ). Exceptionally high capacitance was observed for a few titanium capacitors, which also had unusually large dissipation factors and were excluded in determining the capacitance-voltage relationship. The capacitance-formation voltage product, derived from the curve, was 7.5  $\mu\text{f}\cdot\text{v}/\text{cm}^2$  (47.0  $\mu\text{f}\cdot\text{v}/\text{in.}^2$ ).

The capacitance per unit area of the units formed at a constant voltage of 40, without a prior period at constant current, fitted the straight line of Fig. 35 in the case of a citric acid - glycol electrolyte and was slightly smaller than that for citric acid - ammonia.

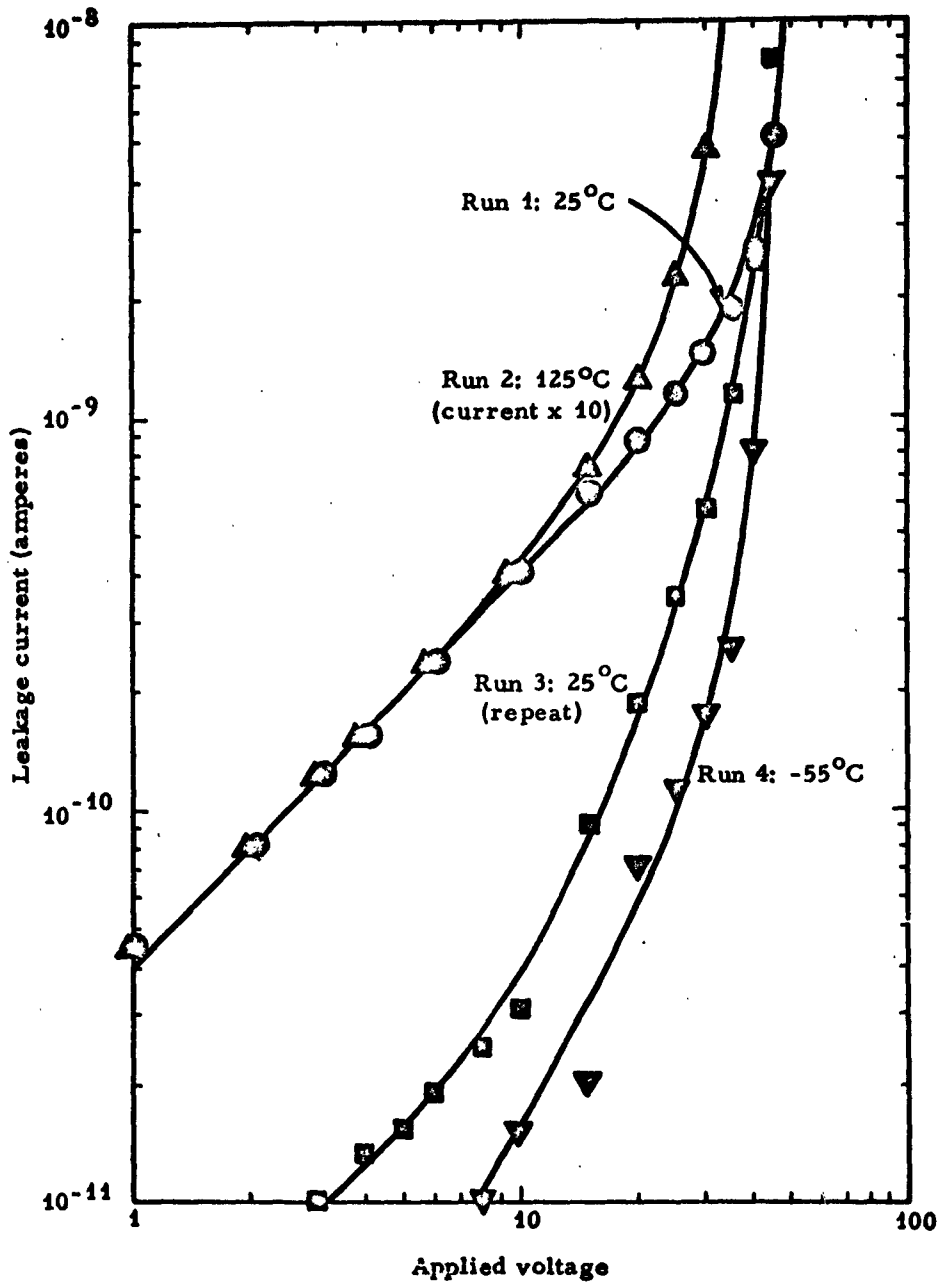


Fig. 34. Leakage current as a function of applied voltage, with temperature a parameter, for a tantalum capacitor anodized at 60 volts.

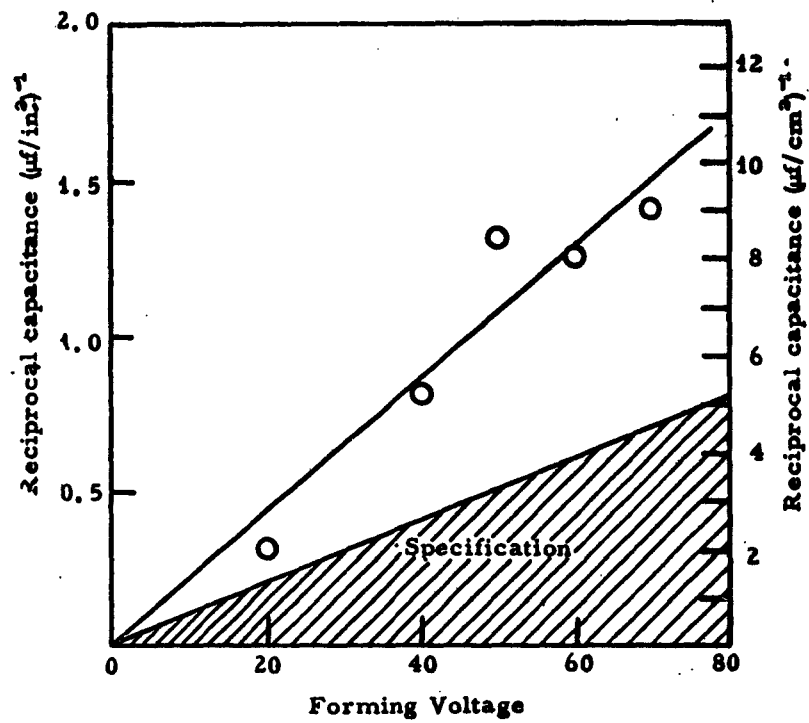


Fig. 35. Reciprocal of capacitance per unit area as a function of forming voltage for titanium capacitors.

After standing for several days, some titanium capacitors showed increased capacitance and dissipation. A number of these were heated in oxygen at 125°C. The capacitance, which had increased by over 50 percent, returned to its original value as a result of this treatment. The dissipation factor fell below its original value. After standing for several days more, the capacitors showed only slight increases in capacitance and dissipation. When other capacitors were heated in oxygen at 200°C, they became short-circuited within one-half hour. A mild heat treatment in oxygen shows promise as a method of stabilizing titanium capacitors. Similar results have been reported elsewhere.<sup>5</sup>

The dissipation factor of titanium capacitors anodized in citric acid - ammonia solutions averaged 0.029. Lower values were obtained by anodizing at constant voltage alone. The dissipation factor of capacitors anodized at constant voltage in citric acid - ethylene glycol solutions averaged 0.018.

The breakdown voltage of titanium capacitors was low and erratic and it was usually preceded by a large leakage current. The leakage current generally increased to the point of destruction if the applied voltage was held sufficiently high to give an initial current of one or two microamperes.

The leakage current of a titanium capacitor as a function of applied voltage is plotted in Fig. 36. With voltage in the forward (anodization) direction, this capacitor had a relatively high resistance over a range of several volts and then became highly conductive at 5 volts.

4. Tungsten. A scatter diagram of capacitance vs dissipation factor, together with their numerical distributions, is presented in Fig. 37 for tungsten capacitors anodized in sulfuric acid at 50 volts.

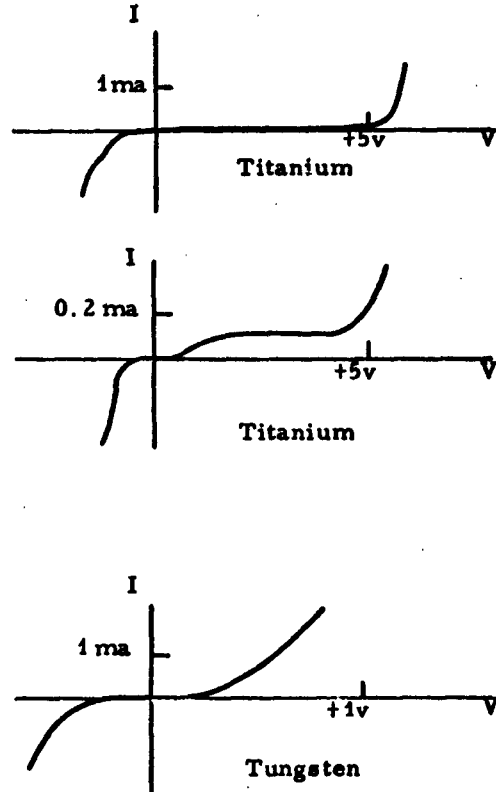


Fig. 36. Current-voltage characteristics for titanium and tungsten thin-film capacitors having high leakage. Indicated polarity of the voltage applies to the forward (anodization) direction.

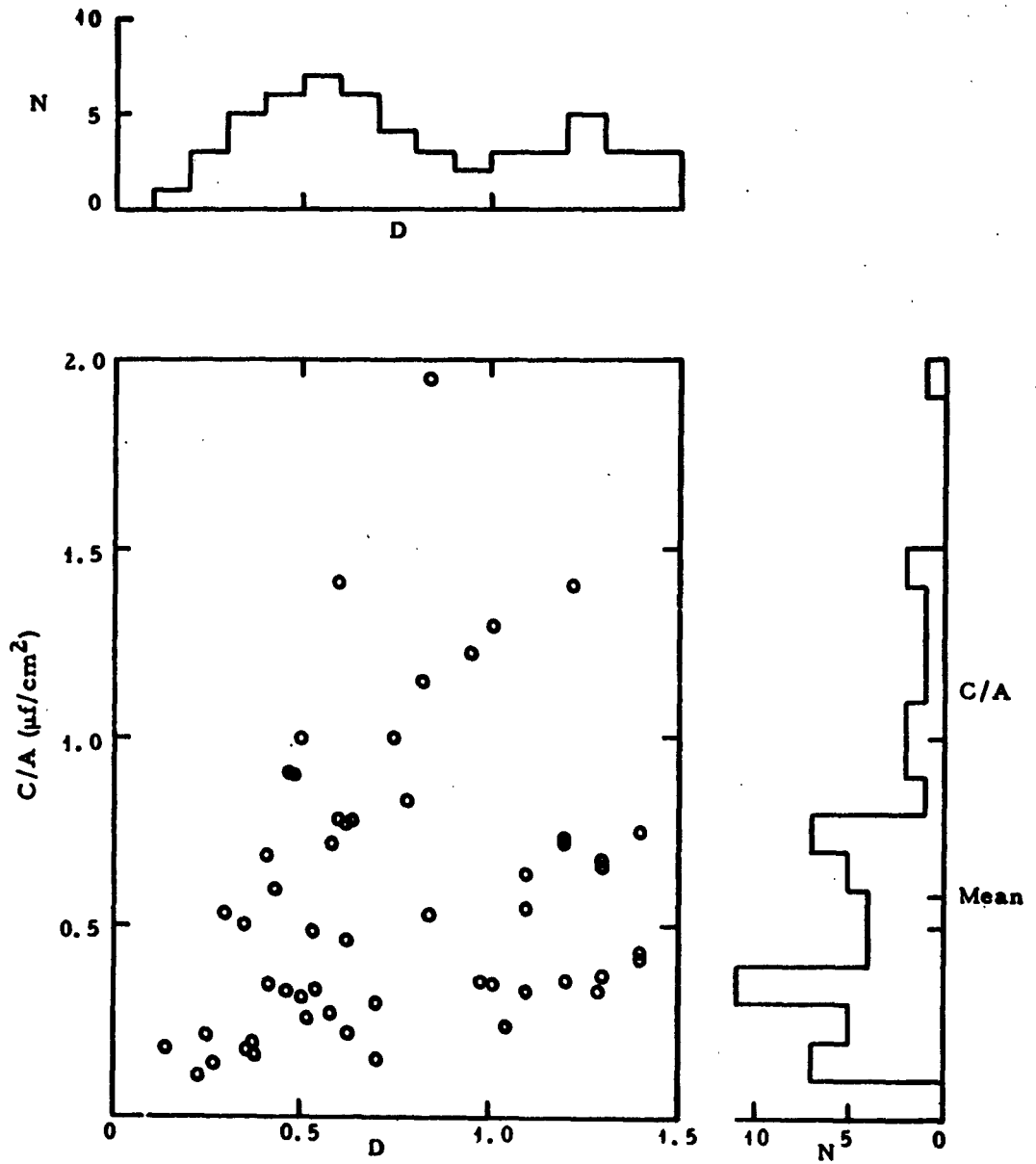


Fig. 37. Capacitance per unit area vs dissipation factor, and their numerical distributions for tungsten anodized in sulfuric acid at 50 volts.

TABLE IV

Average Capacitances and Dissipation Factors for Tungsten Capacitors Anodized in  $H_2SO_4$  at Different Forming Voltages

No. of panels	Forming voltage (volts)	Average capacitance ( $\mu f/cm^2$ )	Average D
7	30	0.350	0.26
54	50	0.59	0.76
14	60	0.27	0.46

Such plots for 30 and 60 volts showed similar scattering. Average capacitances and dissipation factors are given in Table IV. Other electrolytes produced similar wide spreads and large dissipations. From the data on anodization in sulfuric acid at 50 volts, giving capacitance per unit area of  $0.59 \mu f/cm^2$  ( $3.8 \mu f/in.^2$ ), the capacitance-formation voltage product was determined to be  $29.5 \mu f \cdot v/cm^2$  ( $190 \mu f \cdot v/in.^2$ ).

Capacitance per unit area and dissipation factor, measured over a period of days, are listed in Table V together with oxide thickness data for a group of tungsten capacitors formed at 50 volts in sulfuric acid solutions. From these data the inverse capacitance is plotted against thickness in Fig. 38 for films in three age ranges. Inverse capacitance generally decreased with time, tending to settle toward a line which intercepted the thickness axis at 1370 A. Three of the original values were near a line parallel to this one and passing through the origin. Such a line would represent capacitors whose oxide thickness is inversely proportional to their capacitance. The displacement of the line representing

TABLE V  
Properties of Tungsten Capacitors Anodized in Sulfuric Acid Electrolyte at 50 Volts

Sample No.	Oxide color	Oxide thickness (Å)	C/A ( $\mu\text{f}/\text{cm}^2$ )	$C/A^2$ ( $\mu\text{f}/\text{cm}^2$ ) <sup>-1</sup>	D	Age (days)
902	Yellow-green	1620	1.22	.82	.95	3
			1.51	.67	.70	19
			1.29	.78	1.67	74
881	Yellow	1755	.64	1.56	1.10	1
			.40	2.50	.58	27
			.39	2.56	.64	82
889	Yellow	1755	.32	3.12	.50	1
			.41	2.44	.81	18
			.44	2.28	.69	78
891	Yellow	1890	.67	1.49	1.30	1
			.94	1.06	.83	18
			.85	1.18	.71	78
880	Yellow-orange	2160	.22	4.54	.63	1
			.49	2.04	.90	26
			.50	2.00	.85	82
875	Magenta	2295	.42	2.38	1.40	1
872	Magenta	2430	.18	5.45	.36	1
			.32	3.12	.63	24
			.32	3.12	.63	84
945	Blue	2700	.34	2.94	1.20	2
			.34	2.94	1.20	8
			.36	2.78	1.20	63

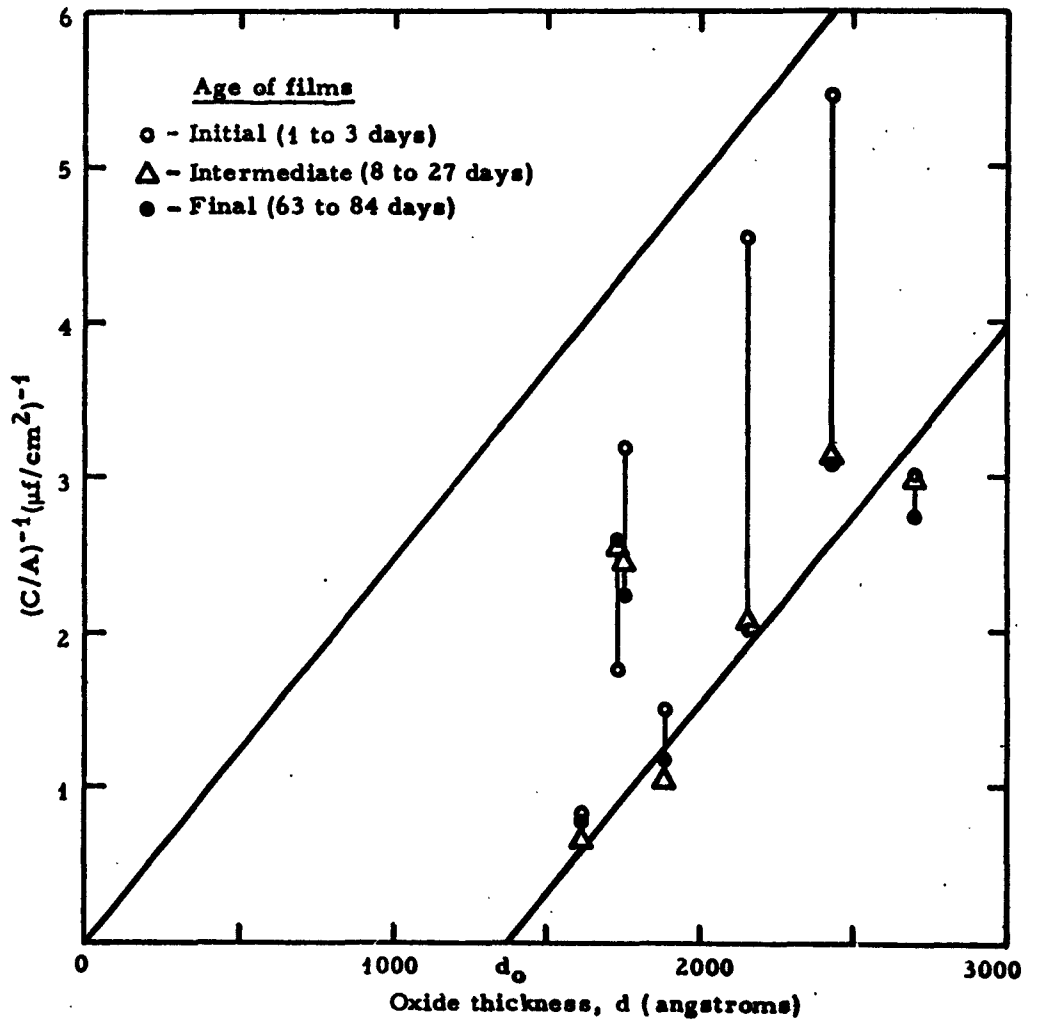


Fig. 38. Inverse of capacitance per unit area vs oxide thickness for films anodized in sulfuric acid at 50 volts (data from Table V), showing changes of capacitance with age of film.

stable values suggests that a portion of the oxide of thickness  $d_0 = 1370 \text{ \AA}$  has been converted to conducting material, thereby shorting out the capacitance which would normally pertain to that portion of oxide.

The apparent dielectric constant of the remaining capacitive layer of thickness  $d - d_0$  is calculated as 46.5, in reasonable agreement with the published value of 41.7 for anodically formed tungsten oxide.<sup>6</sup>

Breakdown voltage was generally less than 10 percent of the forming voltage for tungsten capacitors.

A typical plot of leakage current as a function of applied voltage is shown in Fig. 36 for a tungsten capacitor. In view of the high leakage and high dissipation factors, further measurements of leakage resistance were not warranted.

5. Zirconium. Two groups of zirconium capacitors were formed at 50 volts, one in solutions based on boric acid and the other on ethyl acid phosphate. Both groups had the same average capacitance of  $0.13 \mu\text{f}/\text{cm}^2$  ( $0.84 \mu\text{f}/\text{in.}^2$ ), giving a capacitance-formation voltage product of  $6.5 \mu\text{f}\cdot\text{v}/\text{cm}^2$  ( $42 \mu\text{f}\cdot\text{v}/\text{in.}^2$ ). A scatter diagram of capacitance vs dissipation factor with their numerical distributions is presented in Fig. 39 for both groups.

The effect of ambient temperature on capacitance for a zirconium capacitor at 1 kc is shown in Fig. 40. Capacitance increased with temperature, giving a temperature coefficient computed from the end points of 356 ppm per  $^{\circ}\text{C}$ .

Dissipation factor had a slightly better average of 0.017 for capacitors formed in boric acid, compared with 0.022 for those formed in phosphate solutions.

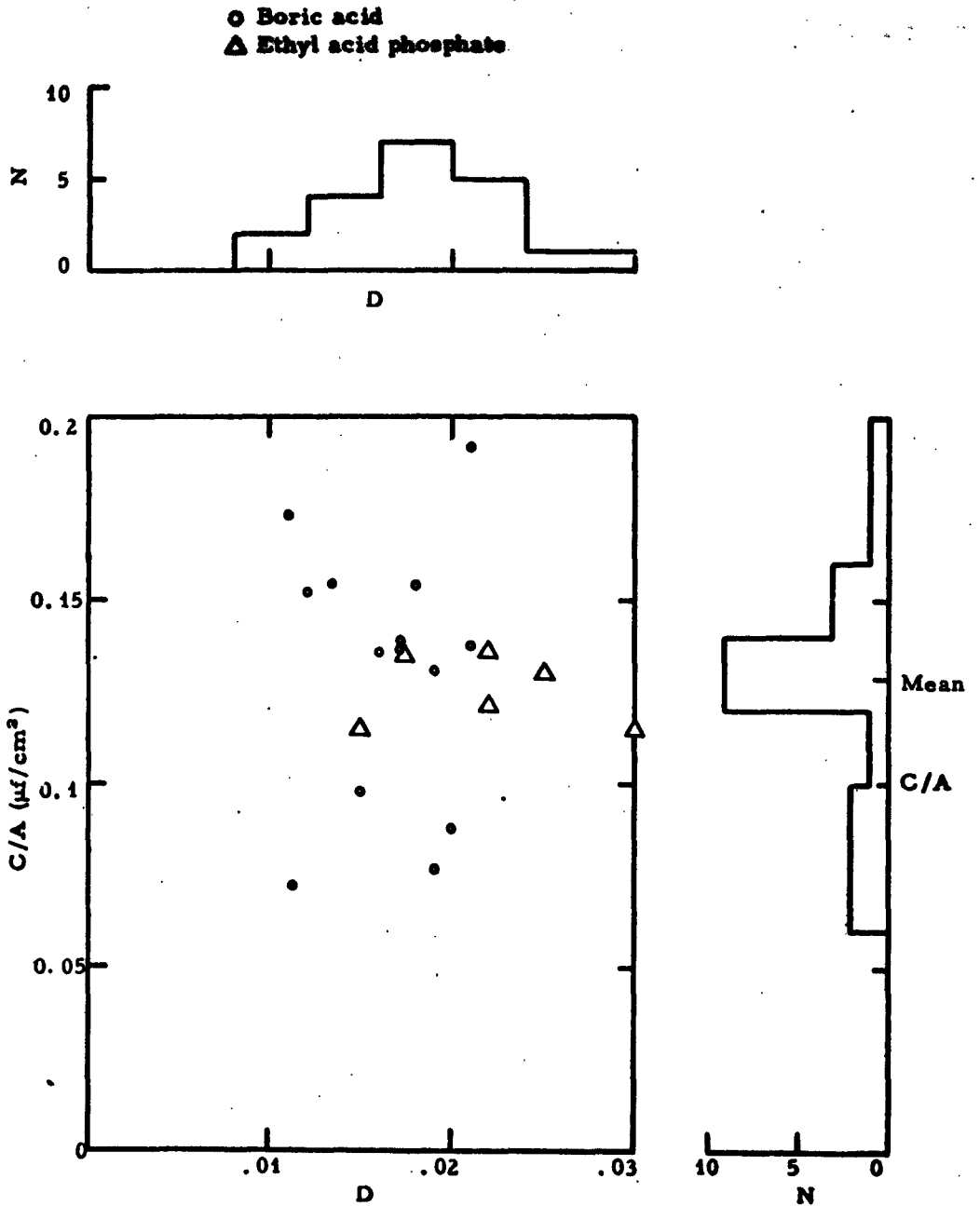


Fig. 39. Capacitance per unit area vs dissipation factor, and their numerical distributions; zirconium anodized in boric acid and ethyl acid phosphate at 50 volts.

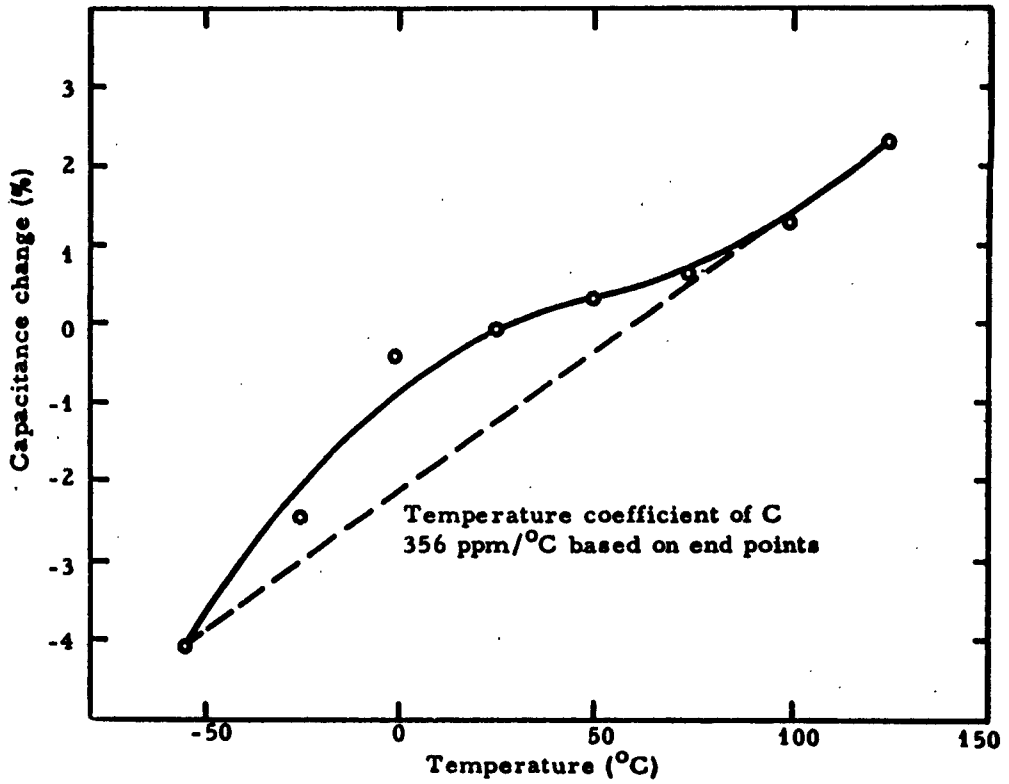


Fig. 40. Percentage capacitance change at 1 kc relative to room temperature value as a function of temperature, for a zirconium capacitor formed at 50 v.

The breakdown voltage characteristics of zirconium capacitors were similar to those for tantalum. In a group of 61 capacitors tested, 36 withstood voltage greater than the forming voltage of 50 without showing appreciable current leakage. Many of the remainder were withdrawn from test after intermittent sparking was observed at voltages from 26 to 49. Only 12 were rejected for short circuiting or current leakage. Some self-healing was noted.

The leakage current of a zirconium capacitor is plotted as a function of applied voltage in Fig. 41. Insulation resistance determined from leakage current at 75 percent of forming voltage was 161 ohm-farads.

## 1.2 THIN-FILM RESISTORS

The technique of preparing thin-film resistors by forming a vacuum-deposited metal in a predetermined pattern and then partially anodizing the deposited metal to a precise value of resistance has been investigated for tantalum and tungsten. The properties of vacuum-deposited films of titanium and zirconium that are related to their use as resistors has also been explored. The resistor properties specified in the contract are:

1. Films with resistance of approximately 6 megohms per square inch.
2. A final resistance within 10 percent of a desired value.
3. Temperature coefficient of resistance (TCR) within  $\pm 200$  ppm/ $^{\circ}$ C over the temperature range  $-55^{\circ}$ C to  $125^{\circ}$ C.
4. Power dissipation up to 2 watts at  $125^{\circ}$ C while maintaining resistance within 1 percent per 1000 hours (10 ppm/hr).

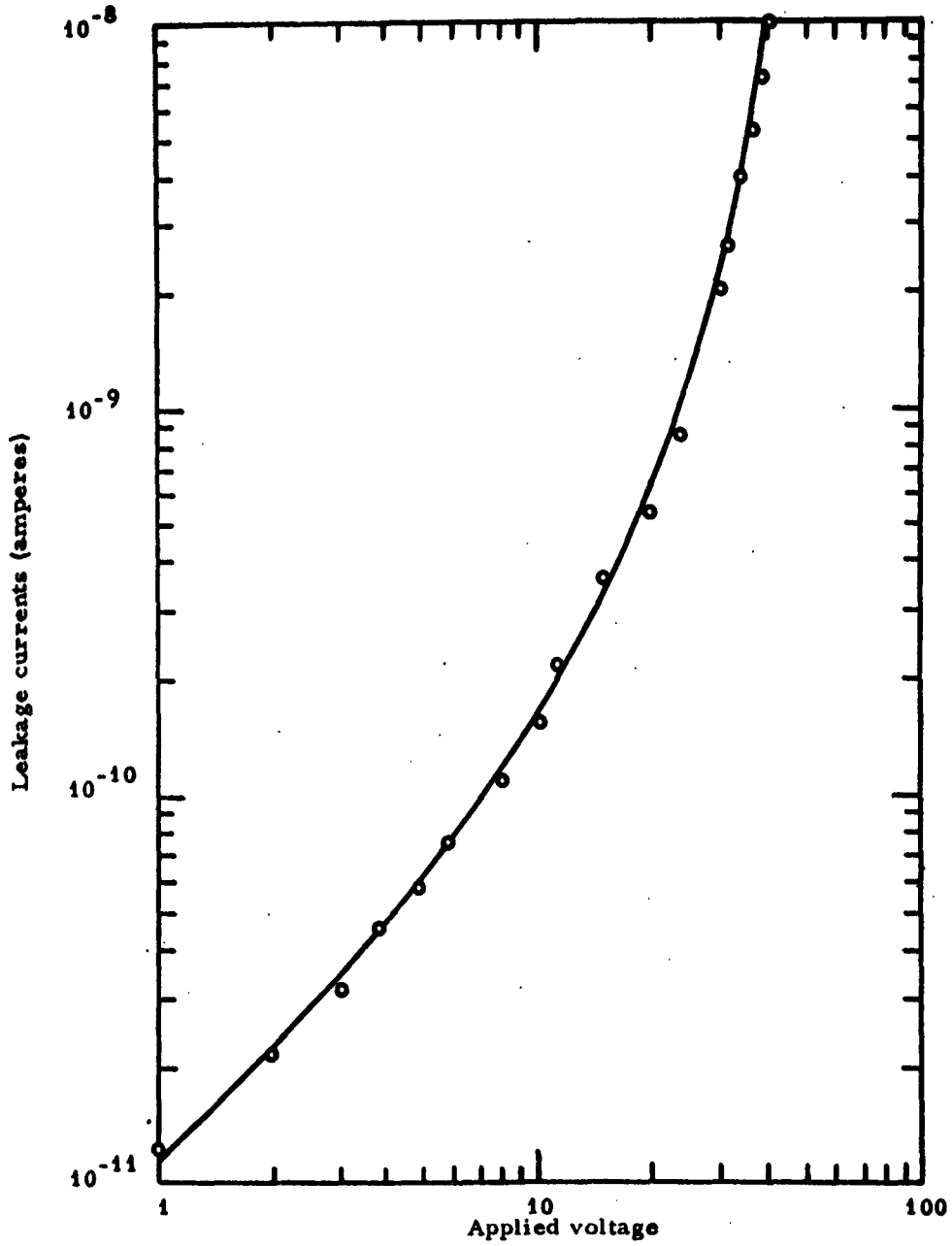


Fig. 41. Leakage current at 25°C as a function of applied voltage for a zirconium capacitor formed at 50 volts.

**1.2.1 Selection and Treatment of Substrates**

Individually selected Type A1 and A3 glass micro slides free from bubbles, scratches and pits were used as substrates. Type A1 glass was used extensively until the later part of the work when newly received slides were found to have visible scratches. At this point, glazed-edge slides of type A3 that were free from defects were employed.

Both types of glass micro slides were cut to the desired test sample size of 5/8 in. x 2 in. They were cleaned in the same manner as capacitor substrates by ultrasonic agitation in an Alconox solution, rinsing, dipping in a chromic - sulfuric acid mixture at 80°C for about 10 seconds, rinsing and flooding quickly with a 1 percent hydrofluoric acid solution followed immediately by rapid rinsing in distilled water and drying with a jet of cold, filtered, compressed air.

**1.2.2 Film Deposition Techniques**

**1.2.2.1 Sputtering**

Films of tantalum, zirconium and tungsten were prepared by sputtering in the vacuum bell jar system described in Section 1.1.3.2. The substrates were held in holders with masks on the work table or anode, approximately 1-1/2 inches from the cathode. The system had an argon leak that supplied 99.995% argon at the desired pressure. The glass substrate was shielded during the pumping and during the pre-sputtering. The cathode dark space was maintained approximately 1 inch thick. The values of pressure, current density and rate used for each of the above metals are given in Table VI.

Sputtering was carried out in 5-second steps with a 60-second cooling period to prevent buckling of the metal masks from excessive heating. Patterns that were to be formed subsequently by etching did

TABLE VI  
Sputtering Parameters

Metal	Pressure ( $10^{-3}$ Torr)	Current density (ma/cm <sup>2</sup> )	Cathode potential (volts)	Rate (A/sec)
Tantalum	75	2.5	6000	20
Zirconium	68	1.7	5000	9
Tungsten (Masked pattern)	60	2.0	5000	7
Tungsten (Etched pattern)	75	5.2	5000-5400	18

not require the use of a mask; therefore the deposition rates indicated could be used without a cooling period.

Some data concerning the uniformity of sputtered tungsten films was obtained from 20 samples prepared at different times. Under the conditions of Table VI, and using a total sputtering time of 10 seconds, the average sheet resistivity was 135 ohms/sq with a standard deviation of 21 ohms/sq. The average TCR was  $-70$  ppm/ $^{\circ}$ C with a standard deviation of 17 ppm/ $^{\circ}$ C. The effect of the rate of sputtering on the TCR of tungsten will be discussed later.

Examination of sputtered films of thickness below 100 A revealed a nonuniform deposition across the breadth of the resistor pattern as shown in Fig. 42. This defect was also found subsequently in thicker films, although it could not be observed as readily. It was postulated that a nonorthogonal field on the surface of the substrate at the beginning of the sputtering caused a nonuniform distribution of the sputtered atoms. A curved field distribution could arise from the

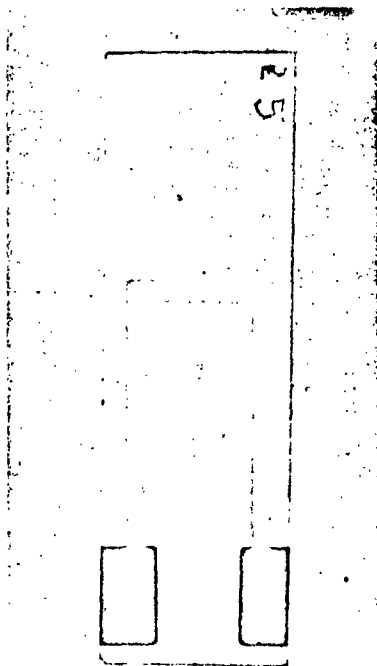


Fig. 42. Nonuniform deposition in a sputtered film.

grounded metal mask which imposed a potential boundary around the insulating glass substrate.

Either of two corrective procedures proved to be successful. The first was to pre-sputter the entire glass substrate with a thin metal layer. This allowed the substrate surface to be electrically grounded to the mask and holder, thereby obtaining an equipotential surface. The second, used in most of this work, was to employ a holder of Supermica to insulate the metal mask from ground, thus reducing the field perturbations. Since patterns produced by etching were not prepared with masks, nonuniform field distribution was not encountered.

#### 1.2.2.2 Evaporation

Titanium films were prepared by vacuum evaporation from a tungsten filament in a Consolidated Vacuum bell jar system with the substrate 15 cm above the filament. Steel masks were held in place by magnets. Titanium wire (25-mil) was wrapped on a standard tungsten filament, Sylvania Type A1109D. The slides were subjected to an ion bombardment current of 300 ma in a dc glow discharge at 2500 volts for approximately ten minutes at a pressure of  $5 \times 10^{-2}$  Torr. The system was then pumped down to approximately  $10^{-6}$  Torr. Filament current during the evaporation was held constant at approximately 100 amperes. Film thickness was monitored by measuring the relative light transmission through a control sample with an Edwards modulated-beam photometer.

Tantalum and the majority of the tungsten films were prepared by vacuum evaporation in the electron bombardment system described in Section 1.1.3.3. The tungsten vapor source was a sessile drop formed on 1/16-in.-diameter B-type tungsten rod, by electron bombardment heating. The electron beam is focused by a grid cavity surrounding the tip of the rod and filament. Films were evaporated at a chamber pressure between  $3 \times 10^{-7}$  and  $2 \times 10^{-6}$  Torr.

Aluminum contact tabs were prepared by vacuum evaporation in a 12-in.-diameter bell jar system. Aluminum wire slugs of 99.99% purity were rapidly evaporated from a heated tungsten filament at approximately  $10^{-4}$  Torr.

### 1.2.3 Measuring Techniques

#### 1.2.3.1 Interferometry

The thickness of the deposited metal film was measured interferometrically at a step where a vacuum-evaporated aluminum contact tab was deposited over the edge of the metal film. The opacity of the aluminum film (1000 Å) eliminated phase shift effects usually encountered at metal-glass boundaries. Film thicknesses greater than 300 Å were measured with a Zeiss interference microscope; thicknesses less than 300 Å were measured by a multiple-beam interferometric technique described in detail in Appendix III.

#### 1.2.3.2 DC Resistance

Film resistances were measured with a Leeds and Northrup Model 5300 bridge and an external galvanometer to increase the sensitivity of measurement. Measurements were made over the temperature range from -55 to 125°C in a Wyle Laboratories C106-640 high-low temperature test chamber.

#### 1.2.4 Resistor Patterns

Most of the test resistors were prepared as shown in Fig. 43. The tab mask, resistor mask and holder are shown in Fig. 44. The U-shaped pattern in line widths down to 18 mils was obtained by deposition through a metal mask held in contact with the glass substrate. The effective dimensions of the resistor deposits between the evaporated aluminum contact tabs were 2.0 in. long x 0.08 in. wide (0.16 sq. in. with 25 squares). This short length of path design was used to keep the resistance of the higher sheet resistivity deposits to values small enough for a reasonably precise measurement of resistance with the available

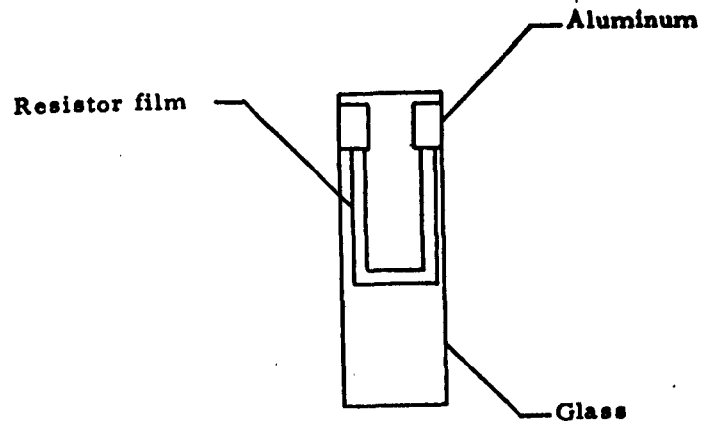


Fig. 43. Test film resistor.

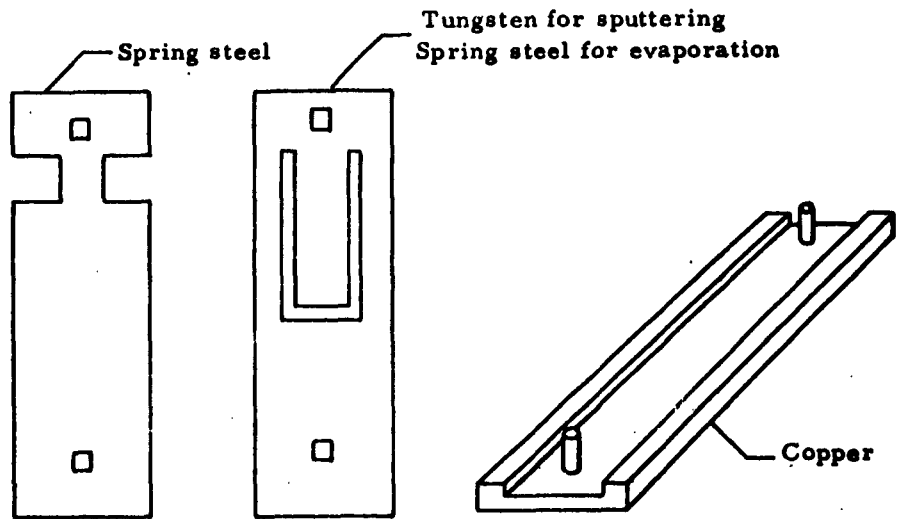


Fig. 44. Resistor masks and substrate holder.

dc bridge. When suitable methods were found for the preparation of film resistors, narrower and longer path patterns, like that shown in Fig. 45, were used to obtain high resistances over a smaller substrate area. For example, a pattern which was specifically designed to yield a one-megohm tungsten resistor with a zero TCR was 16 in. long by 0.005 in. wide (3200 squares) over a substrate area of 1/6 square inch. Turns in the pattern were curved to avoid sharp corners, because thin deposits were found to be preferentially attacked at these sharp corners during anodization as shown diagrammatically in Fig. 46. These fine patterns were prepared by photoengraving the tungsten deposit rather than by evaporating through a mask. Kodak Photo Resist was used as an etching resist and the exposed tungsten was removed by Murakami's Reagent.<sup>7</sup>

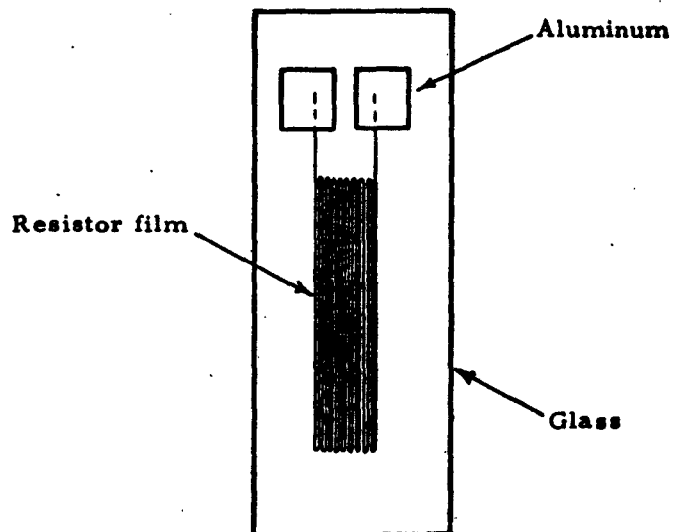


Fig. 45. Narrow path resistor pattern.

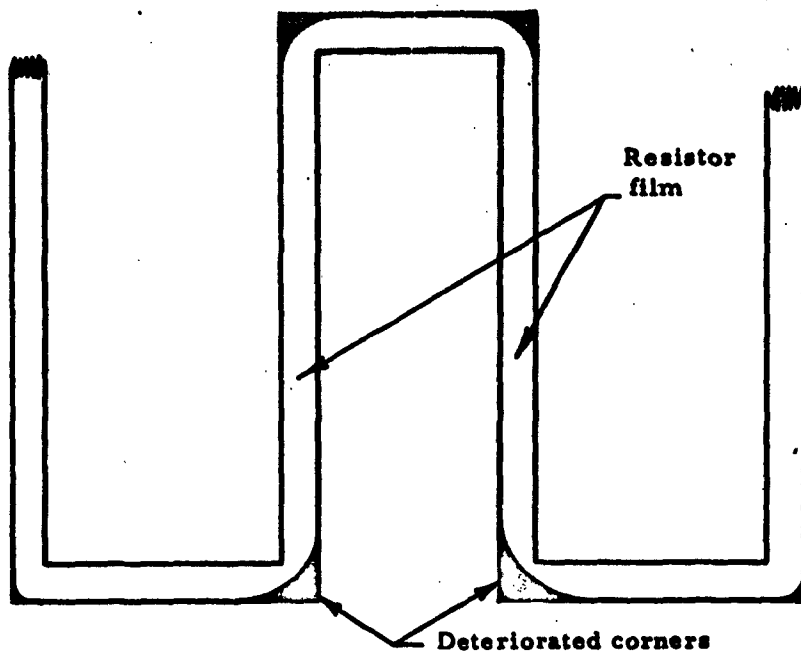


Fig. 46. Deterioration of sharp-cornered pattern.

1.2.5 Anodization (see also Section 1.1.4)

1.2.5.1 Apparatus

Anodization of tantalum and tungsten films were carried out in an electrolytic cell shown diagrammatically in Fig. 47. The cell was resin reaction kettle with a Teflon-covered stirrer and two electrode holders. One holder carried a coiled platinum wire which served as the cathode and the other the deposited metal film which served as the anode. The anode holder, designed to provide a low-resistance contact to the resistive film, is shown in Fig. 48. Contact to each aluminum tab of the resistor was made by a spring-loaded brass plug. Each plug was connected with platinum wire to the two external terminals of the electrode holder. Two nylon set screws held the substrates firmly against two rubber O-rings that provided a leak-tight seal for the contact.

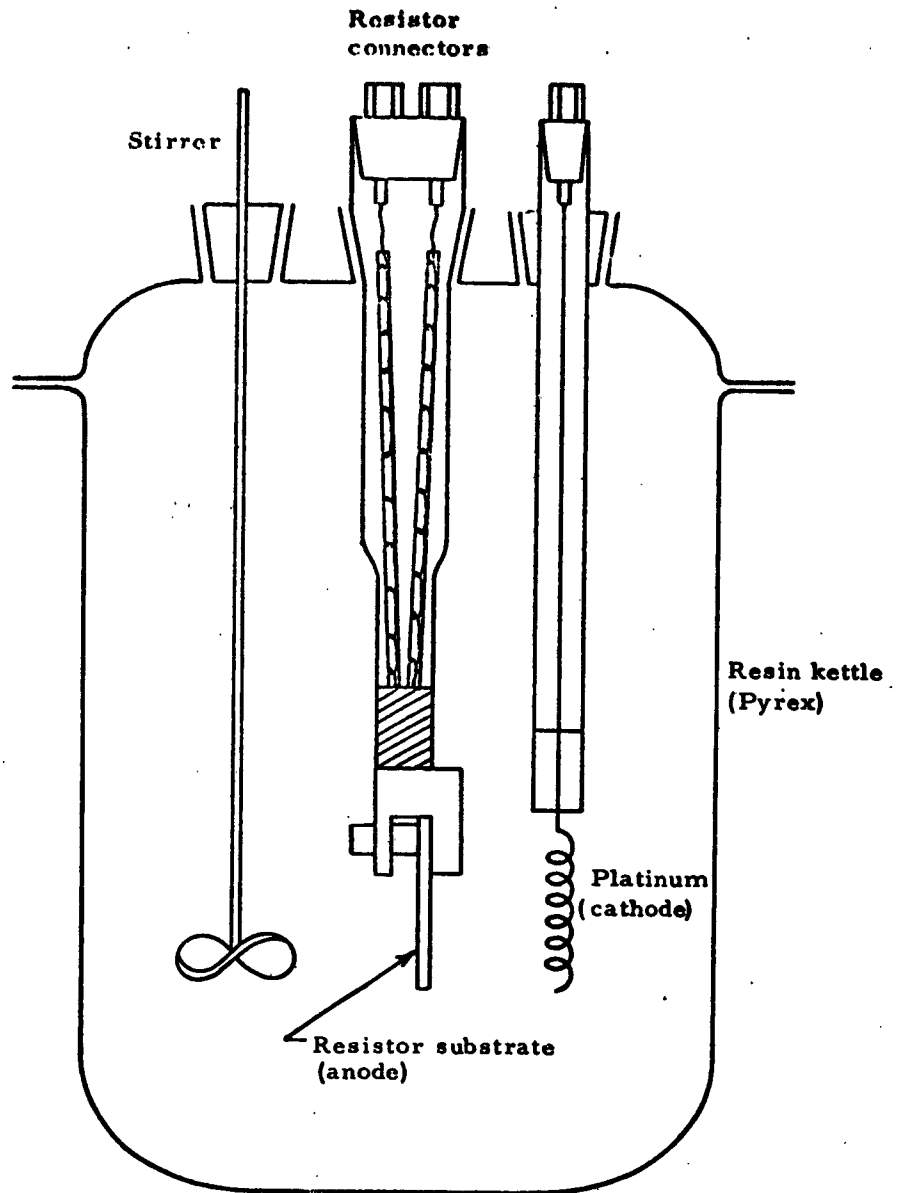


Fig. 47. Anodizing cell.

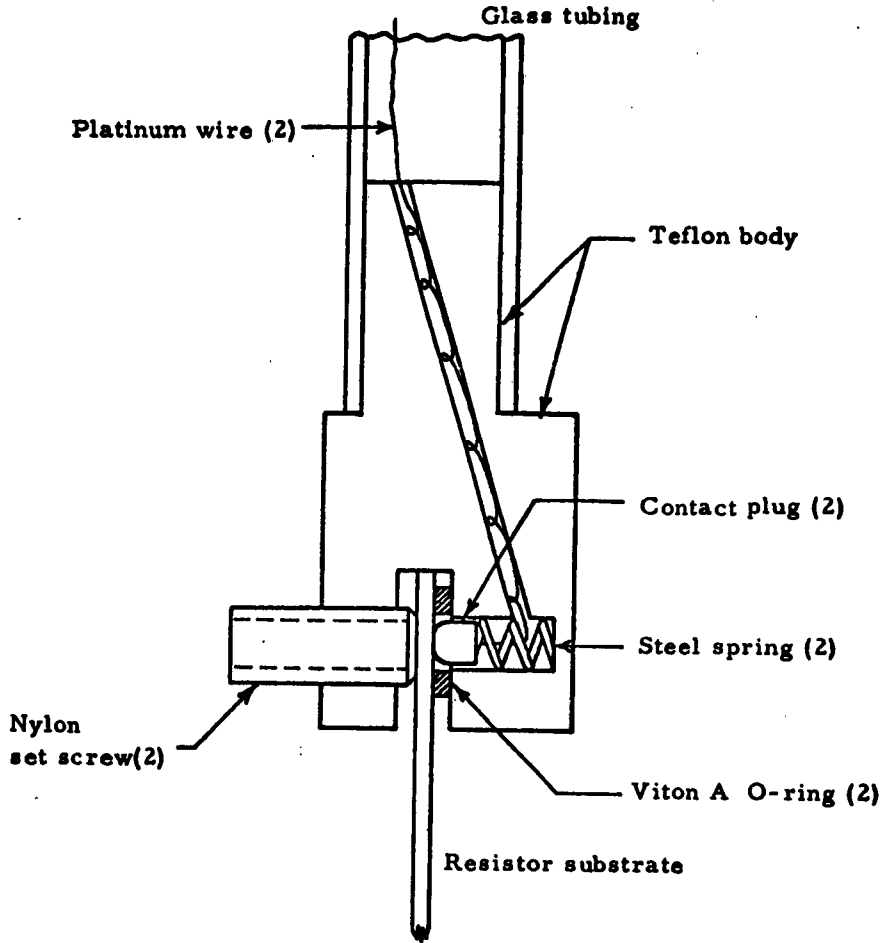


Fig. 48. Sample holder.

1.2.5.2 Electrolytes

The electrolytes used to anodize the metal films were as follows:

For tantalum

a.	Oxalic acid	17% (by weight)
	Ethylene glycol	50%
	H <sub>2</sub> O, distilled	33%
b.	Boric acid	4%
	H <sub>2</sub> O, distilled	96%
	Ammonium hydroxide to pH	6.8

For tungsten

KOH	23 gms
H <sub>3</sub> PO <sub>4</sub>	49 cc
H <sub>2</sub> O, distilled	800 cc
Ethylene glycol	300 cc
pH (measured)	2.0
Used at 5°C.	

The solutions were prepared from reagent-grade chemicals and each was filtered to remove suspended particles. Both of the solutions used to anodize the tantalum metal provided satisfactory oxide coatings. Although the oxalic acid - glycol solution, unlike the ammonium borate solution, deteriorated the aluminum tab by dissolving the aluminum oxide formed, it was preferred because a more stable null identification was obtained on a dc bridge used to monitor anodization.

The solution employed to anodize tungsten provided an unblemished oxide layer and offered few difficulties in monitoring the anodization process. It was cooled to prevent the aluminum oxide surface of the

contact tabs from rapidly dissolving in the electrolyte and in turn deteriorating resistor film surfaces. Although the exposed surfaces of the aluminum tabs were partially anodized in the cooled electrolyte, sufficient metal remained to maintain a low resistance contact. The electrolyte was cooled by suspending the resin kettle in an ice bath.

#### 1.2.5.3 Current Density

In general, anodizing can be accomplished by applying constant current or voltage, or a succession of both. Constant current was chosen because the oxide formation rates made it convenient to use automatic resistance monitoring equipment. Appropriate limits for applied current densities were established.

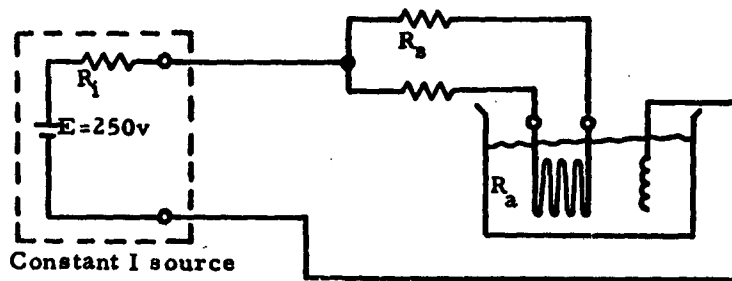
The total applied current is divided between film forming ionic currents and leakage currents. At low current densities, leakage currents constitute the greater fraction. It was experimentally found that the formation rate of tungsten oxide was greatly reduced below a current density of  $30 \mu\text{a}/\text{cm}^2$ , indicating a low efficiency of oxide formation below this value.

Excessively high current densities, on the other hand, will accentuate nonuniform oxide growths owing to a larger IR drop along the underlying metal film. This causes the resistive film to thin-out near the aluminum tab. The effect is particularly troublesome with tungsten films because of the relatively high sheet resistivities used. It was also observed that large current densities produce bare patches at various locations on tungsten films. This deterioration increased when the film was further anodized. Inspection of the films at successive intervals during anodization showed that the deterioration began with the appearance of small holes between 0.001 and 0.006 in. in diameter. These defects

could be eliminated by using current densities below  $1 \text{ ma/cm}^2$ . Subsequently, anodizing currents between  $50 \text{ } \mu\text{a/cm}^2$  and  $200 \text{ } \mu\text{a/cm}^2$  were used for the formation of tungsten oxide. At a current density of  $70 \text{ } \mu\text{a/cm}^2$  a typical oxide coating would be formed in 20 minutes. For tantalum films, it was possible to use a high current density of  $1 \text{ ma/cm}^2$ , which formed a film in about 10 minutes.

Small holes also occurred in tungsten films when the voltage across the oxide film exceeded approximately 35 volts. Most of the resistors were therefore formed without exceeding this voltage.

When the same anodic current source was connected to both ends of a long resistive path, e.g., 16 inches, the current to each end was not equal. Since an unbalance occurring as the film is anodized would cause one leg of the path to become comparatively thinner, the currents to each leg were balanced by inserting a series resistor approximately equal to the internal resistance of the current source into each leg. This circuit is illustrated in Fig. 49 with typical values for the resistors.



$$R_a = 1 \text{ megohm over 16 inches}$$
$$R_2^a = R_1 = 8.2 \text{ megohm}$$

Fig. 49. Balancing of anodizing currents for long resistive paths.

#### 1.2.5.4 Automatic Method of Anodization

An automatic method of anodizing the tungsten film to a specific resistance is shown schematically in Fig. 50. Essentially, the control circuit has a switch which alternately connects the anodizing current source and the monitoring bridge to the immersed film. The bridge, a Wheatstone type, indicates a null when the immersed film resistor, which acts as an arm of the bridge, becomes equal to an external preset calibrated resistance, which acts as the other corresponding arm. The anodizing current supply is switched off when a null is obtained. To obtain a sensitive null indication for precision monitoring, a dc amplifier with a gain of 2500 is used as the null detector. The output of the amplifier controls a relay that opens the current source when the desired preset value of resistance is obtained. The precision of the final anodized resistors, measured with a bridge of 0.5 percent accuracy with a chosen

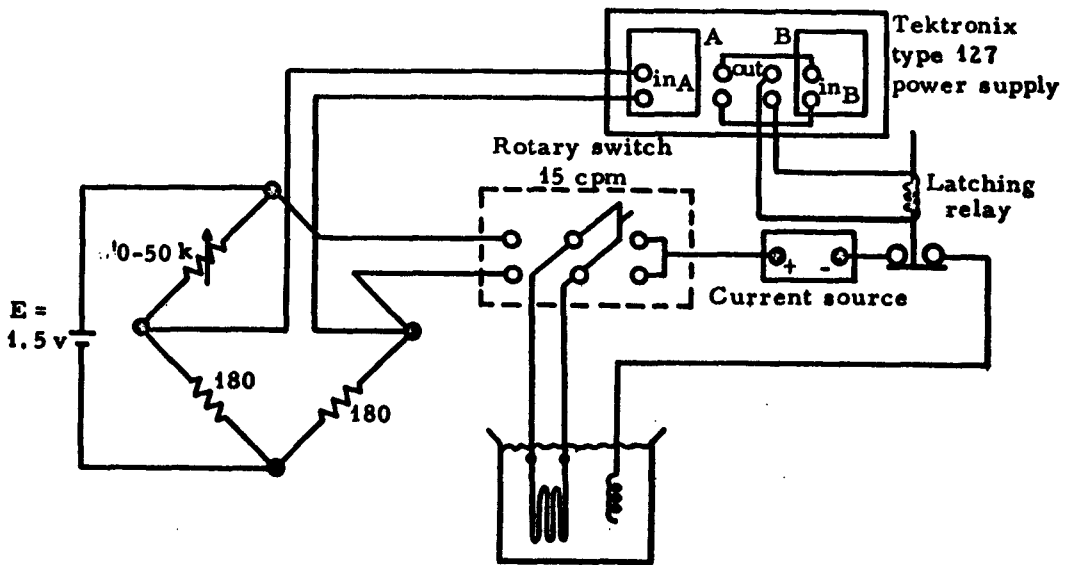


Fig. 50. Automatic anodization schematic.

pre-set resistance, was approximately 0.5 percent for films below 25 kilohms and 1 percent for films to 50 kilohms. The resistance of test resistors was usually kept less than 50 kilohms.

#### 1.2.6 Heat Treatment of Anodized Films

It has been observed that the rate of resistance change of an anodized film exposed to air at temperatures up to 125°C increases with temperature and is largest at the start of heating. It is known that this rate of resistance change can be reduced by heat treating these films in air at higher temperatures. Anodized tantalum deposits, for example, heated at 200°C for 6 hours in air have shown resistances stable within 1 ppm/hr at 125°C up to sheet resistivities of 150 ohms/sq. This treatment, however, thermally oxidizes the film to some extent. High resistivity tungsten films suffer an appreciable change in resistance when similarly treated. A change in resistance after anodization is undesirable since it is this step that adjusts the resistor to the value desired. In addition, thermal oxidation increases the TCR (to higher negative values).

It was found, however, that heat treating anodized tungsten films at high temperatures in vacuum stabilized the resistance without any appreciable change in resistance. Data are presented in Table VII. The first eight entries are preliminary data obtained with the use of a vacuum oven where the minimum obtainable pressure was approximately 0.2 Torr. The average change in resistance was approximately 1 percent for sheet resistivities up to 1000 ohms/sq and increased to 2 percent for sheet resistivities up to 2000 ohms/sq.

**TABLE VII**  
**Change in Resistance (R) as a Result**  
**of Heat Treatment in Vacuum**

Temp. (°C)	Time (Hrs)	Pressure (Torr)	Resistance before treatment (ohms)	Resistance after treatment (ohms)	Resistivity (ohms/sq)	ΔR (%)
140	2	0.2	48,535	49,510	1940	+2.0
150	4	0.2	38,060	39,090	1525	+2.7
150	4	0.2	47,400	48,090	1900	+1.4
150	2	0.2	41,780	42,640	1670	+2.0
120	2	0.2	25,200	25,480	1004	+1.1
140	3	0.2	1,186.5	1,202.8	47	+1.4
130	3	0.2	9,625	9,708	380	+0.8
150	4	0.2	18,930	19,220	44	+1.5
150	5	$1.5 \times 10^{-7}$	622,300	623,000	195	+0.11
150	5	$1.5 \times 10^{-7}$	2,390,000	2,377,000	750	-0.54
150	3	$4.0 \times 10^{-7}$	767,400	763,300	240	-0.53
150	3	$4.0 \times 10^{-7}$	1,364,000	1,365,000	427	+0.0734
150	3	$4.0 \times 10^{-7}$	413,900	415,200	129	+0.31
150	3	$4.0 \times 10^{-7}$	542,850	542,500	169	-0.06
180	4	$3.0 \times 10^{-7}$	340,300	341,100	107	+0.23
180	4	$3.0 \times 10^{-7}$	1,053,000	1,044,000	328	-0.85
150	5	$0.6 \times 10^{-7}$	990,300	993,500	310	+0.32
150	5	$0.6 \times 10^{-7}$	372,300	374,150	117	+0.50
150	25	$1.0 \times 10^{-7}$	20,800	20,650	831	-0.72

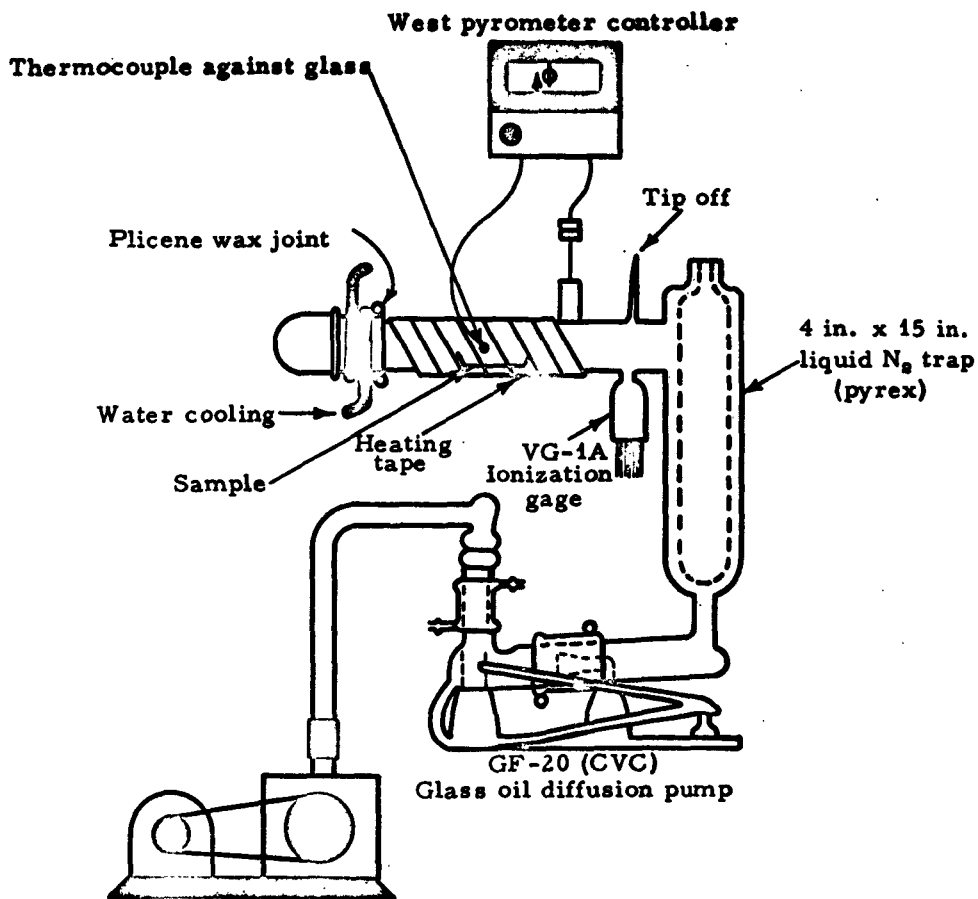


Fig. 51. High-vacuum heat-treating equipment.

A vacuum oven, shown in Fig. 51, was constructed to heat treat anodized films at pressures between  $10^{-8}$  and  $10^{-6}$  Torr. Although the samples tested all had sheet resistivities below 1000 ohms/sq, an average decrease in the percentage change in resistance compared with those samples heat treated at 0.2 Torr may be noted. Some samples have exhibited small decreases in resistance. This behavior suggests a critical pressure, temperature and time of heat treatment for which the resistance change will be zero.

### 1.2:7 Resistor Properties

The three properties by which the different metals were evaluated for use as thin-film resistors were:

1. High sheet resistivity to obtain large resistance values over small substrate areas.
2. Low temperature coefficient of resistance (TCR) to maintain a precise resistance over a wide temperature range.
3. Stable resistance over a wide range of temperature under load and no-load conditions.

#### 1.2.7.1 Temperature Coefficient of Resistance

The sheet resistivities of metal deposits of tantalum, titanium, tungsten and zirconium were determined within the range of TCR specified in the contract,  $\pm 200$  ppm/ $^{\circ}$ C. As mentioned, tantalum and tungsten films were carried through the anodization process and sheet resistivity vs TCR data were obtained for these films.

It may be noted that the range of TCR under consideration includes both positive and negative values, as will be shown, for example, in Fig. 53. As the films are made thinner the positive TCR associated with metallic conductivity becomes smaller, passes through zero and then becomes increasingly negative. When metallic films are very thin, the available electron path becomes a fraction of the normal mean free path for the conduction electrons. With such films, the available path is no longer temperature dependent as it is with thick films where the mean free path is reduced by scattering with increasing temperature. The result is that the TCR approaches zero as the thickness falls below the mean-free-electron path length. Metallic conductivity apparently becomes

replaced by semiconductor behavior as the films become thinner, since the resistivity continues to increase and the TCR becomes increasingly negative. This behavior suggests a departure from an otherwise continuous metal path to an array of metal aggregates or islands, separated by gaps where conduction depends on the transfer of charge across an insulator, or semiconductor gaps between these metal aggregates.<sup>8</sup>

The TCR as a function of sheet resistivity rather than thickness has been measured for all the metals because it provides a direct comparison of the electrical properties of interest and because of the relative ease of measurement. In general, it may be stated that sheet resistivity is a decreasing function of film thickness. Data for tungsten, which include the region of sheet resistivity where zero TCR is found, are given in Fig. 52.

Detailed data for tungsten, titanium, tantalum and zirconium, followed by a tabular summary, are given below:

1. Tungsten. Anodized evaporated tungsten films at zero TCR have sheet resistivities between 150 and 320 ohms/sq, and 2000 ohms/sq at  $-200 \text{ ppm}/^{\circ}\text{C}$ , as shown in Fig. 53. A review of the data has indicated that the use of lower pressures during metal deposition resulted in more positive temperature coefficients for the lower resistivity films and higher resistivities in the region of zero TCR. This suggested that contaminants in the system such as moisture and residual oxygen contributed significant amounts of material of negative TCR to the deposited films.<sup>9</sup> When the evaporation system was recently modified to obtain pressures below  $1 \times 10^{-7}$  Torr during evaporation instead of the  $3 \times 10^{-7}$  Torr employed for the data of Fig. 53, a TCR of  $+400 \text{ ppm}/^{\circ}\text{C}$  was obtained at 30 ohms/sq in contrast to the +80 given in Fig. 53.

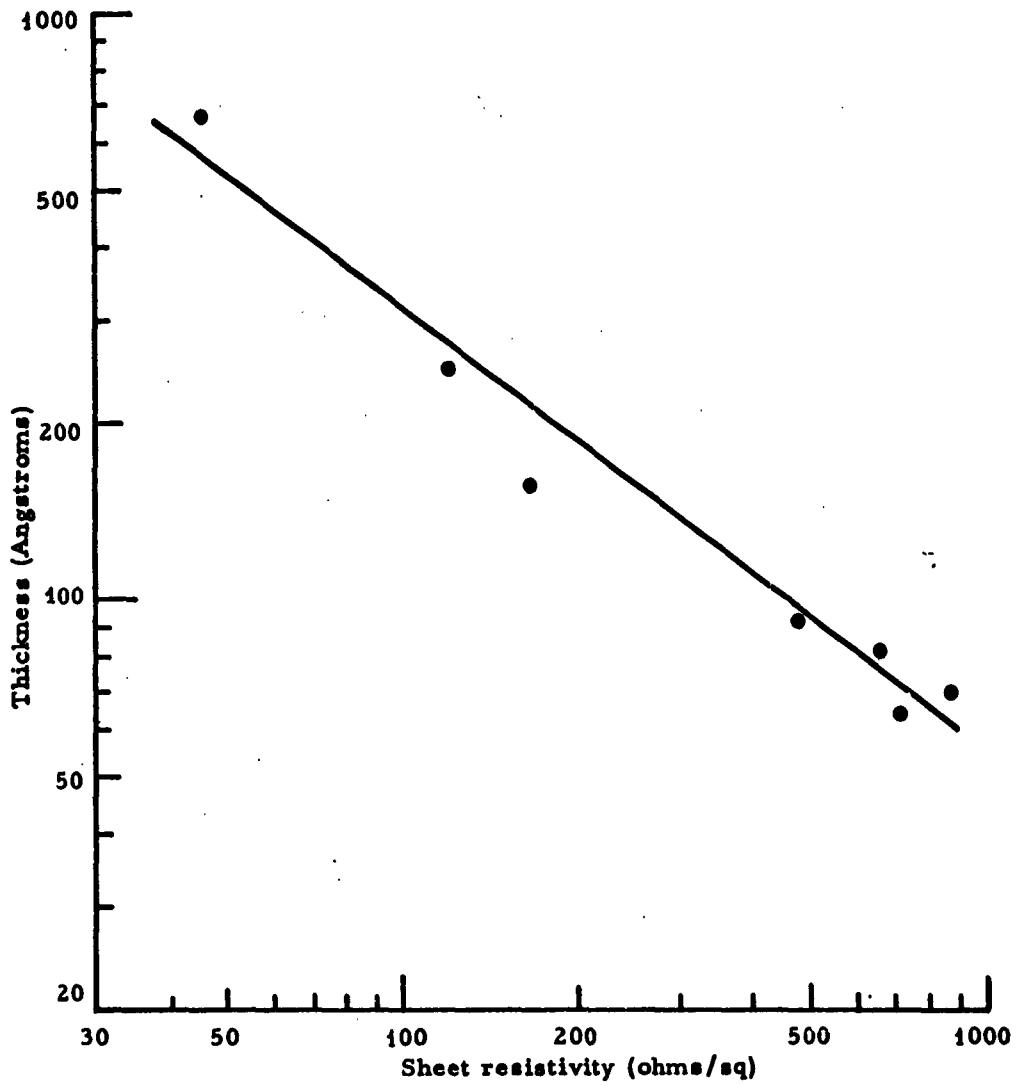


Fig. 52. Tungsten thickness vs sheet resistivity .

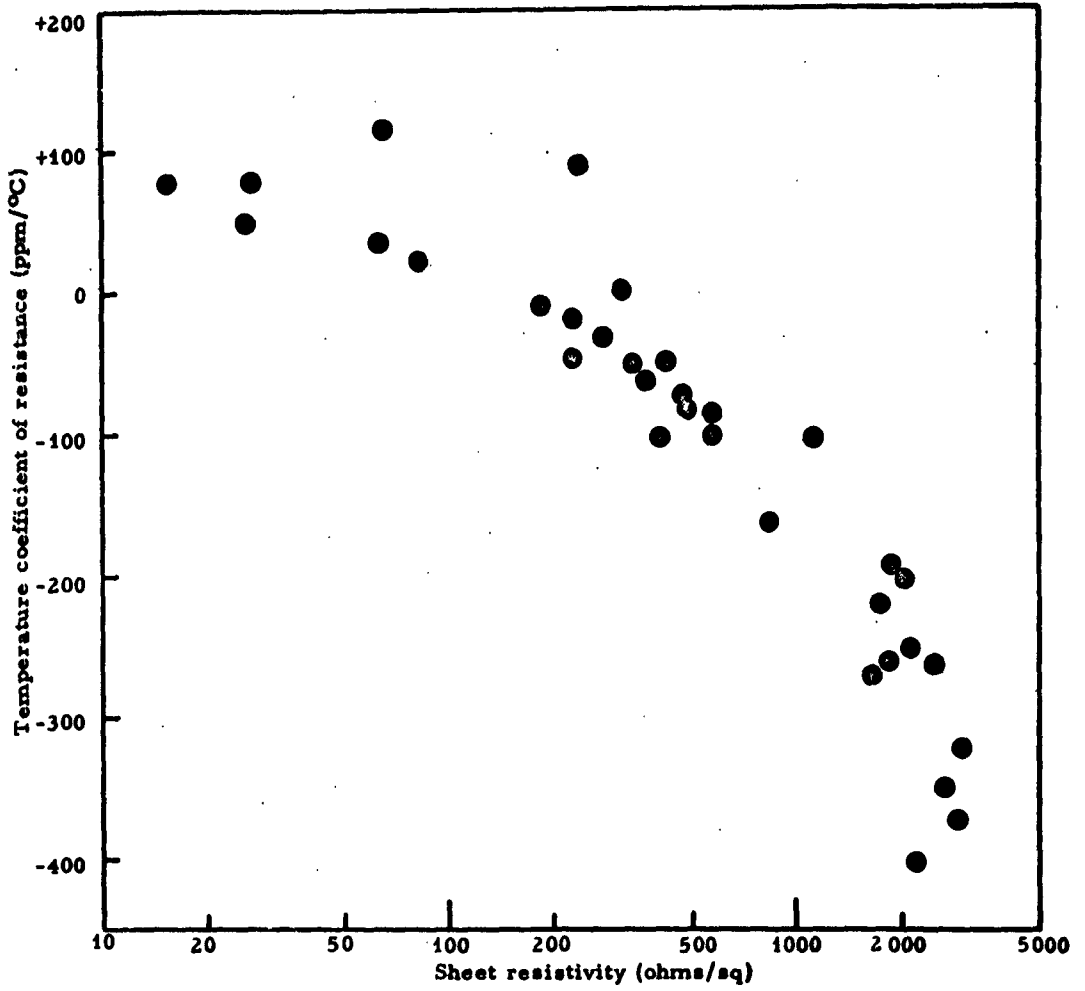
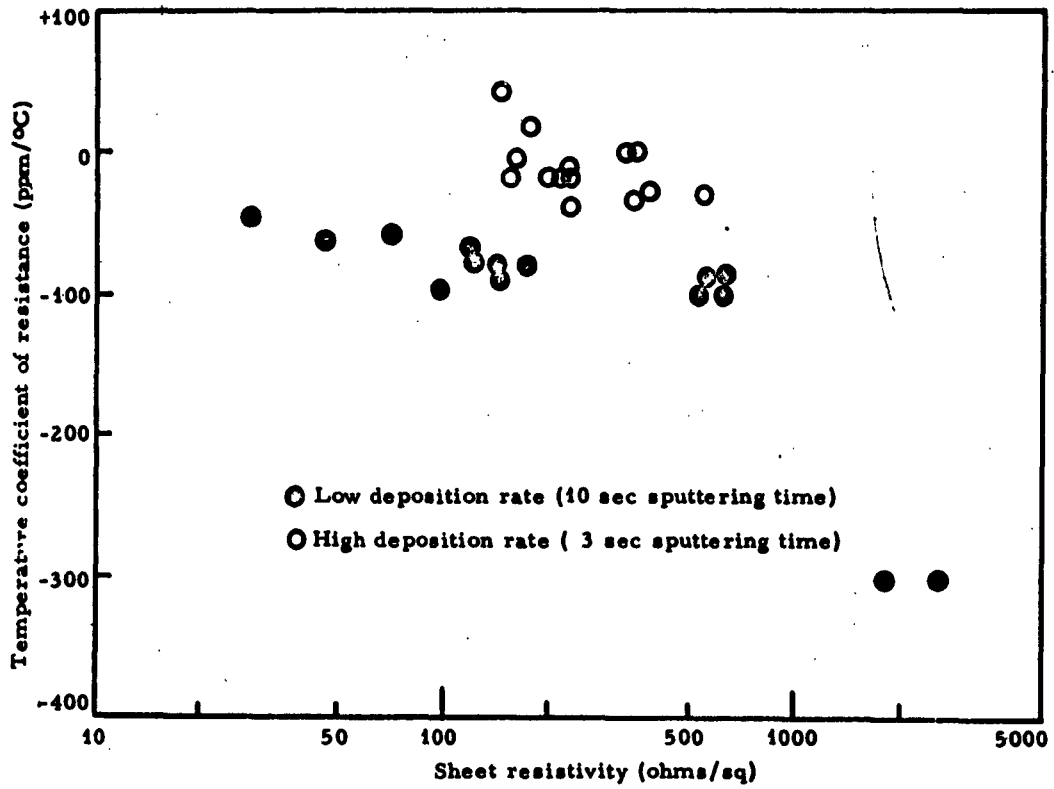


Fig. 53. Temperature coefficient of resistance vs sheet resistivity of anodized evaporated tungsten films.



The data for sputtered tungsten films are shown in Fig. 54. A sheet resistivity at zero TCR close to values for evaporated films was obtained when resistors were prepared by photoengraving patterns on unmasked deposits which were sputtered at high rates. A zero TCR value of sheet resistivity was not obtained for resistors produced by masking during sputtering at the conventional low rate. This supports the evidence that the presence of contaminants during tungsten film deposition results in deposits with larger amounts of negative TCR material.

2. Titanium. Sheet resistivity vs TCR for evaporated titanium films is shown in Fig. 55. A zero TCR exists at a sheet resistivity of 130 ohms/sq and the specified lower limit of TCR at  $-200$  ppm/ $^{\circ}$ C occurs at a sheet resistivity of 700 ohms/sq. The TCR increased to higher negative values when the films were allowed to stand in air at  $25^{\circ}$ C. When samples were heated in air, the TCR was greatly increased to higher values as shown in Fig. 55.

3. Tantalum. The temperature coefficient of anodized evaporated tantalum films vs sheet resistivity is illustrated in Fig. 56. The temperature coefficient of resistance varies from  $+200$  ppm/ $^{\circ}$ C at approximately 30 ohms/sq to  $-200$  ppm/ $^{\circ}$ C between 90 and 120 ohms/sq. A zero TCR is found at approximately 60 ohms/sq. The temperature coefficient vs thickness of the tantalum film is shown in Fig. 57. Thicknesses were computed to a first approximation from an experimentally determined sheet resistance-thickness product.

4. Zirconium. The temperature coefficient of zirconium film resistors vs sheet resistivity is shown in Fig. 58. A sheet resistivity of 250 ohms/sq is obtained at a TCR of  $-200$  ppm/ $^{\circ}$ C. A zero TCR lies

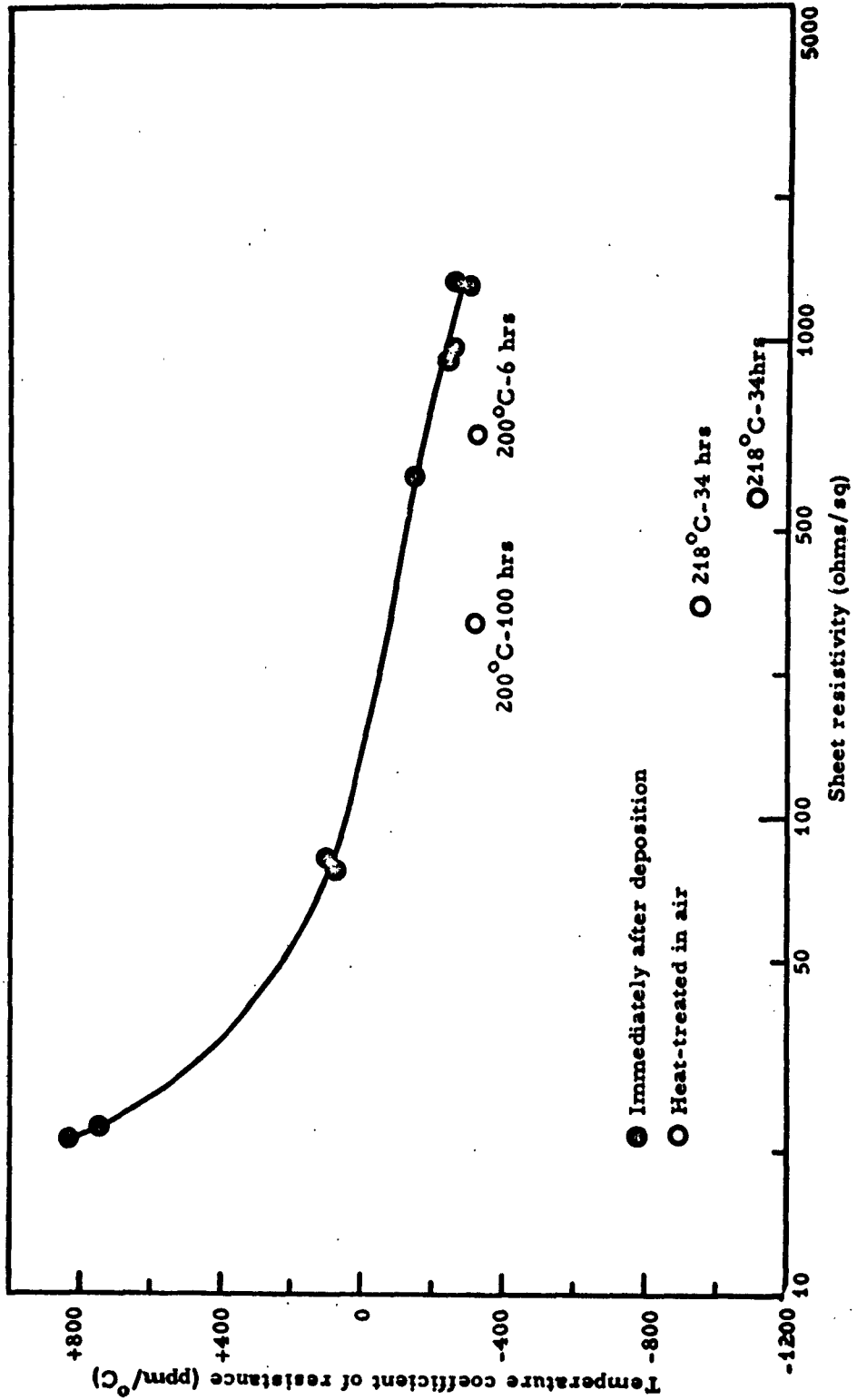


Fig. 55. Temperature coefficient of resistance vs sheet resistivity of evaporated titanium films.

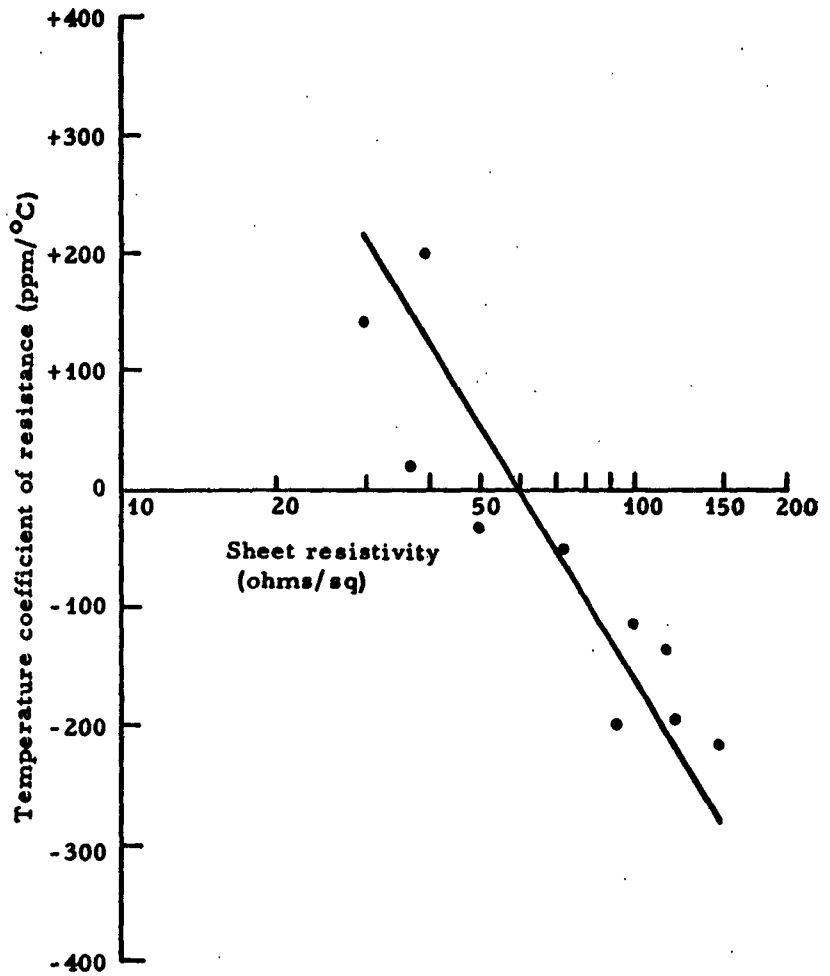


Fig. 56. Temperature coefficient of resistance vs sheet resistivity of anodized evaporated tantalum.

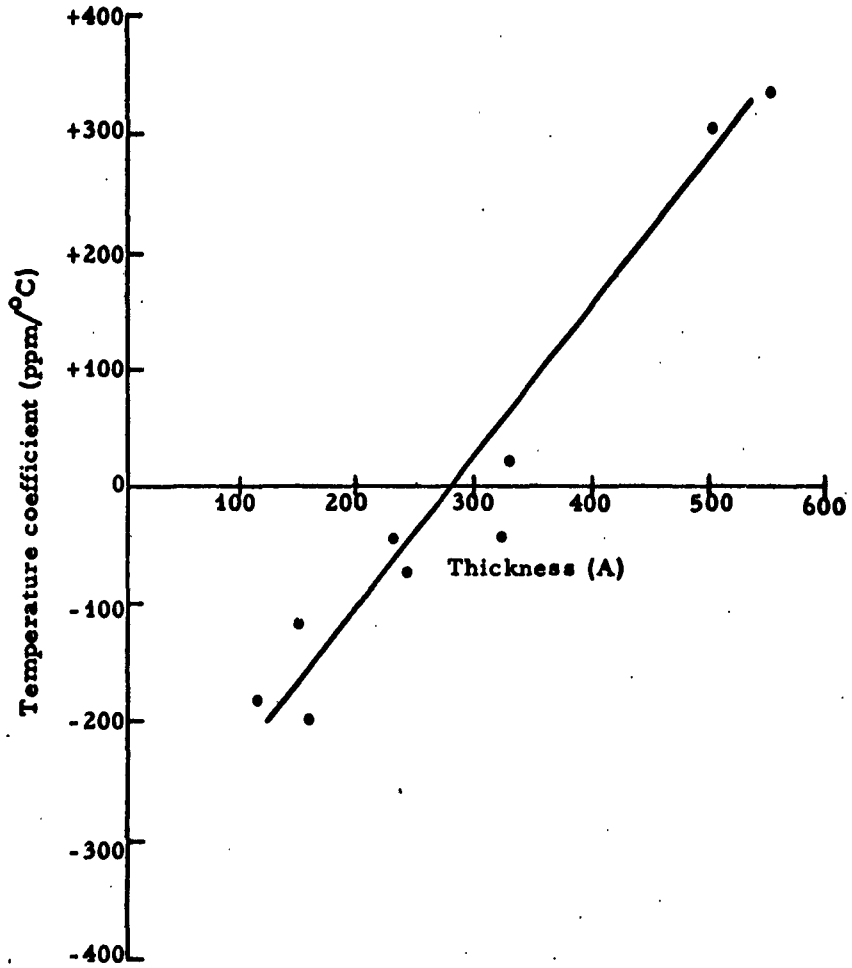


Fig. 57. Variation of temperature coefficient with film thickness of tantalum.



between sheet resistivities 20 and 100 ohms/sq. All the films in this region were sputtered at the pressure and current density given in Table VI at sputtering times of 60 to 80 seconds. The films lacked metallic luster and exhibited a pale brown interference color. This suggests that the zirconium reacted with residual impurities in the sputtering chamber.

Table VIII summarizes the most pertinent sheet resistivity data.

TABLE VIII  
Sheet Resistivities at Given Temperature  
Coefficients of Resistance

Film	Sheet resistivity (ohms/sq)	
	At zero TCR	At -200 ppm/°C
Tungsten (anodized evaporated)	150-300	2000
Titanium (evaporated)	130	700
Tantalum (anodized evaporated)	60	90-120
Zirconium (sputtered)	20-100	250

1.2.7.2 Stability of Resistance

The stability objective specified in the contract is a change of resistance of less than 1 percent per 1000 hours (10 ppm/hr) at worst case operation at 125°C with power dissipation up to 2 watts/sq. inch of total enclosed substrate area.

Exposure of thin films of the refractory metals to air at room temperature and above results in an increase in resistance of the films. Data for tungsten and titanium films are given in Figs. 59 and 60. When tungsten films are anodized, the effect is considerably reduced. When the anodized films are heat treated in air, the resistance is increased

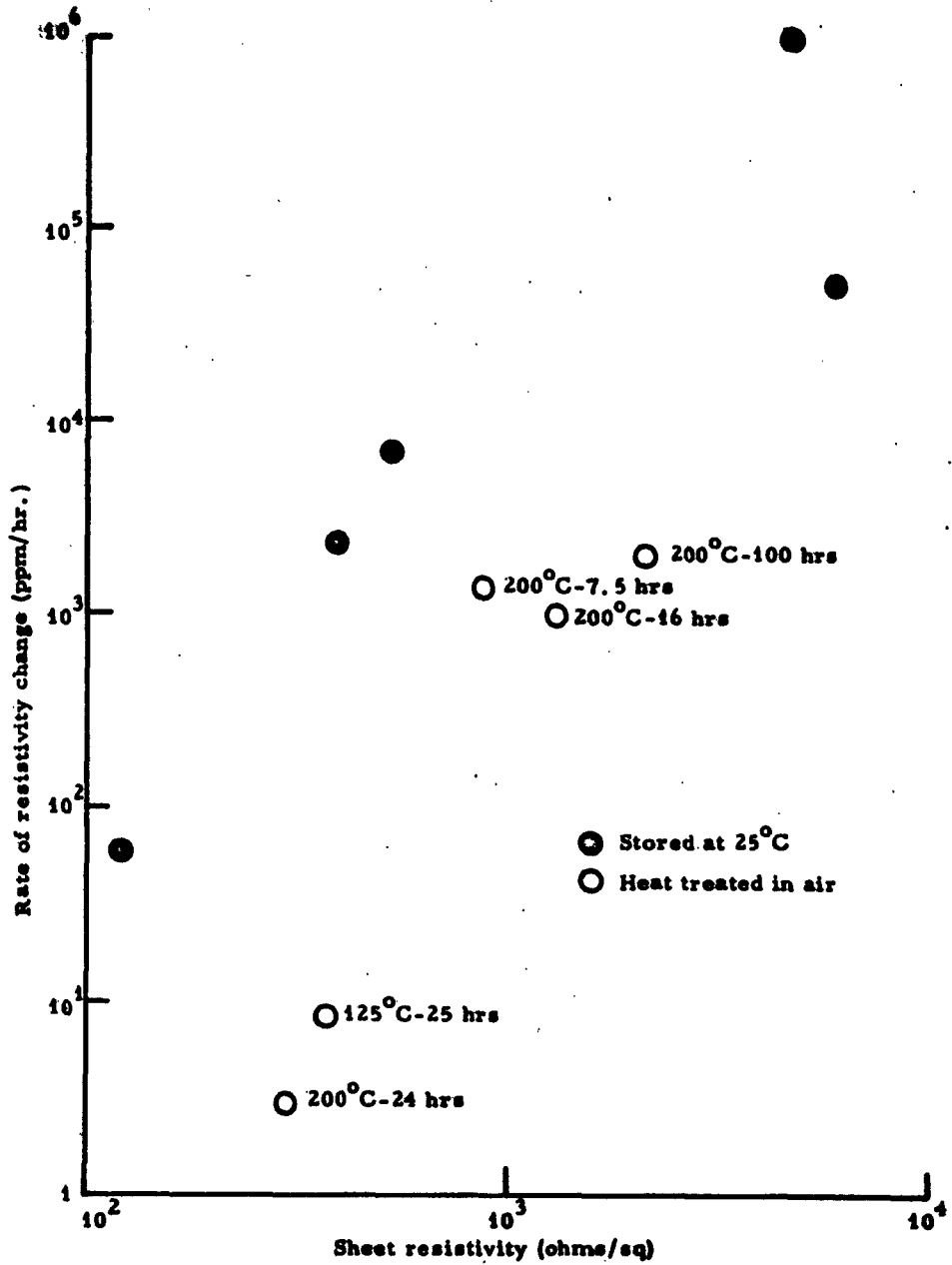


Fig. 59. Stability of resistance vs sheet resistivity for tungsten (not anodized) films. Note: Resistivities measured at 25°C.

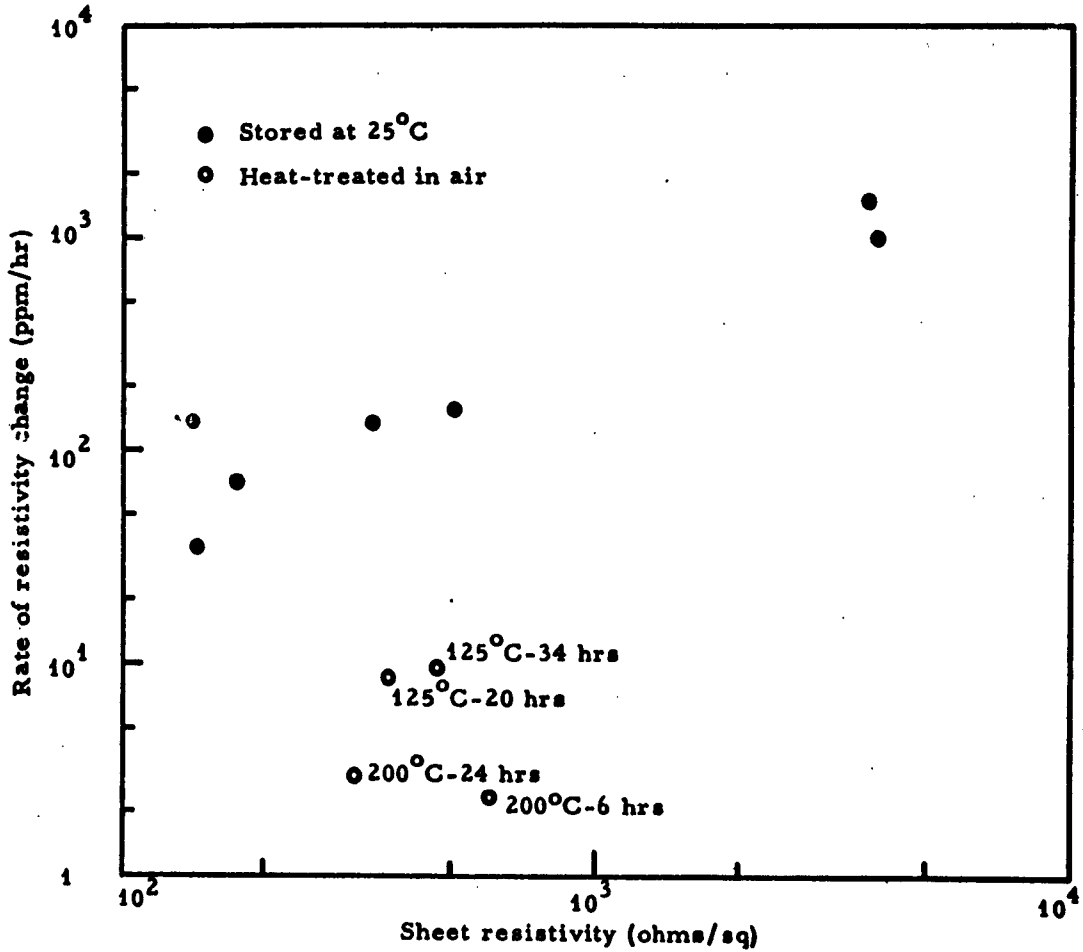


Fig. 60. Stability of resistance vs sheet resistivity for titanium metal films.  
Note: Resistivities measured at 25°C.

but becomes stabilized. When the anodized films are heat treated in vacuum as described in Section 1.2.6, the resistance changes only slightly and becomes stabilized. This set of observations may be explained by attributing increases in resistance to air oxidation. Heat treatment accelerates the oxidation. Anodization protects the metal from it. Heat treating anodized films causes a reaction of the metal with residual traces of air or moisture on the metal and the treatment may be called an accelerated aging process. Heat treating anodized films in vacuum reduces the amount of residual air or moisture available for reaction with the metal.

Stability data for resistors prepared from the metals investigated are as follows:

1. Tungsten

a. Stability under no-load. Stability of resistance tests were carried out in air for periods of 100 to 200 hours. Data for anodized films prepared from both evaporated and sputtered tungsten were obtained. Figure 61 shows that stability within 10 ppm/hr on exposure at 125°C is maintained for evaporated tungsten samples up to 700 ohms/sq and for sputtered tungsten samples up to 100 ohms/sq. Data for tungsten films exposed at 65°C are shown in Fig. 62. Evaporated films are stable up to 2600 ohms/sq and sputtered samples up to 1000 ohms/sq. The spread of points is within the present capability of measurement, which is approximately  $\pm 2$  ppm/hr.

The lower stability of the sputtered samples is believed to be related to the tapered edges in the film deposit caused by the use of masks to define the deposit. These edges of relatively thin metal account for about 10% of the total film width and are expected to be more susceptible during exposure to air oxidation.

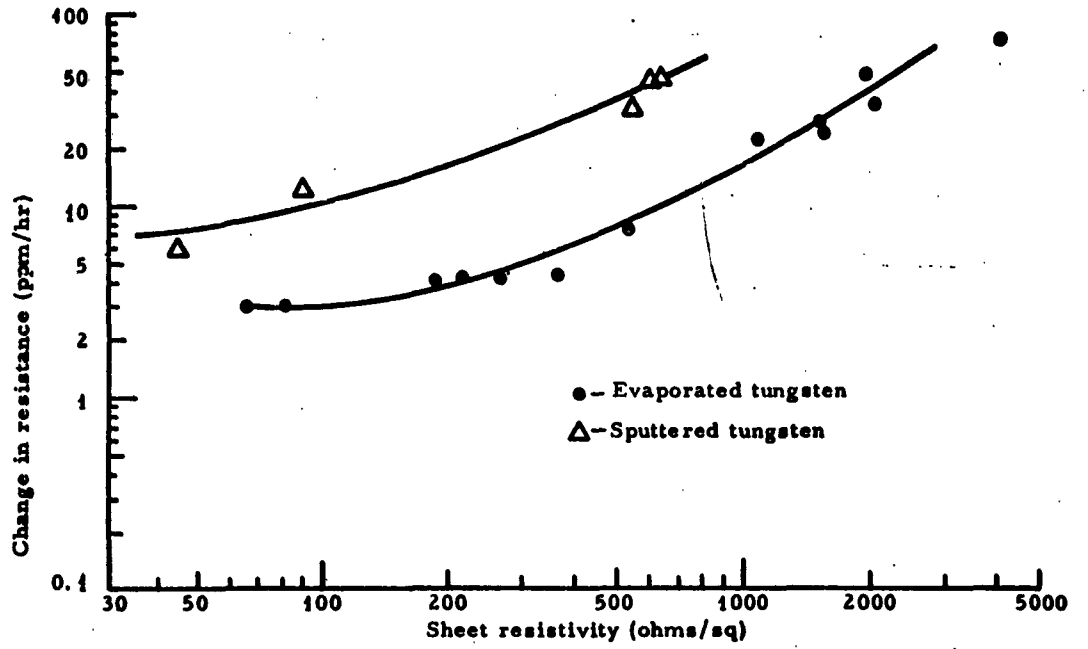


Fig. 61. Stability of resistance of anodized tungsten films measured at 125°C under no-load vs sheet resistivity.

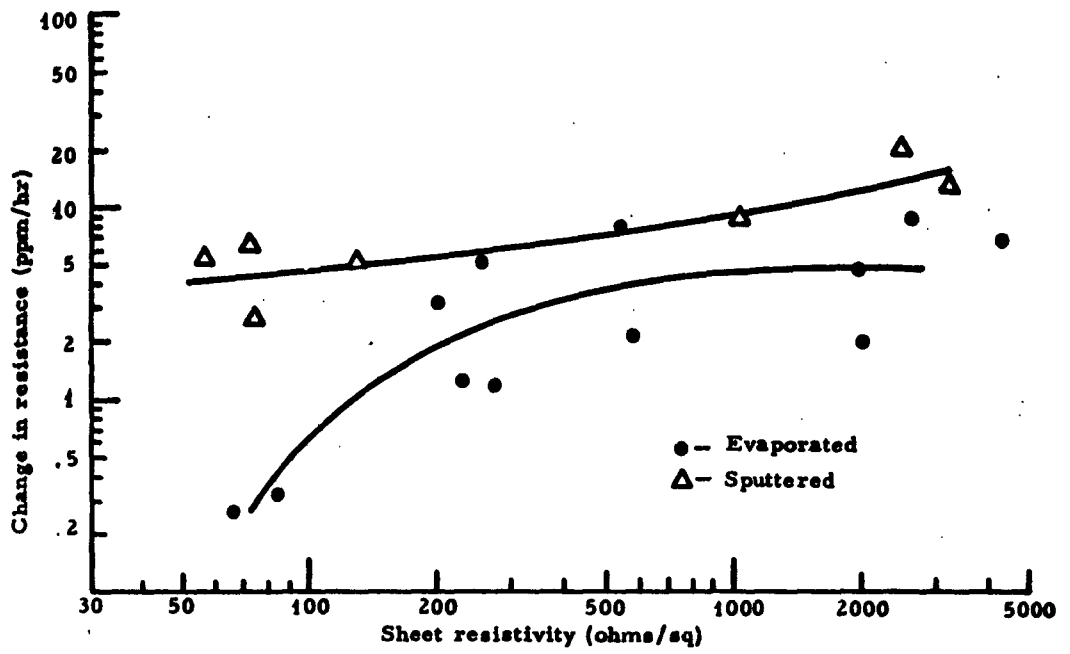


Fig. 62. Stability of resistance of anodized tungsten films measured at 65°C with no-load vs sheet resistivity.

The change in sheet resistivity for nine evaporated anodized samples in the "U" shape pattern that were stored for 4000 hours under room conditions is as follows:

<u>Sheet resistivity</u> <u>ohms/sq</u>	<u>Percent change after</u> <u>4000 hours</u>	<u>Average rate</u> <u>ppm/hr</u>
60	<0.01	<0.025
270	0.024	0.06
318	<0.01	<0.025
405	<0.01	<0.025
400	0.036	0.09
476	0.009	0.022
370	0.015	0.035
400	0.26	0.65
1106	0.04	0.10

Eight samples exhibited a drift no greater than 0.04 percent per 4000 hours (0.1 ppm/hr). The one sample which changed by 0.26 percent, was found to have a defect in the resistor pattern.

b. Stability under load. The ability of the anodized evaporated tungsten films to dissipate power at elevated temperatures is shown in Fig. 63. These data were compiled using seven samples of the "U" shaped pattern of Fig. 43. The power and temperature of each sample was successively increased until the rate of change of resistance, measured at 25°C, was approximately ± 10 ppm/hr. The data presented represent the maximum power dissipation of a resistive film at a particular temperature within the required stability of ± 10 ppm/hr. Two of the seven samples exhibited negative resistance changes and are indicated on the curve. These negative changes in resistance suggest that mechanisms other than oxidation are responsible for the resistance instability.

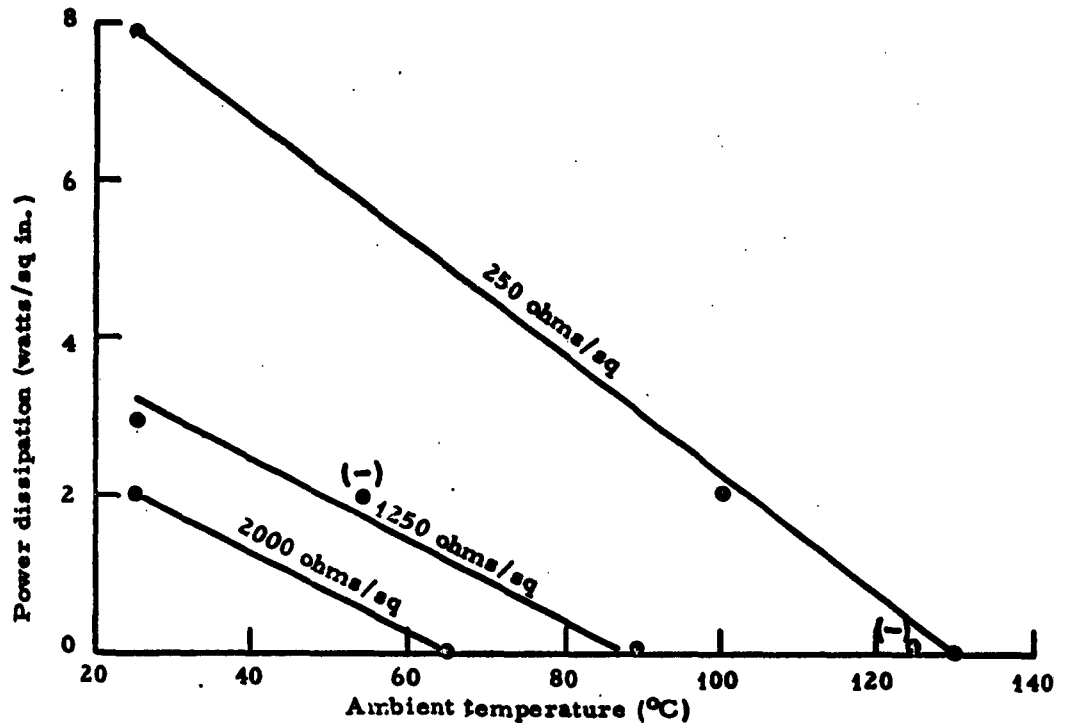


Fig. 63. Power dissipation of anodized evaporated tungsten resistors vs temperature. Stability is maintained within 10 ppm per hour.

2. Titanium

Metal titanium films of 100 ohms/sq sheet resistivity were found to drift 10 percent per 1000 hours (100 ppm/hr) on storage. No further data were taken.

3. Tantalum

a. Stability under no-load. The stability of resistance of anodized films was measured at 25°C and 125°C (in air) after heat treatment at 200°C for 6 hours in air. Although heating in air resulted in small increases in resistance from the value selected during anodization, the resistance of the films was stabilized.

The changes in resistivity of four samples after a 7200-hour life test at room conditions (shelf life) are as follows:

<u>Resistivity</u> <u>(ohms/sq)</u>	<u>Percent change after</u> <u>7200 hours</u>	<u>Average rate</u> <u>ppm/hr</u>
120	0.16	0.22
72	1.0	1.4
71	0.05	0.07
53	1.07	1.5

Anodized films up to sheet resistivities of 150 ohms/sq were found to be stable within 0.07% after 70 hours (10 ppm/hr) at 125°C in air.

b. Stability under load. The power dissipation prior to film breakdown at a temperature of 125°C in air was measured. For tantalum films of 40 ohms/sq sheet resistivity the dissipation immediately before breakdown was 40 watts/sq in. Examination of the glass substrates with circularly polarized light showed that the glass was in a state of radial compression, indicating that the glass melted at the site of breakdown. In some cases this stress was sufficient to crack the glass.

#### 4. Zirconium

The resistance stability of metal zirconium films was not tabulated because they exhibited a high degree of instability — estimated to be in excess of 100 ppm/hr at room conditions. Of the four metals deposited, zirconium was rated the lowest.

### 2. CONCLUSIONS

#### 2.1 THIN-FILM CAPACITORS

Techniques have been established for depositing on microscope slide glass substrates adherent, unblemished films of tantalum, tungsten and zirconium by sputtering, and films of aluminum, titanium and tungsten by vacuum evaporation. Methods of preliminary selection and cleaning of substrate surfaces were developed. These techniques in large part accounted for increasing the voltage at which breakdown occurred. Suitable electrolytes were selected and procedures established for the anodization of the films to produce clear, smooth oxide films of tantalum, aluminum and zirconium that are suitable for use as micro-circuit capacitor dielectrics.

Evaluation of electrical properties of capacitors formed with these films indicated that tantalum, aluminum and zirconium approach the basic requirements of low dissipation factor and high breakdown voltage. The electrical characteristics of thin-film capacitors prepared from these metals as well as titanium and tungsten are summarized and compared with the contract specifications in Table IX. When all properties are considered, tantalum best approaches the contract specifications.

TABLE IX  
Thin Film Capacitor Characteristics

Material	Capacitance		Dissipation factor D at 1 kc	Breakdown VB/VF (%)	Insulation resistance RLC at 0.75 VF (ohm-f)	Temperature coefficient of capacitance ppm/°C
	C/A at VF = 50 (µf/cm²)	CVF/A (µf-v/cm²)				
Specs.*	.31 (min)	15.5 (min)	.05 (max)	100	1000 (min)	200 (max)
Aluminum	.088	4.5	.005 - .01	80 - 96	1450	539
Tantalum	.22	13.5	.01	100	400	222
Titanium	.15	7.5	.02	<25**	--	--
Tungsten	.59	29.5	.8	<10**	--	--
Zirconium	.13	6.5	.02	100	160	356

\* Specifications of contract.

\*\* Difficult to estimate; low and erratic.

Symbols: A area

C capacitance

RL leakage resistance

VB breakdown voltage

VF forming voltage

## 2.2 THIN-FILM RESISTORS

Of the four metals investigated, tantalum, titanium, tungsten and zirconium, tungsten best fulfilled the specifications of the contract. A summary of the properties of thin-film anodized tungsten resistors obtained in the period of the contract is given in Table X.

The temperature coefficient of resistance (TCR) of tungsten films as a function of sheet resistivity is significantly dependent on the impurity gas content in the film deposition system. More positive temperature coefficients have been found for the lower sheet resistivity films when the impurity content has been reduced.

The resistance of anodized tungsten films can be stabilized by heat treatment at 150°C for 3 hours at a pressure of  $4 \times 10^{-7}$  Torr or less without appreciably changing the resistance from that obtained by anodization.

TABLE X

Properties of Anodized Tungsten Resistors Compared with Contract Specifications

<u>Property</u>	<u>Specifications</u>	<u>Tungsten</u>	<u>Tantalum</u>
Film resistor "density"	$6 \times 10^6$ ohms/sq. in.	$6 \times 10^6$ ohms/sq. in.	$1.2 \times 10^6$ ohms/sq. in.
Precision of preselected resistance	10%	1.5%	1.5%
Temperature coefficient of resistance	200 ppm/°C	Nominally 0	Nominally 0
Stability	1% per 1000 hours	1% per 1000 hours	---
Power dissipation at 125°C	2 watts/sq. in.	1/16 to 1/8 watt/sq. in.	---

### 3. REFERENCES

Page in text

- 26 1. H.A. Johansen, G.B. Adams, Jr., and P. Van Rysselberghe, *J. Electrochem. Soc.*, 104, 339 (1957).
- 37 2. G. Hass, *J. Optical Soc. Amer.*, 39, 532 (1949).
- 48 3. L. Maissel, J. Simmons, and M. Casey, *IRE Trans. Comp. Parts, CP-8*, 70 (1961); R.W. Berry and D.J. Sloan, *Proc. IRE*, 47, 1070 (1959); R.W. Berry, U.S. Pat. 2,993,266 (1961); N. Schwartz, M. Gresh, and S. Karlik, *J. Electrochem. Soc.*, 108, 750 (1961).
- 61 4. *Electromechanical Design*, 52 (Dec. 1960).
- 64 5. H.G. Rudenberg, J.R. Johnson, and L.C. White, *Solid State Design*, 3, 27 (1962).
- 70 6. L. Young, "Anodic Oxide Films," Academic Press (1961).
- 81 7. *Metals Handbook*, 1948 Ed., 396, Amer. Soc. for Metals, Metals Park, Ohio.
- 93 8. C.A. Neugebauer, Final Report, July 1962, Contract AF-19(604)-5566 (ASTIA Document 278557),
- 93 9. Oxidation of Tungsten, DMIC Report 155 (July 17, 1961).

#### 4. RECOMMENDATIONS FOR FUTURE WORK

##### 4.1 THIN-FILM CAPACITORS

1. Attempt to increase leakage resistance and reduce breakdown by counteracting metals or metallic ions that may be frozen into the anodized layer. Counteractants may be incorporated during metal film deposition, e.g., as a residual gas, or during anodization as solutes.

2. Reduce breakdown and leakage by seeking counter-electrode materials and deposition techniques that will promote agglomeration of the counter-electrode film to avoid penetration of the film into fissures in the anodized layer.

3. Improve long-term stability by use of low alkali glass (with smoother surfaces than are presently available).

4. Generally improve the capacitor properties of anodized zirconium by further testing different electrolytes.

##### 4.2 THIN-FILM RESISTORS

1. Obtain higher tungsten resistivities at zero temperature coefficient of resistance by eliminating as far as practicable those conditions involved in depositing tungsten films that contribute to negative temperature coefficients. These conditions and the direction expected for improvement are increased purity of the tungsten source, reduction of contaminants in the deposition system, higher rates of deposition and higher substrate temperatures.

2. Investigate the extent to which fine resistor patterns of tungsten can be made without sacrificing reproducibility or stability, to obtain a higher film resistor density.

## APPENDIX I

### ELECTRICAL TESTING UNIT FOR THIN-FILM CAPACITORS

A compact testing unit was assembled for initial tests, clearing of short circuits and breakdown voltage measurements. A schematic diagram is shown in Fig. I-1.

With the 3-section switch S1 in the "ac or clear" position, the ac supply is connected to the capacitor under test, provided that switch S2 is in the "ac" position. Supply current is limited by the 10-kilohm rheostat.

To clear short circuits, switch S2 in the "clear" position. A 1- $\mu$ f capacitor, which is charged through a 1-megohm resistor to a voltage established by a potentiometer across the dc supply, is then discharged through the capacitor under test by pressing switch S3.

With the 3-section switch S1 in the "dc" position, the dc supply is connected to the capacitor under test through a 1-megohm resistor. Applied voltage is controlled with the potentiometer.

A dual-trace, direct-coupled oscilloscope monitors the voltage across the capacitor under test (trace B) and the voltage of the supply (trace A). The two oscilloscope signals are made equal for a test sample of infinite resistance by the use of a second 1-megohm resistor leading to trace A. This compensates for the 1-megohm input impedance of the scope. Shorting switches are used to ground both scope inputs and the capacitor momentarily while zero settings or gain changes are made.

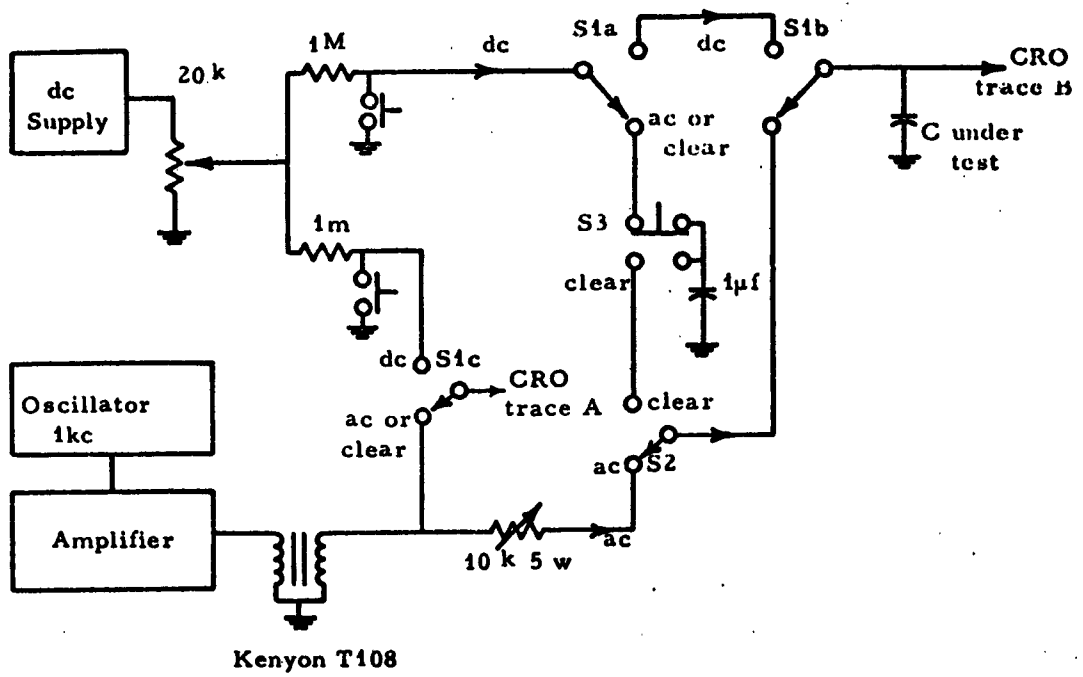


Fig. I-1. Schematic diagram of electrical testing unit for thin-film capacitors.

APPENDIX II

MEASUREMENT OF CAPACITANCE AND DISSIPATION FACTOR  
OVER A FREQUENCY RANGE

Capacitance and dissipation factor were measured with a General Radio 1650-A impedance bridge over a range of frequencies from 0.1 to 100 kc. External oscillators were provided: a Krohn-Hite 430A for frequencies above 10 kc, and a Hewlett-Packard 201C for frequencies below 10 kc where greater power was required. The null detector was an oscilloscope with a deflection sensitivity of 0.02 volt per inch, coupled through a 30-pf capacitor to minimize hum. Sensitivity in measuring dissipation was increased by wiring a decade resistor box with 0.01-ohm steps in series with the D rheostat of the bridge. External leads were shielded.

Because the bridge was designed for an upper limit of 20 kc, it was calibrated with a standard mica capacitor and known series resistors to approximate the equivalent circuits of thin-film capacitors. Values of dissipation factor computed from these standards were compared with D readings on the bridge and found to agree within 5 percent. Small corrections for capacitance were also determined.

### APPENDIX III

#### MULTIPLE-BEAM INTERFEROMETRY FOR THIN-FILM MEASUREMENT BELOW 300 Å

A modified Bausch and Lomb interference microscope objective was mounted on a metallurgical microscope having provision for vertical illumination. The objective was comprised of a lens and an optical flat with a partly reflecting front surface coating. The original coating had insufficient reflectivity for multiple beam interferometry; consequently it was replaced by evaporated aluminum with a reflectivity of more than 90%. The flat was lowered against the surface of the sample, which had previously been aluminized. A screw adjustment provided an air wedge between the flat and the sample, giving rise to interference fringes which were extremely narrow because of the multiple reflections. The tungsten lamp and the interference filter supplied with the microscope were replaced by a mercury arc and filter to give monochromatic illumination at 5460 Å. The arc was focused on the back focus of the objective lens, so that the sample is illuminated by light collimated by the objective before it strikes the flat and the sample below.

A photomicrograph of the edge of a tungsten film resistor as seen through the interferometer is shown in Fig. III-1. The deviation of fringes averages 2.5 percent of a fringe space, representing a step height of 69 Å. Improvements in the optical system involving the substitution of aluminum coatings by silver coatings for the sample and a multi-dielectric layer mirror with high reflectivity and low absorption are expected to permit measurement of thinner films, if they are deposited with sharply defined edges.

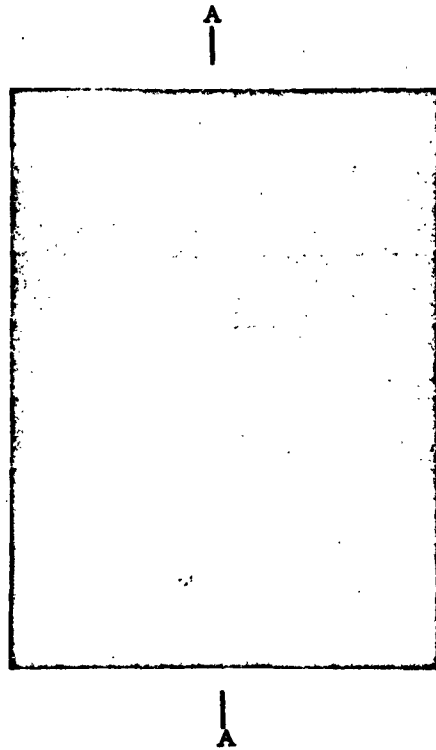


**Fig. III-1. Tungsten film resistor edge AA as seen through multiple beam interference microscope.**

**MAN HOURS EXPENDED BY KEY PERSONNEL**

For period Dec. 1, 1962 - February 28, 1963, Contract No. DA 36-039  
SC-90744

A. L. Solomon, Project Supervisor	68
E. R. Bowerman, Project Director	391
J. W. Culp	405
P. F. Hudock	447

Total man hours expended under Contract No. DA 36-039 SC-90744,  
for period June 1, 1962 to February 28, 1963

A. L. Solomon, Project Supervisor	170
E. R. Bowerman, Project Director	768
J. W. Culp	1261
P. F. Hudock	1279
F. Leder	<u>360</u>
Total hours	3838

Total man hours expended under Contract No. DA 36-039 SC-87305  
for period June 1, 1961 to May 31, 1962

A. Solomon, Project Director	149.0
E. R. Bowerman, Project Director	1438.0
J. Culp	1463.8
A. Esbitt	834.3
H. Woods	1.0
P. Lublin	<u>14.0</u>
Total hours	4048.1

GT&E Labs, Inc.  
DA 36-039-sc-90744  
Second Quarterly Report

UNITED STATES ARMY ELECTRONICS RESEARCH & DEVELOPMENT AGENCY  
STANDARD DISTRIBUTION LIST  
RESEARCH AND DEVELOPMENT CONTRACT REPORTS

	<u>Copies</u>
OASD (R&E) ATTN: Technical Library Room 3E1065 The Pentagon Washington 25, D. C.	1
Chief of Research and Development OCS, Department of the Army Washington 25, D. C.	1
Commanding General U. S. Army Materiel Command ATTN: R&D Directorate Washington 25, D. C.	1
Commanding General U. S. Army Electronics Command ATTN: AMSEL-AD Fort Monmouth, New Jersey	1
Director, U. S. Naval Research Laboratory ATTN: Code 2027 Washington 25, D. C.	1
Commander, Aeronautical Systems Division ATTN: ASAPRL Wright-Patterson Air Force Base, Ohio	1
Hq, Electronic Systems Division ATTN: ESAL L. G. Hanscom Field Bedford, Massachusetts	1
Commander, Air Force Cambridge Research Laboratories ATTN: CRO L. G. Hanscom Field Bedford, Massachusetts	1

Copies

<b>Commander, Air Force Command &amp; Control Development Division ATTN: CRZC L. G. Hanscom Field Bedford, Massachusetts</b>	<b>1</b>
<b>Commander, Rome Air Development Center ATTN: RAALD Griffiss Air Force Base, New York</b>	<b>1</b>
<b>Commander, Armed Services Technical Information Agency ATTN: TISIA Arlington Hall Station Arlington 12, Virginia</b>	<b>10</b>
<b>Chief, U. S. Army Security Agency Arlington Hall Station Arlington 12, Virginia</b>	<b>2</b>
<b>Deputy President U. S. Army Security Agency Board Arlington Hall Station Arlington 12, Virginia</b>	<b>1</b>
<b>Commanding Officer Harry Diamond Laboratories ATTN: Library, Room 211, Building 92 Washington 25, D.C.</b>	<b>1</b>
<b>Corps of Engineers Liaison Office U. S. Army Electronics Research and Development Laboratory Fort Monmouth, New Jersey</b>	<b>1</b>
<b>AFSC Scientific/Technical Liaison Office U. S. Naval Air Development Center Johnsville, Pennsylvania</b>	<b>1</b>
<b>USAE LRDL Liaison Office Rome Air Development Center ATTN: RAOL Griffiss Air Force Base, New York</b>	<b>1</b>
<b>Commanding Officer U. S. Army Electronics Materiel Support Agency ATTN: SELMS-ADJ Fort Monmouth, New Jersey</b>	<b>1</b>

DA 36-039-sc-90744

Copies

<b>AFSC Scientific/Technical Liaison Office</b> <b>U. S. Army Electronics Research and Development Laboratory</b> <b>Fort Monmouth, New Jersey</b>	<b>1</b>
<b>Commanding Officer and Director</b> <b>U. S. Navy Electronics Laboratory</b> <b>San Diego 52, California</b>	<b>1</b>
<b>Field Emission Corporation</b> <b>ATTN: Mr. F. M. Charbonnier</b> <b>611 Third Street</b> <b>McMinnville, Oregon</b>	<b>1</b>
<b>P. R. Mallory &amp; Company, Inc.</b> <b>ATTN: Mr. A. S. Doty</b> <b>Indianapolis 6, Indiana</b>	<b>1</b>
<b>Texas Instruments, Inc.</b> <b>ATTN: Mr. Wayne Patterson</b> <b>P. O. Box 5012</b> <b>Dallas, Texas</b>	<b>1</b>
<b>Republic Aviation Corporation</b> <b>ATTN: Dr. F. Huber</b> <b>Farmingdale, L. I., New York</b>	<b>1</b>
<b>Stanford Research Institute</b> <b>ATTN: Dr. Saul W. Chaikin</b> <b>Menlo Park, California</b>	<b>1</b>
<b>General Dynamics Corporation</b> <b>ATTN: Mr. R. L. Layburn</b> <b>P. O. Box 1068</b> <b>Red Bank, New Jersey</b>	<b>1</b>
<b>Bell Telephone Laboratory</b> <b>ATTN: Mr. D. A. McLean</b> <b>Murray Hill, New Jersey</b>	<b>1</b>
<b>Philco Corporation</b> <b>Lansdale Division</b> <b>ATTN: Mr. C. D. Simmons, Mgr. Microelectronics Dept.</b> <b>Lansdale, Pennsylvania</b>	<b>1</b>

Marine Corps Liaison Office  
U. S. Army Electronics Research and Development Laboratory  
ATTN: SELRA/LNR  
Fort Monmouth, New Jersey 1

Commanding Officer  
U. S. Army Electronics Research and Development Laboratory  
ATTN: Director of Research and Engineering  
Fort Monmouth, New Jersey 1

Commanding Officer  
U. S. Army Electronics Research and Development Laboratory  
ATTN: Technical Documents Center  
Fort Monmouth, New Jersey 1

Commanding Officer  
U. S. Army Electronics Research and Development Laboratory  
ATTN: SELRA/ADJ (FU #1)  
Fort Monmouth, New Jersey 1

Advisory Group on Electron Devices  
346 Broadway  
New York 13, New York 2

Commanding Officer  
U. S. Army Electronics Research and Development Laboratory  
ATTN: SELRA/TNR  
Fort Monmouth, New Jersey 3  
(FOR RETRANSMITTAL TO ACCREDITED BRITISH AND CANADIAN  
GOVERNMENT REPRESENTATIVES)

Commanding General  
U. S. Army Combat Developments Command  
ATTN: CDCMR-E  
Fort Belvoir, Virginia 1

Commanding Officer  
U. S. Army Communications-Electronics Combat Development Agency  
Fort Huachuca, Arizona 1

Director, Fort Monmouth Office  
U. S. Army Communications-Electronics Combat Development Agency  
Building 410  
Fort Monmouth, New Jersey 1

DA 36-039-sc-90744

Copies

Metarac, Incorporated  
ATTN: Mr. George N. Fadel  
45-68 162nd Street  
Flushing 58, New York

1

Chief, Bureau of Ships  
Room 3327, Department of the Navy  
ATTN: Mr. J.M. Kerr, Jr., Code 691A2A  
Washington 25, D.C.

1

Headquarters, ARDC  
ATTN: Mr. L. Gubbins, RASGR  
Griffiss Air Force Base, New York

1

Commander, ASD  
ATTN: Mr. C.K. Greene, ASRNE  
Wright-Patterson Air Force Base, Ohio

1

Commanding Officer  
U.S. Army Electronics Research & Development Laboratory  
Fort Monmouth, New Jersey

ATTN: SELRA/PE (Division Director)

1

ATTN: SELRA/PE (Dr. E. Both)

1

ATTN: SELRA/PEP (Dr. H.J. Degenhart)

1

ATTN: SELRA/PEP (Mr. R.A. Gerhold)

1

ATTN: SELRA/PF (Mr. V.J. Kublin)

1

ATTN: SELRA/PEP (Mr. A.J. Raffalovich)

16

75

<p>U.S. Army Electronics Research &amp; Dev. Lab. Fort Monmouth, N.J., THIN FILMS FORMED BY ELECTROCHEMICAL REACTIONS, by E.R. Bowerman, J. Warren Culp and P.F. Hudock. Final Report, June 1, 1961 - Feb. 28, 1963, 123 pages, incl. 65 figures and 10 tables. Unclassified Report</p> <p>The formation of thin-film capacitors by the anodic oxidation of the surfaces of vacuum-deposited, evaporated and sputtered films of Al, Ta, W, Ti and Zr was investigated. Tantalum most nearly approached the contract objectives with breakdown voltage equal to or greater than the anodization forming voltage.</p>	<p>UNCLASSIFIED</p> <p>1. Thin films 2. Resistors 3. Capacitors</p> <p>I. DA Project No. 3A99-15-003 and 3C93-34-001</p> <p>II. Contract No. DA 36-039 SC-90744 (continuation of DA 36-039 SC-87305)</p>	<p>UNCLASSIFIED</p> <p>U.S. Army Electronics Research &amp; Dev. Lab. Fort Monmouth, N.J., THIN FILMS FORMED BY ELECTROCHEMICAL REACTIONS, by E.R. Bowerman, J. Warren Culp and P.F. Hudock. Final Report, June 1, 1961 - Feb. 28, 1963, 123 pages, incl. 65 figures and 10 tables. Unclassified Report</p> <p>The formation of thin-film capacitors by the anodic oxidation of the surfaces of vacuum-deposited, evaporated and sputtered films of Al, Ta, W, Ti and Zr was investigated. Tantalum most nearly approached the contract objectives with breakdown voltage equal to or greater than the anodization forming voltage.</p>	<p>UNCLASSIFIED</p> <p>1. Thin films 2. Resistors 3. Capacitors</p> <p>I. DA Project No. 3A99-15-003 and 3C93-34-001</p> <p>II. Contract No. DA 36-039 SC-90744 (continuation of DA 36-039 SC-87305)</p>	<p>UNCLASSIFIED</p> <p>III. General Telephone &amp; Electronics Laboratories, Inc., Bay Side New York</p> <p>IV. E.R. Bowerman J. Warren Culp P.F. Hudock</p> <p>V. Final Report TR 63-205.3</p> <p>VI. In ASTIA collection</p>
<p>U.S. Army Electronics Research &amp; Dev. Lab. Fort Monmouth, N.J., THIN FILMS FORMED BY ELECTROCHEMICAL REACTIONS, by E.R. Bowerman, J. Warren Culp and P.F. Hudock. Final Report, June 1, 1961 - Feb. 28, 1963, 123 pages, incl. 65 figures and 10 tables. Unclassified Report</p> <p>The formation of thin-film capacitors by the anodic oxidation of the surfaces of vacuum-deposited, evaporated and sputtered films of Al, Ta, W, Ti and Zr was investigated. Tantalum most nearly approached the contract objectives with breakdown voltage equal to or greater than the anodization forming voltage.</p>	<p>UNCLASSIFIED</p> <p>1. Thin films 2. Resistors 3. Capacitors</p> <p>I. DA Project No. 3A99-15-003 and 3C93-34-001</p> <p>II. Contract No. DA 36-039 SC-90744 (continuation of DA 36-039 SC-87305)</p>	<p>UNCLASSIFIED</p> <p>U.S. Army Electronics Research &amp; Dev. Lab. Fort Monmouth, N.J., THIN FILMS FORMED BY ELECTROCHEMICAL REACTIONS, by E.R. Bowerman, J. Warren Culp and P.F. Hudock. Final Report, June 1, 1961 - Feb. 28, 1963, 123 pages, incl. 65 figures and 10 tables. Unclassified Report</p> <p>The formation of thin-film capacitors by the anodic oxidation of the surfaces of vacuum-deposited, evaporated and sputtered films of Al, Ta, W, Ti and Zr was investigated. Tantalum most nearly approached the contract objectives with breakdown voltage equal to or greater than the anodization forming voltage.</p>	<p>UNCLASSIFIED</p> <p>III. General Telephone &amp; Electronics Laboratories, Inc., Bay Side New York</p> <p>IV. E.R. Bowerman J. Warren Culp P.F. Hudock</p> <p>V. Final Report TR 63-205.3</p> <p>VI. In ASTIA collection</p>	<p>UNCLASSIFIED</p> <p>III. General Telephone &amp; Electronics Laboratories, Inc., Bay Side New York</p> <p>IV. E.R. Bowerman J. Warren Culp P.F. Hudock</p> <p>V. Final Report TR 63-205.3</p> <p>VI. In ASTIA collection</p>